

# Measuring Dynamic Strain Induced by Balloon-Expandable Endovascular Stents in Arterial Walls

by

James C. Squire

B.S., United States Military Academy (1989)

Submitted to the  
Department of Electrical Engineering and Computer Science  
in partial fulfillment of the requirements for the degree of

MASTERS OF SCIENCE

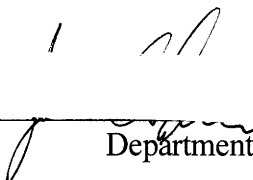
at the

MASSACHUSETTS INSTITUTE OF TECHNOLOGY

December 1996

©1996 Massachusetts Institute of Technology  
All rights reserved

Author

  
Department of Electrical Engineering and Computer Science

December 13, 1996

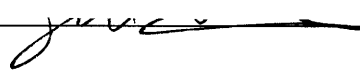
Certified by

  
Elazer R. Edelman

Herman von Helmholtz Associate Professor

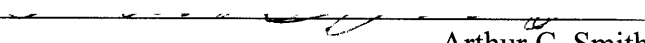
Thesis Supervisor

Certified by

  
Campbell Rogers  
Assistant Professor, Harvard Medical School

Thesis Coadvisor

Accepted by

  
Arthur C. Smith  
Chairman, Committee on Graduate Students

MAR 06 1997

# Measuring Dynamic Strain Induced by Balloon-Expandable Endovascular Stents in Arterial Walls

by  
James C. Squire

Submitted to the Department of Electrical Engineering and Computer Science  
on December 24, 1996, in partial fulfillment of the  
requirements for the degree of  
Masters of Science

## Abstract

Many novel interventions have been developed in the hopes of treating advanced arteriosclerosis. Ironically these very same techniques trigger the uncontrolled growth of cells within the artery that may re-narrow the vessel lumen and limit long term efficacy. This phenomenon, termed restenosis, causes up to one-third of patients who undergo angioplasty to require additional intervention within three months. The biological mediators of restenosis are incompletely understood. Recent discoveries<sup>1,2,3,4,5</sup> suggesting that dynamically-changing strain in particular may trigger smooth muscle cell hyperplasia within the intima, have spurred interest in both the characterization of strain imposed on blood vessels by these treatment modalities and the vascular response to applied mechanical strain.

I have investigated the dynamic, local strain field imposed *in vivo* by endovascular stents. These indwelling devices are becoming increasingly important in treatment of atherosclerosis and take issues of strain to extremes. Stents are expandable metal tubes which are threaded inside an artery to a site of narrowing where they are plastically enlarged and left as permanent implants to scaffold the artery open. During expansion stents induce large-scale strains within the vascular wall which are difficult to measure dynamically *in vivo*. These strains in turn may be critical determinants of stent-vessel biology.

This thesis quantifies the strain tensor imparted by the expanding stent upon the arterial wall as both a function of space and time, and determines whether this dynamically-changing strain field causes injury not apparent from pre-expansion/post-expansion images alone. An understanding of the design-dependence and causative effects of strain may then contribute to the optimal design of endovascular implants that minimizes hyperplasia. Furthermore, the ability to measure the local distention within blood vessels *in vivo* may permit more basic study of general tissue responses to strain.

Thesis supervisor: Elazer. R. Edelman, Associate Professor of Health Sciences and Technology

Thesis coadvisor: Campbell Rogers, Assistant Professor of Medicine, Harvard Medical School

## Acknowledgments

First of all, I would like to thank Professor Elazer Edelman for being an outstanding advisor and mentor, and for his work in creating a research environment that is as much an extended family as a laboratory. He has provided sage advice on matters ranging from thesis selection, presentation, and administration to philosophy, politics, and proper hyphenation, and teaches perhaps the most important lessons through his life example. A wise man once said, “You can disown your family and divorce your wife, but you will *always* be labeled with your advisor’s name.” I will always be proud to have been Elazer’s student.

I would also like to thank Campbell Rogers for his unfailing support and encouragement during my research. His contributions are reflected throughout this thesis; he completed most of the rabbit surgeries and through countless calls to his pager (“Can Dr. Rogers call you back *after* he finishes catheterizing the patient?”) provided much advice.

I am indebted to my friend/teacher Steve Burns for his encouragement and support during the early graduate years. He has reminded me of the joy of teaching and the importance of compassion.

The members of Elazer’s laboratory have made this research rewarding, and I want to thank everyone for their contributions to this work and to my education. Several of Phil Seifert’s expertly-stained histology slides (with his “secret stent sectioning technique”) illustrate this thesis; the Canadian post-doc contingent of Dave Ettenson, Ed Koo, Tony English and Martin Sirois spent many patient hours with me discussing cellular biology and the process of paper-writing; Wade Wan spent nearly as many hours talking about the Canadians; and Mark Lovich and David Tseng often provided insight when I worked and good squash partners when I didn’t. My sincere thanks to Fred Welt who completed one of the rabbit surgeries and whose medical commonsense helped debug one of the first artery-specklers. Mike Jacknis, an undergraduate whom I taught and later supervised, had an unadulterated love of engineering rarely seen even in these environs; I am sure the creativity and enthusiasm he shared in this project will serve him well. Sahil Parikh’s animal experiments provided many of the seeds of this thesis; few first-year medical students have completed as many operating room hours as he. A special thanks to the

administrative skills of Joanne Sorrento and Lisa Court, who provided the behind-the-scenes support that so often goes unrecognized and unthanked.

Two foundations supported this work, and I want to remember and thank Dorothy Poitras and Morton Yohalem. I will not forget their role in giving me an opportunity to complete this work.

I want to thank Carl and Gladys Salva for their care, weekend retreats, and most of all, for their daughter.

My parents, Jim and Marilyn Squire are to blame/credit for my accomplishments. Through love and war, several careers, and countless fool ideas they've been there for me in body or spirit.

Finally, I would like to thank my lovely wife Laura. For the last seven years we have played, studied, laughed, cried, and loved together, from the joys of four graduations to the pain of wartime separation. Laura, we have grown up together and pushed/pulled each other through this. I look forward to a lifetime spent together with you.

# Contents

<b>Acknowledgments</b> .....	<b>3</b>
<b>Contents</b> .....	<b>5</b>
<b>List of Figures</b> .....	<b>8</b>
<b>List of Tables</b> .....	<b>10</b>
<b>1. Introduction</b> .....	<b>11</b>
1.1 Statement of the problem.....	11
1.2 Thesis organization.....	12
<b>2. Background</b> .....	<b>14</b>
2.1 Stenting: an important treatment of cardiac disease.....	14
2.1.1 Cardiac disease in the United States.....	14
2.1.2 Endovascular stents.....	15
2.2 Short vs. long-term stent efficacy.....	17
2.2.1 Excellent short-term results.....	17
2.2.2 Long-term outlook less favorable .....	17
2.3 Mechanical bases of injury leading to hyperplasia.....	21
2.3.1 What is/is not known about mechanically-caused injury .....	21
2.3.2 Direct effect of strain on arterial smooth muscle cells.....	22
2.3.3 Contact abrasion/laceration.....	23
2.3.4 Shear stress.....	24
2.3.5 Of these possible mechanisms, why choose to examine strain?.....	24

2.4 General response of living tissue to strain.....	26
2.4.1 Strain vs. stress effects.....	26
2.4.2 The endovascular stent: an excellent model.....	26
<b>3. Strain Mensuration System.....</b>	<b>28</b>
3.1 Introduction .....	28
3.2 Methods.....	29
3.2.1 Experimental system .....	29
3.2.2 Theoretical.....	30
3.2.3 Analytical .....	33
3.3 Results .....	34
3.3.1 Marking device .....	34
3.3.2 <i>Ex vivo</i> artery segment.....	34
3.3.3 Latex phantom.....	40
3.3.4 Error simulations .....	42
3.4 Discussion.....	44
3.4.1 Strain.....	44
3.4.1.1 Definitions.....	44
3.4.1.2 Finding strain tensor from marker triads.....	46
3.4.2 How others have measured tissue strain .....	47
3.4.3 Error Analysis .....	51
3.4.4 Spatial resolution.....	53
3.4.5 Luminal strain in the thick-walled artery model.....	53
3.5 Summary.....	55
<b>4. <i>In vivo</i> vascular strain induced by the expanding endovascular stent.....</b>	<b>56</b>
4.1 Introduction .....	56

4.2 Methods.....	57
4.3 Results .....	59
4.3.1 <i>In vivo</i> strain components 2 to 8 atm.....	59
4.3.2 Pressure-differential strain.....	63
4.4 Discussion.....	63
4.4.1 The dogbone effect .....	64
4.4.1.1 Proposed mechanism - existence depends only on stent/balloon length, not on material properties .....	64
4.4.1.2 Validating evidence: superficial injury.....	66
4.4.1.3 Validating evidence: deep injury & hyperplasia.....	68
4.4.2 Other findings.....	69
4.4.3 Proposed methods to reduce dogbone.....	70
4.4.2.1 Stent-based methods .....	71
4.4.2.2 Catheter-based methods.....	72
4.4.2.3 Self-expanding stents.....	72
4.5 Summary.....	72
<b>5. Conclusions.....</b>	<b>74</b>
5.1 Accomplishments .....	74
5.2 Future work .....	75
<b>Appendix A: Figure data .....</b>	<b>77</b>
<b>Appendix B: Strain analysis/display code.....</b>	<b>80</b>
<b>References .....</b>	<b>111</b>

## List of Figures

Figure 1: Healthy, patent artery (A) versus diseased (B).....	15
Figure 2: A stainless steel stent mounted upon a balloon catheter .....	16
Figure 3: Cross-sections of healthy and diseased arteries.....	18
Figure 4: Angiograms showing the progression of restenosis .....	19
Figure 5: Pig coronary artery 3 days (A) and (B) 28 days after stenting.....	20
Figure 6: Human saphenous vein graft after stenting.....	20
Figure 7: Strain mensuration system.....	30
Figure 8: Determination of three-dimensional reference point locations.....	31
Figure 9: Bovine coronary explant before and after marking with the inkjet device. ....	34
Figure 10: Bovine <i>ex vivo</i> artery segment at 0 atm. ....	35
Figure 11: Bovine <i>ex vivo</i> artery segment at 2 atm. ....	36
Figure 12: Bovine <i>ex vivo</i> artery segment at 4 atm. ....	37
Figure 13: Bovine <i>ex vivo</i> artery segment at 6 atm. ....	38
Figure 14: Bovine <i>ex vivo</i> artery segment at 8 atm. ....	39
Figure 15: Phantom at early expansion step .....	40
Figure 16: Phantom at late expansion step.....	41
Figure 17: Validation of Monte-Carlo error simulation.....	43



Figure 18: Biaxial Green strain tensor .....	44
Figure 19: The two-dimensional strain field in cylindrical coordinates.....	45
Figure 20: Stent placement in the rabbit femoral artery .....	57
Figure 21: Rabbit femoral artery shown before and after <i>in vivo</i> marking.....	58
Figure 22: <i>In vivo</i> strains in rabbit femoral artery at 2 atm.....	59
Figure 23: <i>In vivo</i> strains in rabbit femoral artery at 4 atm.....	60
Figure 24: <i>In vivo</i> strains in rabbit femoral artery at 6 atm.....	61
Figure 25: <i>In vivo</i> strains in rabbit femoral artery at 8 atm.....	62
Figure 26: Change in the strain tensor as pressure is increased from 4 to 8 atm.....	63
Figure 27: Both stent and balloon open end-first at 4 atm of pressure.....	65
Figure 28: As the center region opens, the surrounding artery contracts axially. ....	65
Figure 29: AgNO <sub>3</sub> stained <i>en face</i> rabbit femoral artery after stenting .....	67
Figure 30: Arterial injury and hyperplasia levels vs. position along the stent.....	68
Figure 31: Balloon/catheter designs, present and proposed.....	71

## List of Tables

Table I: $r^2$ values measuring the validity of the assumption that the artery is axisymmetric and has a quadratic surface.....	42
Table II: Average <i>in vivo</i> errors predicted through the Monte-Carlo simulator. ....	44
Table III: A comparison of strain-imaging methods used in highly-compliant materials .....	50

# 1. Introduction

## 1.1 Statement of the problem

Many novel interventions have been developed in the hopes of treating advanced arteriosclerosis. Ironically these very same techniques trigger the uncontrolled growth of cells within the artery that may re-narrow the vessel lumen and limit long term efficacy. This phenomenon, termed restenosis, causes up to one-third of patients who undergo angioplasty to require additional intervention within three months. The biological mediators of restenosis are incompletely understood. Recent discoveries<sup>1,2,3,4,5</sup> suggesting that dynamically-changing strain in particular may trigger smooth muscle cell hyperplasia within the intima, have spurred interest in both the characterization of strain imposed on blood vessels by these treatment modalities and the vascular response to applied mechanical strain.

I have investigated the dynamic, local strain field imposed *in vivo* by endovascular stents. These indwelling devices are becoming increasingly important in treatment of atherosclerosis and take issues of strain to extremes. Stents are expandable metal tubes which are threaded inside an artery to a site of narrowing where they are plastically

enlarged and left as permanent implants to scaffold the artery open. During expansion stents induce large-scale strains within the vascular wall which are difficult to measure dynamically *in vivo*. These strains in turn may be critical determinants of stent-vessel biology.

This thesis quantifies the strain tensor imparted by the expanding stent upon the arterial wall as both a function of space and time, and determines whether this dynamically-changing strain field causes injury not apparent from pre-expansion/post-expansion images alone. An understanding of the design-dependence and causative effects of strain may then contribute to the optimal design of endovascular implants that minimizes hyperplasia. Furthermore, the ability to measure the local distention within blood vessels *in vivo* may permit more basic study of general tissue responses to strain.

## 1.2 Thesis organization

This thesis describes a coordinated set of *in vitro* and *in vivo* experiments designed to examine endovascular stent-induced strain. Chapter 2 provides background needed to answer the question “Why study strain in the stented blood vessel?” The reasons are interrelated and span clinical, biological, and engineering fields of research. Chapter 3 investigates the system used to measure vascular strain induced by the stent. The capabilities and limitations of the system are characterized *ex vivo* using excised bovine coronary arteries. A Monte-Carlo simulator capable of predicting accuracy of the strain

mensuration system is developed and validated using a latex phantom. Chapter 4 applies the system in a rabbit vascular injury model. The following questions are explored:

- How do balloon-expandable stents inflate *in vivo*? Do they rotate? Do they expand nonuniformly?
- Do the stents abrade the vascular wall during expansion? Is this an important contributor of hyperplasia?
- Can any abrasion present be reduced through catheter choice or redesign, stent choice or redesign, or operator technique?

Chapter 5 summarizes the thesis and considers its various applications, including suggestions for future work.

## **2. Background**

### **2.1 Stenting: an important treatment of cardiac disease**

#### **2.1.1 Cardiac disease in the United States**

Ischemic heart disease, the end result of reduced flow through narrowed, presumably atherosclerotic coronary arteries (Figure 1), is the leading cause of mortality in the Western world; it affects more than 10 million Americans and is responsible for 42.5% of all deaths in the United States<sup>6</sup>. Although percutaneous transluminal coronary balloon angioplasty (PTA) and coronary artery bypass grafting (CABG) have been widely used, lack of long-term efficacy in many patients has prompted the search for new technologies, including laser angioplasty, atherectomy, and implanted endovascular scaffolding devices called stents. Of these, stents are rapidly gaining the lion's share of the vascular intervention market because of their high initial success rate and improved long term efficacy. In 1995 approximately 100,000 patients in the United States received stents and this number is expected to double by 1997<sup>7</sup>.

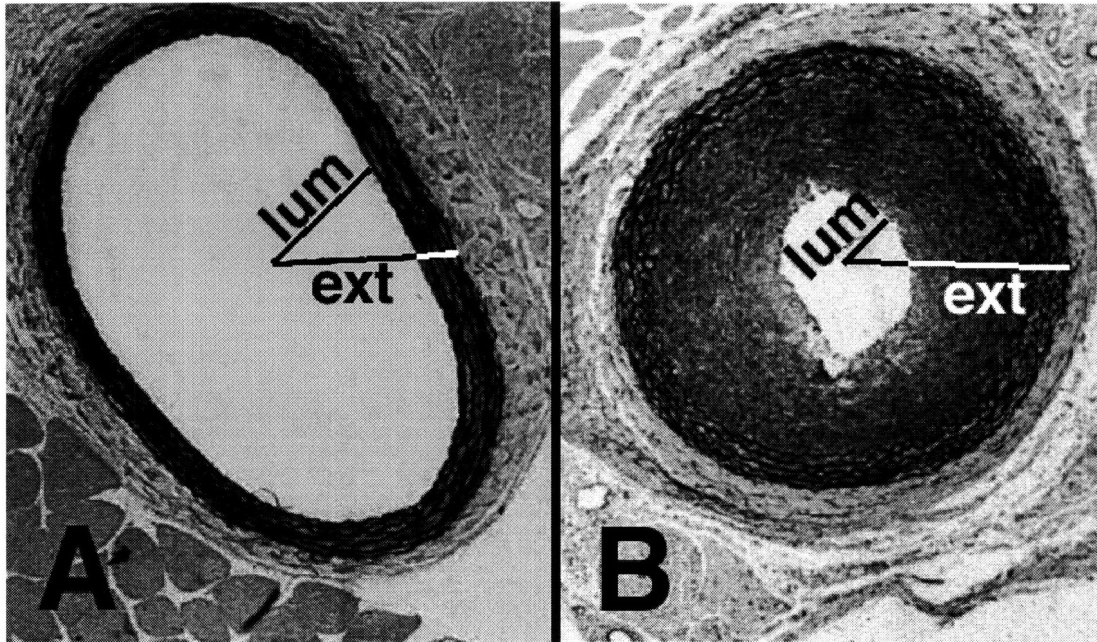


**Figure 1: Healthy, patent artery (A) versus diseased (B).** The most prominent structure in the normal artery is the *tunica media*. This darkly strained collar of concentric elastic lamella bounds the lumen and contains smooth muscle cells. These cells regulate local vessel tone and blood flow by contracting or relaxing leading to constriction or dilation of the artery. The *tunica intima*, the innermost lining of the artery, is barely visible, if at all, at this magnification (100x). In the diseased artery the *tunica intima* is now occupied by a hyperplastic mass; in this artery the mass is principally comprised of smooth muscle cells. These cells have now undergone phenotypic transformation from their contractile state to a synthetic or proliferative state. In place of tone regulation they now grow and stimulate further growth so as to progressively occlude the lumen. Although the exterior radii (ext) of both arteries are similar (as measured at the advential-medial boundary), the luminal radius (lum) of the healthy artery is three-fold that of the diseased vessel.

### 2.1.2 Endovascular stents

Endovascular stents are expandable metal tubes 6 mm to 60 mm in length and 3 mm to 10 mm in diameter made from a variety of materials that include stainless steel, titanium, and the nickel-titanium alloy nitinol. In a compressed state the stent is mounted on a catheter and threaded through the vascular tree to a site of narrowing. The stent is next enlarged in

diameter approximately 50%: nitinol stents expand as they are freed to resume their natural expanded shape as dictated by a thermally-triggered shape memory effect; stainless steel stents are plastically deformed under the influence of a cylindrical balloon inflated within the stent to 8-20 atmospheres (atm) of pressure. Once the catheter is withdrawn the stent is left as a permanent implant within the artery (Figure 2).

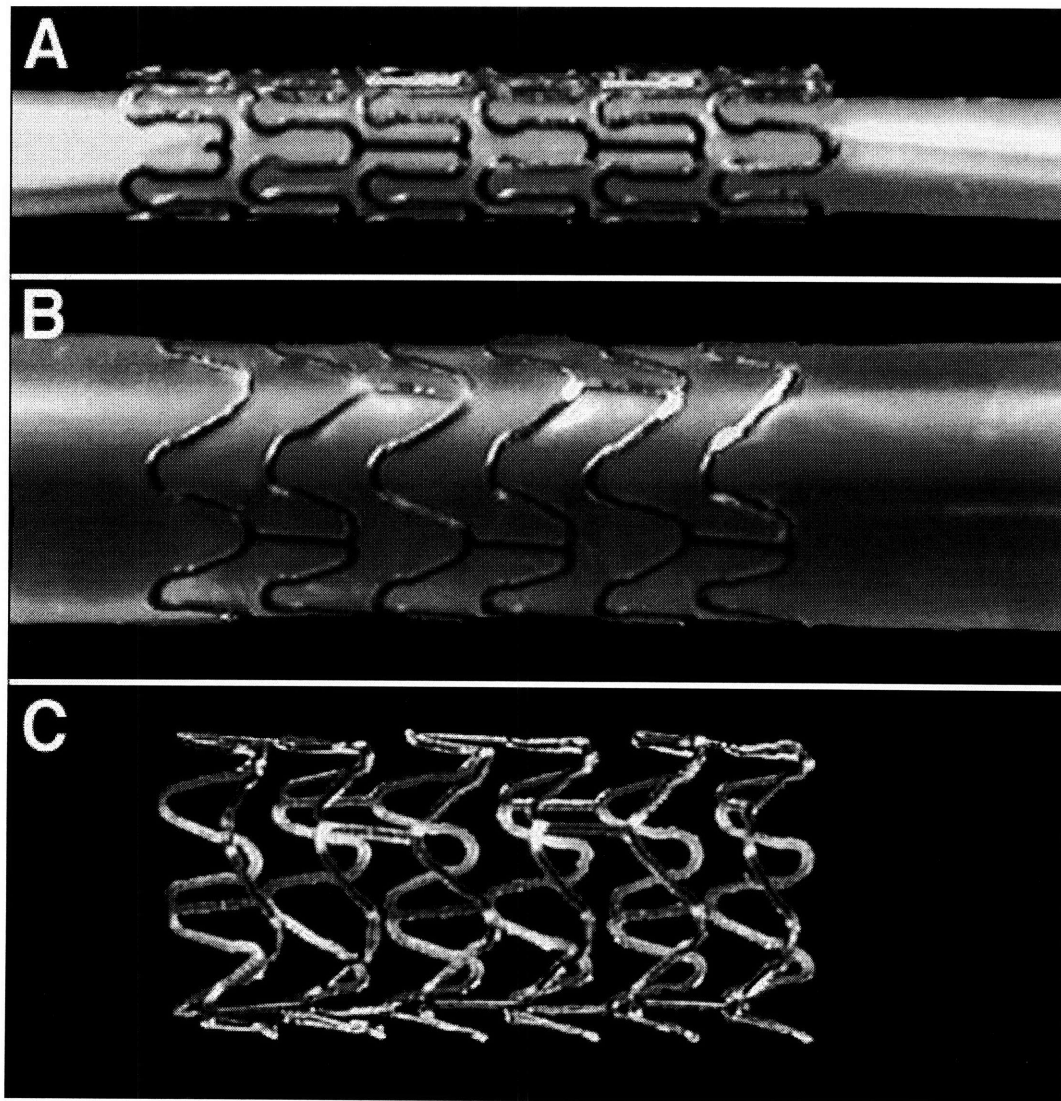


**Figure 2: A stainless steel stent mounted upon a balloon catheter (A) before and (B) after balloon inflation, and (C) after balloon withdrawal**



## **2.2 Short vs. long-term stent efficacy**

### **2.2.1 Excellent short-term results**

Before successful implantation, the endovascular stent must be delivered through more than one meter of tortuous vasculature; moreover, emplacement often requires 1 mm accuracy.

The stent must enlarge with limited recoil under the force of the surrounding artery, which responds to this stress with spasms of vasoconstriction. Finally, vessel patency must be restored without complications such as vessel hemorrhage, acute thrombosis, or obstruction by delamination of surrounding plaque. These issues formed significant obstacles to early stenting procedures although improved clinical techniques now result in far fewer complications; subacute thrombosis rates, for example, have declined six-fold and are now lower than 3%<sup>8,9</sup>.

### **2.2.2 Long-term outlook less favorable**

Despite initial success rates, the permanent addition of a stent to the arterial wall may induce a persistent and aggressive vascular response. Unlike acute complications, these reactions have not been greatly reduced by refinements to the implantation procedure.

Approximately 33% of the patients receiving stents require further intervention within six months<sup>10</sup> to restore patency after thrombosis, fibrosis, and rapidly proliferating smooth muscle and inflammatory cells progressively occlude the lumen (Figure 3). The biological underpinnings of vascular response to injury are complex and include platelet aggregation,

monocyte infiltration, and change in smooth muscle cell phenotype<sup>11</sup>. Despite continued investigation into the biological causes and remedies, restenosis from the combined effects of neointimal hyperplasia, medial degeneration, and vascular remodeling remains an unsolved problem in modern interventional cardiology.

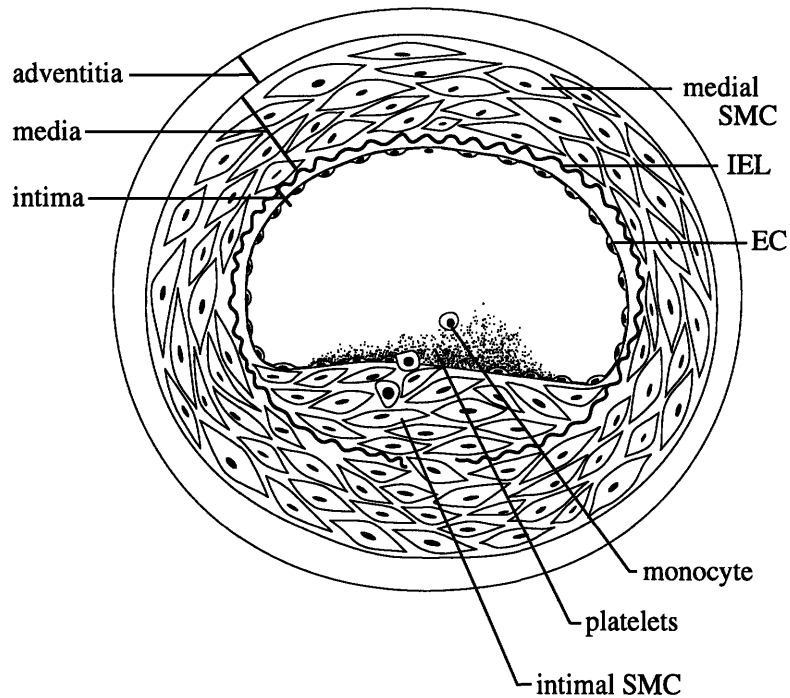


**Figure 3:** The upper portion of this figure shows a cross-section of a healthy artery. The endothelial cell (EC) monolayer rests upon basement membrane covering the internal elastic lamina (IEL). The media is composed of smooth muscle cells (SMC). After EC injury (bottom), platelets are adhering to the exposed thrombogenic surface of the vessel wall and are attracting monocytes, and SMC have begun to proliferate and migrate to form a neointima.

The progression of restenosis can be seen in the angiograms of Figure 4 of a left anterior descending coronary artery, showing restoration of patency immediately after stenting (A), and restenosis six months postoperatively (B). The stented region is boxed. The stainless steel stent itself cannot be seen as it is not sufficiently radio-opaque.

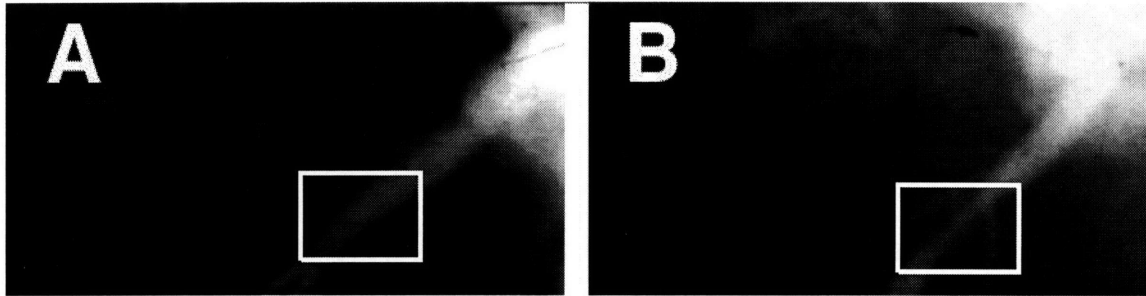


**Figure 4: Angiograms showing the progression of restenosis in a porcine LAD coronary artery immediately after stenting (A) and 3 months post-operatively (B).\***

Many experimental animal models of vascular injury and repair are used to study mechanisms underlying restenosis. One of the most common models used is injury to the iliac arteries of the New Zealand White Rabbit. We chose this model as it allowed direct visualization of the stented artery. Although this rabbit model lacks the atherosclerotic plaque, fibrosis, necrosis, and lipid pools commonly found in human diseased vessels, it does exhibit a proliferation of smooth muscle cells in the intima that restricts luminal flow and is a characteristic of human restenosis. A cross section of a stented rabbit femoral artery is shown in Figure 5 3 days and 28 days after stenting. Although the vessel was healthy before stent deployment, a neointimal cap of smooth muscle cells has formed after 28 days, appearing grossly similar to the restenosis found surrounding the stent in the human vessel in Figure 6\*.

---

\* Angiogram and human coronary photomicrograph courtesy of Campbell Rogers, M.D., Brigham and Women's Hospital, Boston, MA

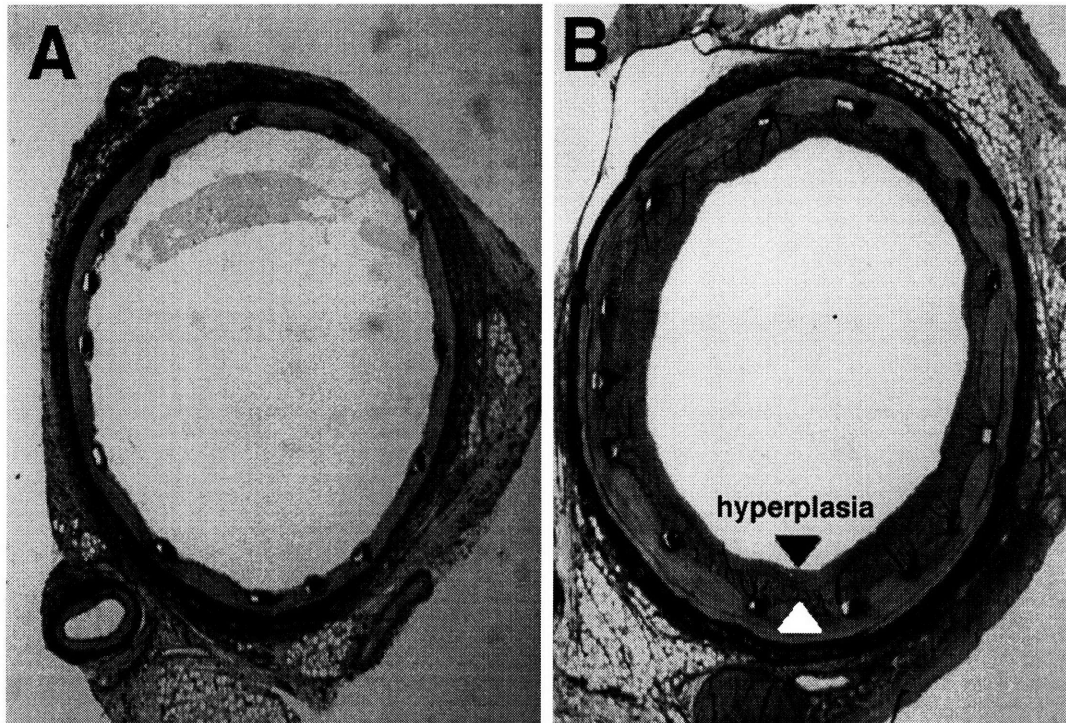


Figure 5: Pig coronary artery 3 days (A) and (B) 28 days after stenting. The decrease in luminal area from intimal hyperplasia is highlighted.

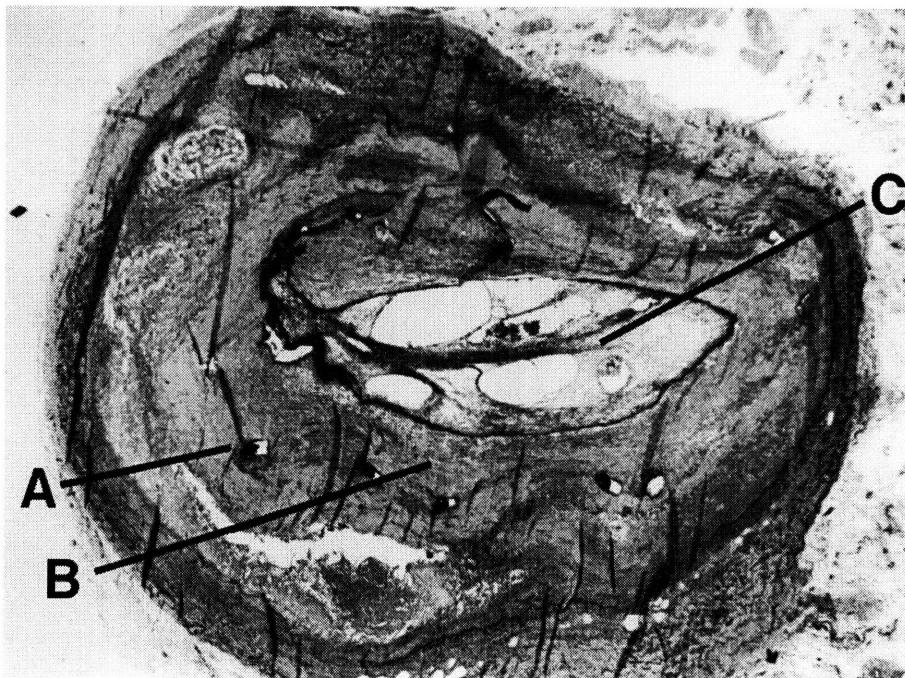


Figure 6: Human saphenous vein graft after stenting with strut legs (A), neointima (B), and lumen (C) partially occluded with postmortem thrombus. The struts are deeply embedded in a matrix of intimal smooth muscle cells formed after the deployment of the stent.

## 2.3 Mechanical bases of injury leading to hyperplasia

A new approach to understanding why neointimal hyperplasia develops after stenting comes from examining the *mechanical* events that initiate the biologic response to vascular injury, rather than the well-studied question of how the response to injury results in thrombosis, fibrosis, and hyperplasia. Three mechanical events have been shown to be closely correlated with a SMC proliferative response: compressive strain<sup>1</sup>, denudation or laceration that violates the integrity of the endothelial cell barrier or deeper layers of the vessel wall<sup>4</sup>, and changes to shear stress imparted by blood flow at the luminal surface<sup>17</sup>.

### 2.3.1 What is/is not known about mechanically-caused injury

Stent implantation causes focal mechanical injury to the vessel wall, ranging from denudation of the endothelial cell monolayer covering the interior of the lumen to progressive laceration of deeper vascular structures. Schwartz described a linear relationship between the extent of eventual restenosis and these effects. Mechanical trauma is also directly linked to hyperplasia. Imposed strain, without causing observable injury, can increase DNA production in human vascular smooth muscle cells and increased production of several potent growth factors<sup>1</sup>. The amount of injury inflicted by the stent, and therefore restenosis rates, is not only a function of the final vessel enlargement ratio but also of the stent geometry. Stents of identical weights and stent-to-vessel contact areas, etched from the same lot of stainless steel and inflated by the same

pressure to identical post-inflation diameters and differing in only in configuration produced varying amounts of deep laceration and restenosis.<sup>40</sup>

These studies raise the following questions:

- 1) What are the mechanical components of stent-induced vascular injury? Is it a function of stress, strain, direct cell injury, blood flow, ion diffusion, or an inflammatory response?
- 2) Is the injury a function of only chronic parameters (e.g. final strain distribution) or does it arise from acute mechanical trauma inflicted during stent expansion?

We have developed a method to measure the dynamic and chronic strain tensor imposed by the stent *in vivo* as a function of position along the surface of the vascular wall. These data will not only demonstrate the impact of strain but can be used to determine whether strain is responsible for the observation that different stent designs cause different amounts of injury. The ability to measure vascular strain *in vivo* lays the foundation for optimal design of endovascular implants that minimize restenosis and may provide a valuable tool for further investigation of the response of any tissue to strain.

### **2.3.2 Direct effect of strain on arterial smooth muscle cells**

Smooth muscle cells which provide the bulk of tissue in restenosis have been shown to exhibit both mitogenic and chemotactic behavior in response to an applied strain, providing a direct link between strain and restenosis. When subjected to a physiologic,

periodic stretching, cultured smooth muscle cells reorient themselves in the direction of the applied force<sup>12</sup>. Recent research by Grodzinsky demonstrated that a transient strain of 80% can also directly stimulate smooth muscle cell growth, increasing thymidine incorporation (which indicates cell replication) four-fold, and upregulating fibroblast growth factor-2 (FGF-2) production more than eight-fold<sup>1</sup>. FGF-2 has earlier been demonstrated to mediate migration and proliferation of smooth muscle cells in the intima<sup>3,13,14</sup>.

### **2.3.3 Contact abrasion/laceration**

Withdrawal of an inflated balloon catheter across the arterial surface is a well-accepted and frequently-used model of endothelial denudation. Yet even the subtle injury that occurs with the gentle rubbing of a nylon monofilament loop against the arterial wall can completely deendothelize an artery. The denudation that occurs under the considerably more forceful contact with a metal stent expanded under 8 atm of pressure will expose the underlying basement membrane and deeper layers of the blood vessel wall to potent growth factors circulating in the blood, and permit platelets to attach to newly-exposed subendothelial thrombogenic sites. These events are postulated to initiate hyperplasia, and form the most commonly cited cause of restenosis resulting from angioplasty<sup>15</sup>.

Direct stent-arterial contact is not the only means of vascular abrasion; the balloon catheter that inflates the stent also may contact the arterial lining by protruding through

the stent leg openings, or the balloon's unconstrained ends may denude if sized longer than the stent.

#### **2.3.4 Shear stress**

Endothelial cells have long been known to be sensitive to the shear stress imparted by surrounding blood flow. The shear stress in healthy human arteries varies from 2 to 20 dyne/cm<sup>2</sup><sup>16</sup>. Dewey showed in an *ex vivo* experiment that although a constant 8 dynes/cm<sup>2</sup> shear stress field did not alter endothelial cell endocytosis rates, a single *increase* from 0 to 8 dynes/cm<sup>2</sup> doubled them<sup>17</sup>. Prostacyclin production *in vivo* is even more sensitive to changes in shear, increasing from 0.004 ng/min/10<sup>6</sup> cells at rest to 2.0 ng/min/10<sup>6</sup> cells at the onset of a 16 dyne/cm<sup>2</sup> shear field<sup>18</sup>. Other aspects of endothelial behavior influenced by shear stress include intercellular fibronectin production<sup>19</sup>, membrane permeability<sup>20</sup>, and cell proliferation rates<sup>21</sup>. Large-scale mockup visualization experiments seem to demonstrate that endovascular implantation indeed induces local disruption of blood flow<sup>22</sup>, although no quantitative information has yet been obtained through *in vivo* measurements or computational modeling.

#### **2.3.5 Of these possible mechanisms, why choose to examine strain?**

While some vascular strain is clearly imposed by vasodilatation and contraction in response to internal stimuli and the natural rhythm of the cardiac cycle, these events alone do not cause neointimal hyperplasia. The strain field imparted to the artery by an



expanding stent is fundamentally different than these physiologically-derived sources, however, and we believe that it may be a significant determinant of intimal hyperplasia through both direct and indirect mechanisms.

Direct support for the hypothesis that stent-imparted strain initiates intimal hyperplasia comes from the recent discovery noted above that an imposed strain stimulates smooth muscle cell replication<sup>1</sup>. In addition, using the well-established fact that hyperplasia forms in response to vessel injury, substantial evidence exists that strain is an *indirect* determinant of hyperplasia as there are several mechanisms linking excessive strain to vascular injury. For instance, any local difference of the strain field between the artery and the expanding stent implies slippage at that point; if this occurs at sufficient inflation pressure, vascular abrasion, endothelial denudation, and subacute laceration will result. It is also known that endothelial cells are anchored to the underlying basement membrane at discrete integrin binding sites and to each other at vinculin adhesion sites<sup>23</sup>; if the underlying matrix is stretched more than the endothelial cells can distend some of the junctions joining the endothelial cells must break and compromise the integrity of the endothelial barrier. Knowledge of the strain field imposed by the expanding stent could predict through these mechanisms vascular injury and eventual hyperplasia.

## **2.4 General response of living tissue to strain**

### **2.4.1 Strain vs. stress effects**

Biological responses to mechanical injury may in general be considered as either stress-mediated or strain-mediated. Usually the material properties of the affected tissue inextricably bind applied stress to induced strain, and yet the ability to divorce these issues is fundamental, perhaps distinguishing the differing pathologies of diseases including the stress-bearing bone diseases of osteoarthritis and movement-sensitive inflammatory rheumatoid arthritis. The ability to differentiate and quantify these mechanical origins of injury *in vivo* is becoming increasingly important as the use of prosthetics and permanent implants in humans become more common. What strains are induced by these implants? Does this strain injure the surrounding tissue? And how can we reduce these effects? This thesis examines a system that determines the pattern of arterial deformation as measured by the Green strain tensor induced by a chronically indwelling vascular prosthesis, a metal stent. The knowledge of how stents dynamically expand may assist in the development of less-injuring devices and advance understanding of how vascular tissues react *in vivo* to applied strain.

### **2.4.2 The endovascular stent: an excellent model**

The endovascular stent provides an excellent model to study the effect of strain on tissue for three reasons:

- **Biological:** The stent takes strain-related effects to extremes, as at 8 atm it imparts a chronic force per unit area approximately 75 times physiologic blood pressure. By design this force approaches the maximum tolerable before structures, such as the internal elastic lamina, are observed to tear.
- **Clinical:** Stenting procedures are becoming increasingly common as a low-risk minimally-invasive alternative to more complex interventions such as coronary artery bypass grafting.
- **Analytic:** The regular geometry of many stent designs lends itself to analytic modeling, often with reduction in the order of the model because of symmetry. This makes cause-and-effect processes much more apparent than when analyzing quantities of numerical data produced by the three-dimensional finite element models that are used to model general three-dimensional force-displacements.

## 3. Strain Mensuration System

### 3.1 Introduction

We developed a method using a single camera to measure the dynamic, local Green strain tensor developed along the surface of a cylindrical wall as it deforms in an axisymmetric manner. The method was tested *ex vivo* on excised bovine coronary arteries deformed by endovascular stents to show the system's feasibility to determine *in vivo* strains. The system's accuracy was modeled with a Monte-Carlo simulation, and the results validated using a large-scale inflatable latex phantom. This chapter will focus on the strain mensuration system itself; results and implications of the *in vivo* tests will be discussed in the following chapter.

To measure the surface strain tensor over the vessel wall, a section of the artery was first marked with reference points and imaged as the luminal stent was expanded. A three-dimensional axially-symmetric parametric model of the arterial section was determined whose projection best matched each frame, and the image and its reference points were then back-projected onto this adaptive model. The back-projected reference points were then automatically grouped and analyzed to determine the

circumferential, axial, and torsional components of the strain tensor developed within each arterial subsection.

The surface strain tensor was determined in the excised bovine artery as a compliant balloon catheter was inflated to a maximum pressure of 8 atmospheres (atm) in 2 atm steps. The Green strain tensor was calculated with circumferential, axial, and torsional components ranging from  $0.00 \pm 0.10$  to  $0.70 \pm 0.10$  and a spatial resolution of 0.75 mm. The system is capable of measuring *in vivo* strains of the same magnitude with similar accuracy and spatial resolution.

## **3.2 Methods**

### **3.2.1 Experimental system**

The strain mensuration system is shown in Figure 7. The exterior of the bovine coronary was cleaned of fascia in preparation for marking. An arteriotomy was performed, and a corrugated ring stainless steel stent premounted on a 3 mm polyurethane balloon catheter (Advanced Cardiovascular Systems/Guidant) (Figure 2) was advanced into a section of the artery that had no anterior side-branches. A grid of reference marks was applied to the exterior of the artery over the region to be using a modified ink -jet printer cartridge (Cannon CJ-3A) driven by a waveform generator. Benchtop testing showed this device could form regular 50  $\mu\text{m}$  to 250  $\mu\text{m}$  marks when driven by a 24 V pulse train with a pulse-on duration from 1 to 20  $\mu\text{s}$ . For arterial marking, a 10 Hz train of 5  $\mu\text{s}$  pulses was

used to produce 150  $\mu\text{m}$  markings. After the artery was marked the stent was expanded to 8 atm of pressure, held at this pressure for one minute, and then released. The procedure was recorded with an imaging system comprised of a CCD camera (Hitachi VC-C370) and a deep-field zoom lens (Computar 18-108 mm, f2.5) with a polarizing lens to reduce glare. A VCR (Sony SLV-920) recorded the procedure, and the data was later digitized to 640x400 pixel resolution by a Raster-Ops 24XLTV frame grabber.

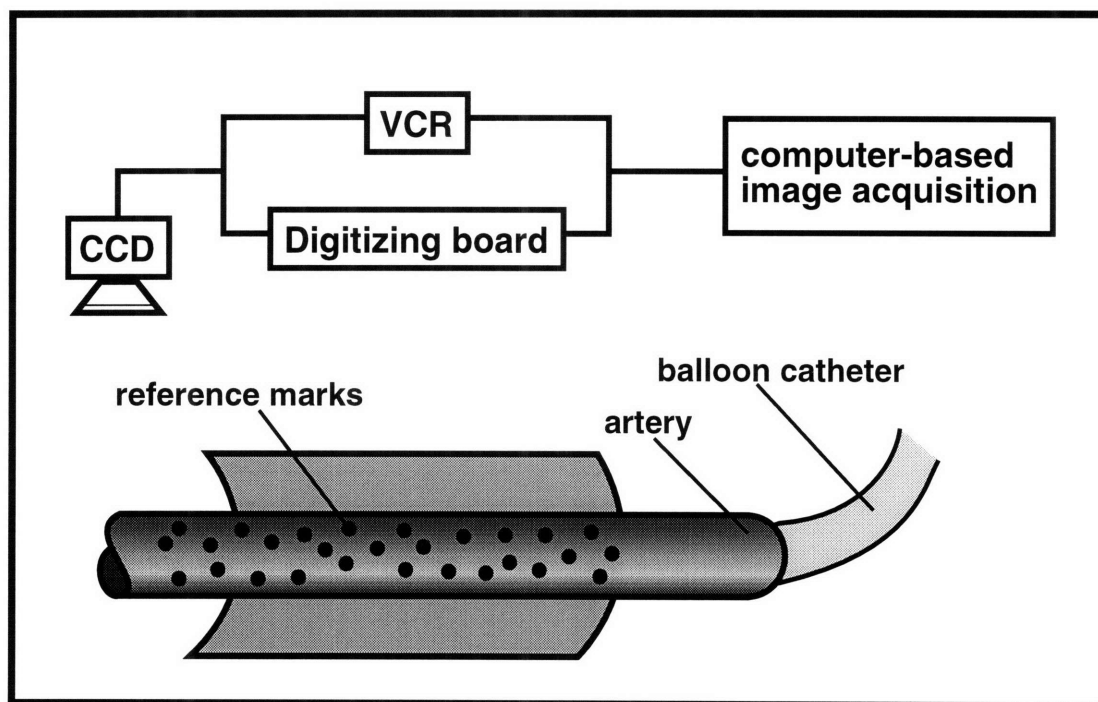


**Figure 7: Strain mensuration system consists of a computer-based image acquisition subsystem that records and analyzes a sequence of digitized video images of an artery marked with ink reference points as a stent is expanded inside the marked region.**

### 3.2.2 Theoretical

Each digitized frame represented the two-dimensional projection of the curved artery. To determine three-dimensional data from each two-dimensional frame, the artery was

assumed to be axially-symmetric; i.e. in  $\{r, \theta, z\}$  cylindrical coordinates of equation  $r = f(z)$ . The outer envelope of the vessel was digitized and a general two-dimensional quadratic equation fit to the envelope. The general quadratic equation,  $Ax^2 + Bxy + Cy^2 + Dx + Ey + F = 0$ , was chosen because of its flexibility; with few coefficients it can model two line segments that are parallel, converging (a section cut from an ellipse), or diverging (a hyperbola of two sheets). The coefficients were determined using the Nelder-Mead non-linear least-squares algorithm<sup>24</sup> implemented in the Matlab programming language. Once the two-dimensional equations describing the stent envelope were determined, their paths were swept around their longitudinal axis to create a three-dimensional axially-symmetric quadratic surface model (Figure 8). The locations of the reference marks from each two-dimensional frame were back-projected onto this three-dimensional model and the three-dimensional locations stored for strain analysis.

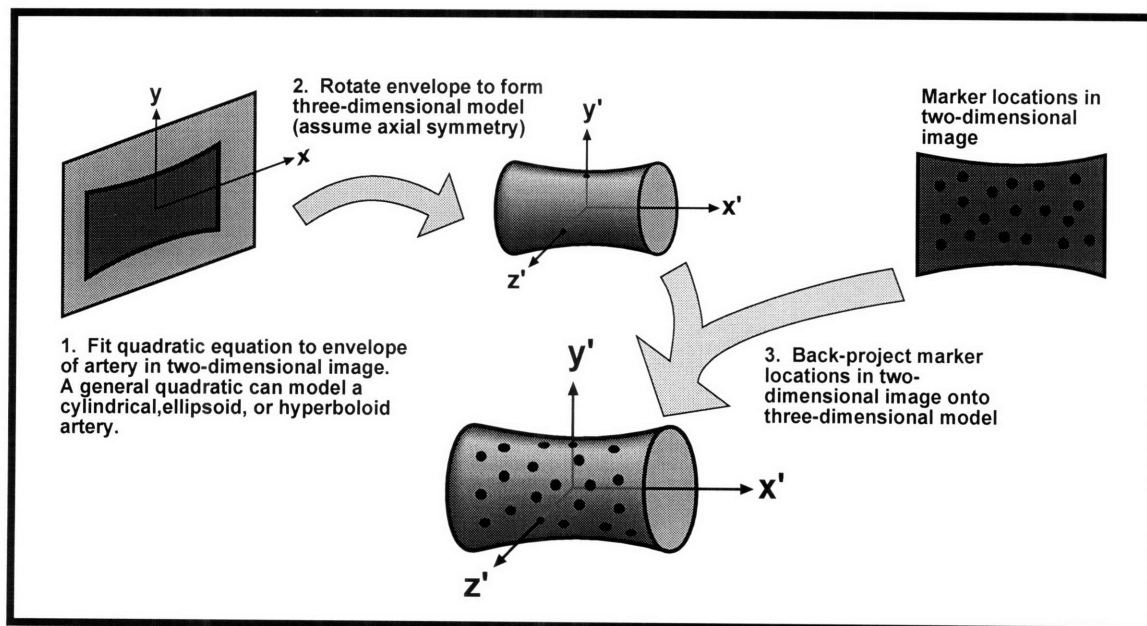


**Figure 8: Determination of three-dimensional reference point locations given a two-dimensional image of an axisymmetric surface.**

The surface strain components  $\epsilon_{\theta\theta}$ ,  $\epsilon_{zz}$ ,  $\epsilon_{\theta z}$  that exist within a uniformly-deformed, axially-symmetric membrane are derived as a function of the locations of three reference points in the undeformed and deformed states in section 3.4.1.2. To determine the strain field, triads of reference points were automatically grouped by computer under the assumption that the strain, although highly non-uniform over the length of the stent, varied in space sufficiently gradually between neighboring markers so that a good local approximation could be found using adjacent markers. The algorithm that grouped the reference points assigned a weighted score to each potential triad. A positive weight was associated with triads including points separated by an empirically-determined optimal distance. Points separated too widely average-out the locally varying tensor field and so reduce the spatial resolution of the system. Points grouped too close together suffer from a high error-to-measurement ratio caused by additive uncertainties in position. A negative score was associated with triads constraining points progressively closer to the envelope of the artery model as they generate exaggerated position measurement error because of the sensitivity of the back-projection. Once grouped, the strain tensor within each reference-point triad was determined and associated with the corresponding area on the arterial surface. Areas of the arterial surface that lacked suitable reference point triads were associated with the strain tensor from the nearest reference point triad. If the earlier assumption of axial symmetry was valid each axial slice should have the same strain tensor, independent of  $\theta$ . The strain tensor for all segments within each axial slice was



therefore replaced with the average tensor for the entire slice, and an alert was generated if any of the values varied from the average by more than 10%.

### 3.2.3 Analytical

The algorithmic grouping of reference points into triads for strain mensuration is a highly nonlinear process. Therefore we constructed a Monte Carlo simulator to determine the accuracy of the strain mensuration system using as parameters the errors introduced by back-projection, assumption of a quadratic surface, and limited resolution of the digitizing device. We verified the accuracy of the simulator by conducting an expansion of a large-scale balloon phantom, and compared the estimated error of the simulator (run with new error parameters appropriate for the phantom) with the actual error of the imaging system. The *in vivo* arterial experiment and the phantom mockup experiment were each simulated using 10,000 independent runs. Following the experimental results of Weizsacker, the phantom was constructed from a latex tube as a reasonable first-order model of an artery. We hand-marked a grid upon the phantom, and recorded data as the tube was inflated in step increments from an average diameter of 46 cm to 175 cm. After each step the tube was allowed to stabilize for 1 minute to reduce creep or other viscoelastic effects that could interfere with manual measurements, the image was digitized with a comparable field-of-view to the *in vivo* experiments, and distances between markings hand-measured to determine the true strain tensor.

### 3.3 Results

#### 3.3.1 Marking device

The ink jet marking device was successful at laying down an even grid of fine, high-contrast reference points in a moist environment. Results of *ex vivo* marking on an excised bovine coronary artery are shown in Figure 9. Note the regular mark size of 150  $\mu\text{m}$ . The artery appears light gray because the blood has been drained.

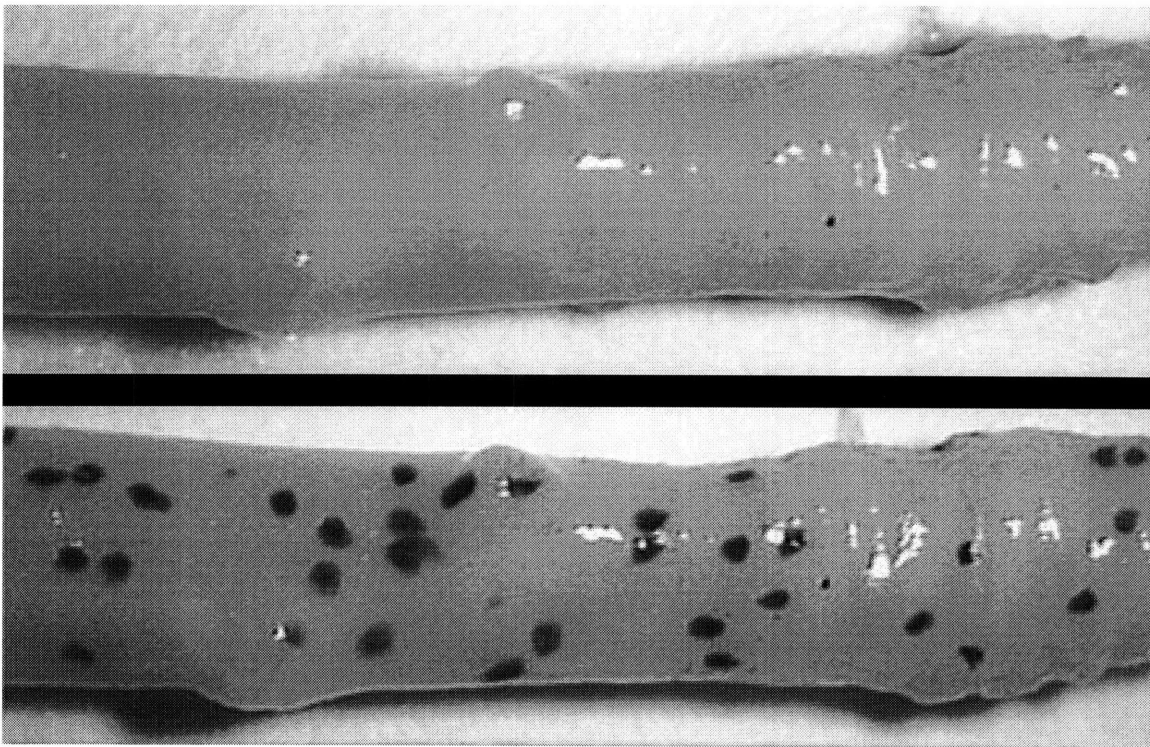


**Figure 9: Bovine coronary explant, shown in the same aspect before and after marking with the inkjet device.**

#### 3.3.2 *Ex vivo* artery segment

The surface strain tensor has three independent components which develop along the artery as both a function of location and stent inflation pressure. With no distending

pressure (0 atm) all strain components are zero as there is no deformation of the artery (upper panel of Figure 10). The lower panel is a three-dimensional reconstruction of the arterial envelope, as given by the best-fitting quadratic surface of revolution (see section 3.2.2). Only the portion of the artery directly surrounding the stent is shown.

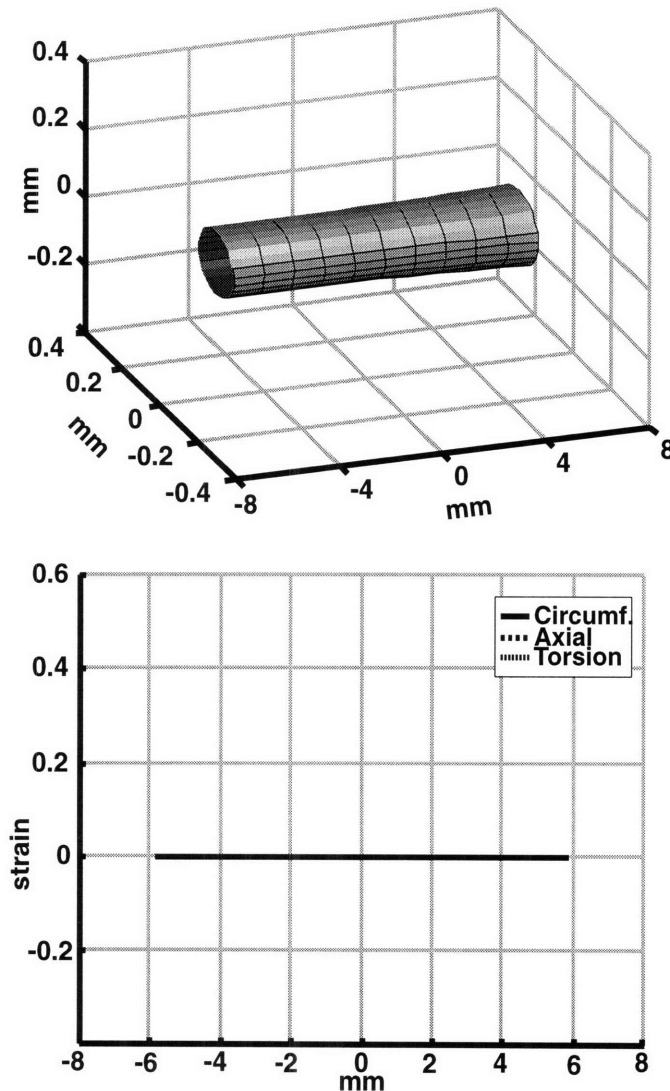


**Figure 10:** Reconstructed view of bovine arterial segment before *ex vivo* expansion (top panel). The axes represent dimensional distances in mm. The arterial surface strain tensor components are shown in the lower panel as a function of the longitudinal distance along the artery. At zero atmospheres of balloon catheter inflation pressure, all components are identically zero. Raw data is presented in Appendix A.

At 2 atm of pressure (Figure 11) the stent has not yet begun to inflate as the balloon is not yet distended sufficiently to contact the arterial wall. The reconstructed arterial surface is shown with a strip from the lower surface removed to show for comparison the original position of the artery at 0 atm. There is so little circumferential expansion at this point that both proximal and distal ends appear slightly bowed *inwards*, although this is likely measurement error since the system, as will be later derived, is not sensitive to strains less than approximately 10%.

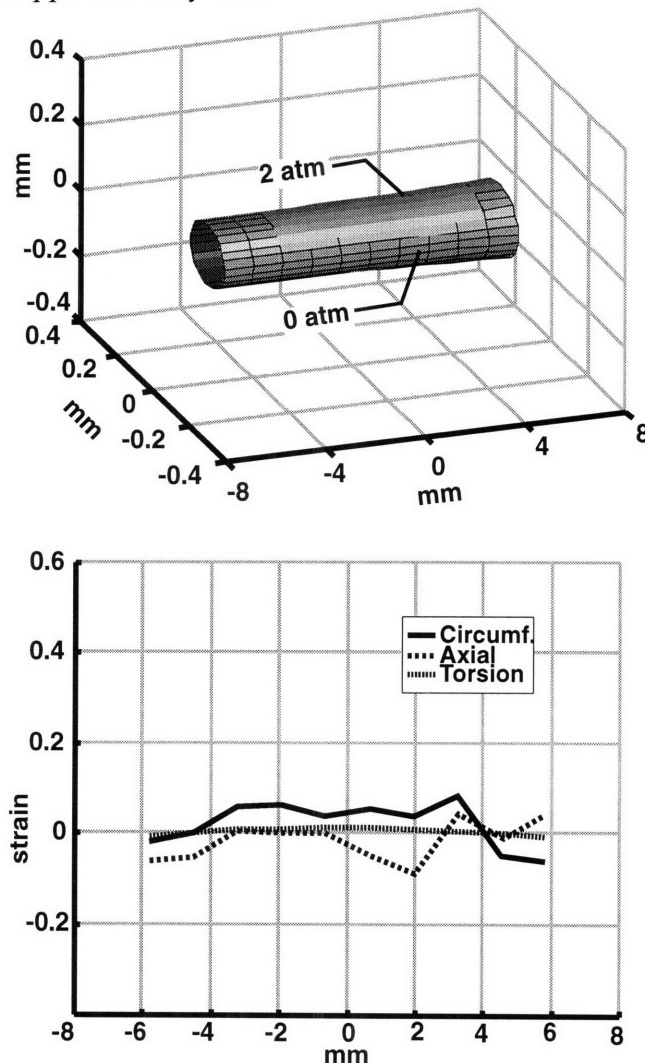


**Figure 11: Reconstructed view of bovine arterial segment before and after *ex vivo* expansion to 2 atm (top panel). The axes represent dimensional distances in mm. The arterial surface strain tensor components are shown in the lower panel as a function of the longitudinal distance along the artery. Raw data is presented in Appendix A.**

As balloon catheter pressure is increased to 4 atm the proximal (left in Figure 12) end of the stent is inflated first. The cutaway reference in the lower panel shows relatively small gain in luminal area at this pressure (compare with the cutaway of the arterial surface at 0 atm in the lower panel).

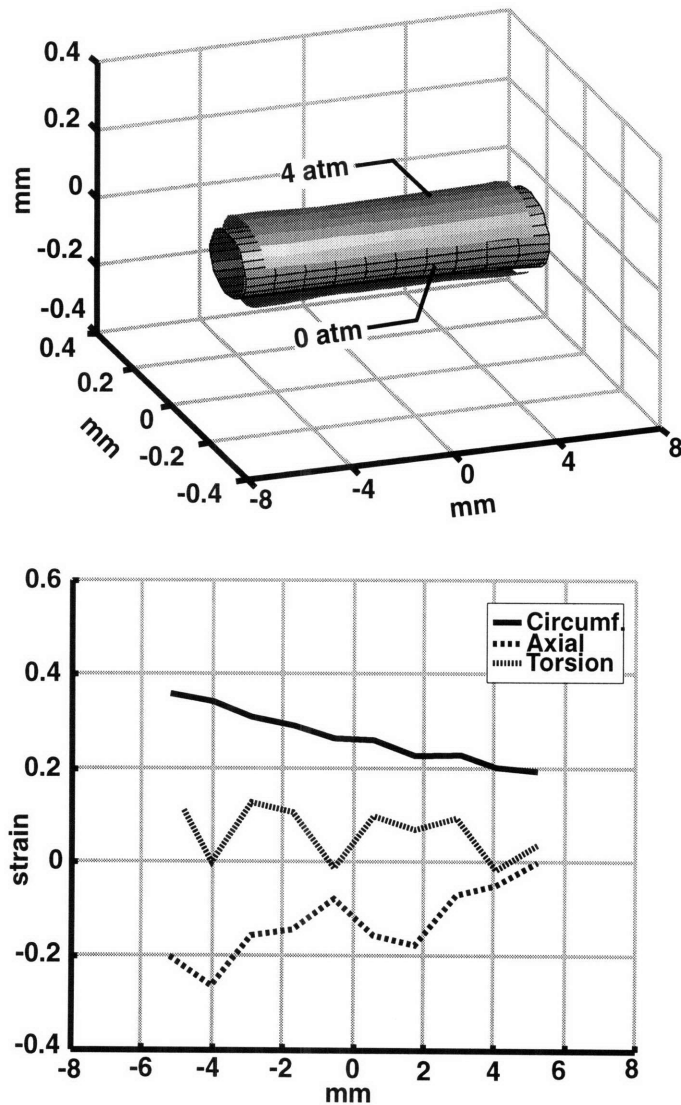


**Figure 12: Reconstructed view of bovine arterial segment before and after *ex vivo* expansion to 4 atm (top panel). The axes represent dimensional distances in mm. The arterial surface strain tensor components are shown in the lower panel as a function of the longitudinal distance along the artery. Raw data is presented in Appendix A.**

At 6 atm the proximal side opens abruptly (Figure 13), expanding by approximately 25% more than the final average circumferential strain. The axial strain has meanwhile become clearly negative, i.e. the arterial segment shortens in length as the radius increases.

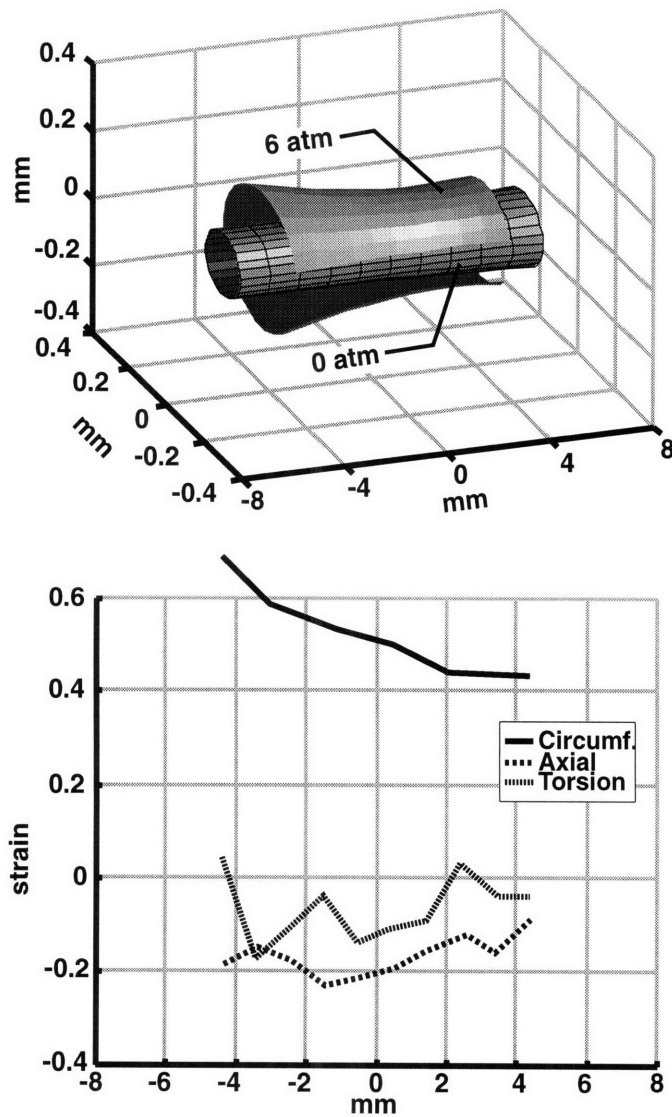


**Figure 13:** Reconstructed view of bovine arterial segment before and after *ex vivo* expansion to 6 atm (top panel). The axes represent dimensional distances in mm. The arterial surface strain tensor components are shown in the lower panel as a function of the longitudinal distance along the artery. Raw data is presented in Appendix A.

As the pressure increases to 8 atm the balloon/stent unit expands to fully contact the arterial wall along its length and the arterial surface regains a cylindrical appearance (Figure 14). The proximal end relaxes inwards, and is now slightly less open than the distal region. The low torsional component of strain indicates that twisting around the longitudinal axis has remained nearly zero throughout the expansion, although the axial component indicates a 10% to 20% contraction in length.

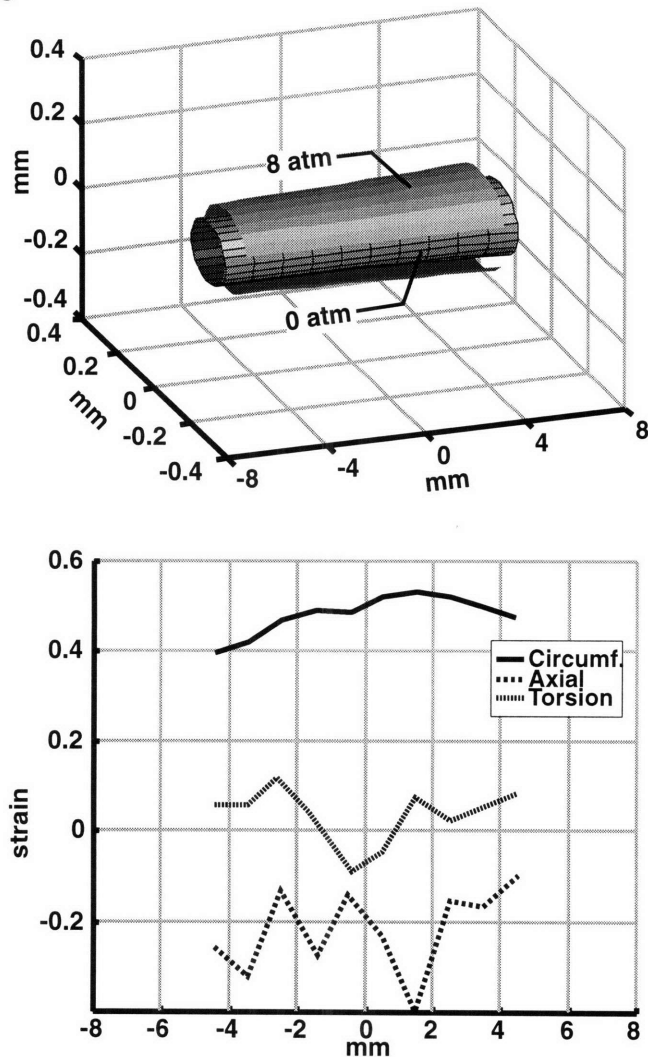


**Figure 14: Reconstructed view of bovine arterial segment before and after *ex vivo* expansion to 8 atm (top panel). The axes represent dimensional distances in mm. The arterial surface strain tensor components are shown in the lower panel as a function of the longitudinal distance along the artery. Raw data is presented in Appendix A.**

### 3.3.3 Latex phantom

In order to examine the errors inherent in the strain mensuration system we used a large-scale cylindrical latex phantom. The phantom was inflated and strain was computed both by hand-measurement (considered to be the true strain tensor for reasons given in section 3.4.3) and with the less-accurate strain mensuration system. Because the phantom was easily inflated to large volumes even at low pressures, six sets of measurements were taken at incremental steps of increasing balloon radius. The mensuration system's analysis of balloon strain for the lowest and highest pressure steps are shown below (Figure 15 and Figure 16).

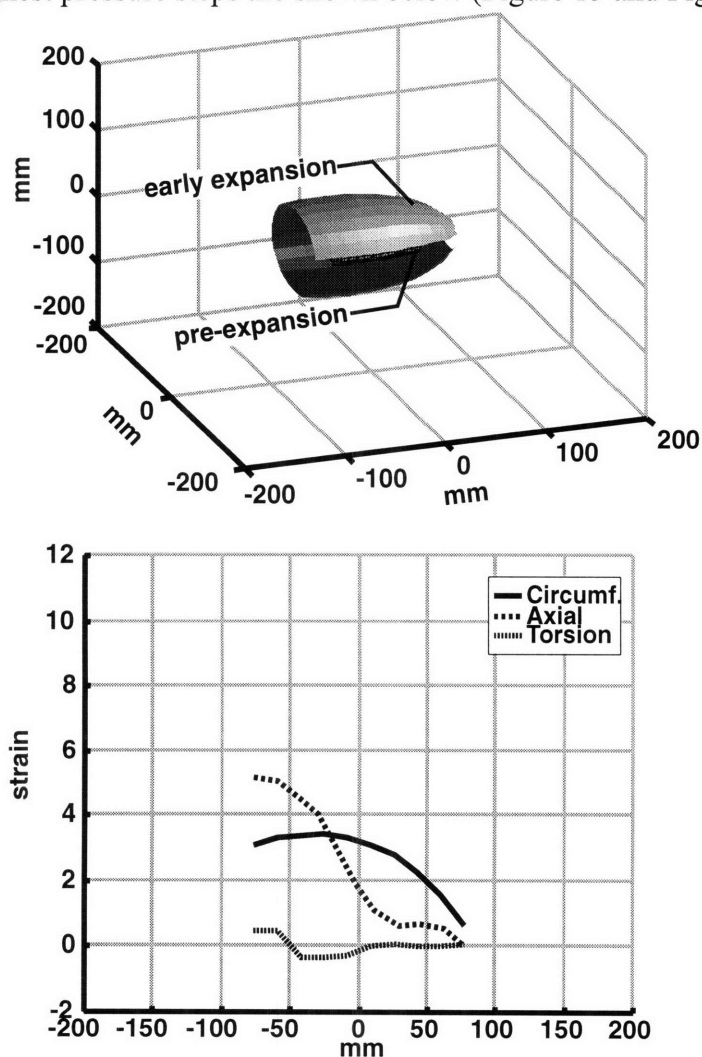


**Figure 15: Reconstructed view of phantom before deformation and at early expansion step (top panel). The axes represent dimensional distances in mm. The surface strain tensor components are shown in the lower panel as a function of the longitudinal distance along the phantom. Raw data is presented in Appendix A.**



The system tracked changes in strains correlating to 20 fold enlargements. Unlike the artery expanded with a balloon catheter inside a stent, which showed negative axial strain during circumferential enlargement, large positive increases in axial expansion occurred as the phantom increased in circumference.

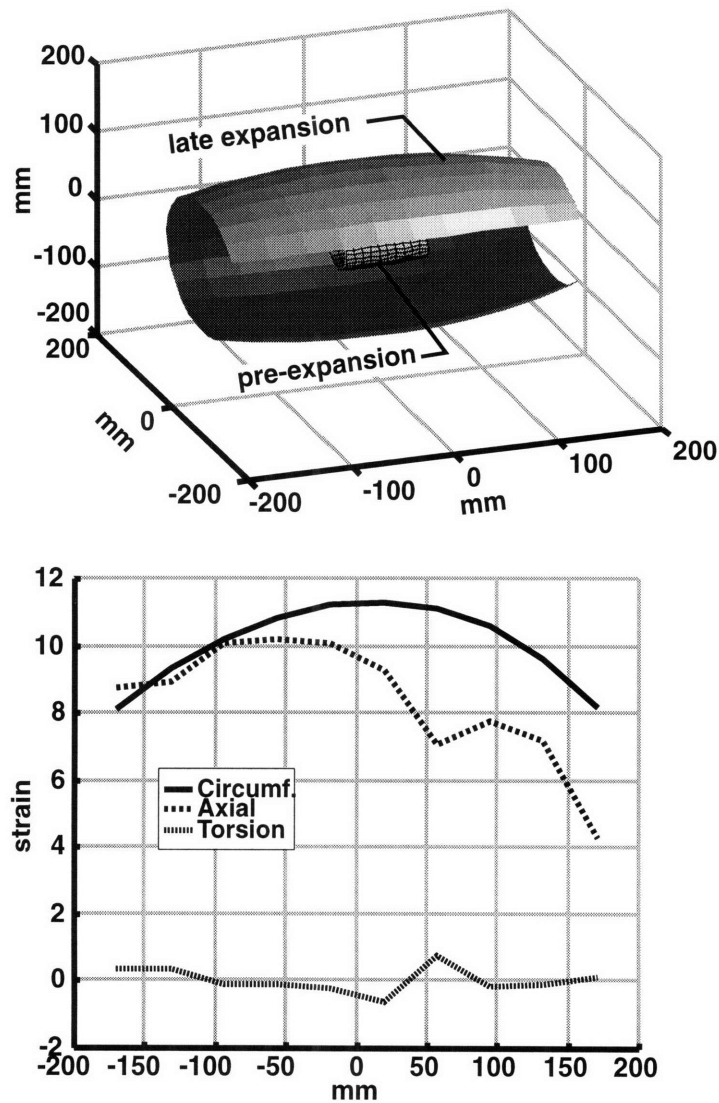


**Figure 16: Reconstructed view of phantom before deformation and at late expansion step (top panel). The axes represent dimensional distances in mm. The surface strain tensor components are shown in the lower panel as a function of the longitudinal distance along the phantom. Raw data is presented in Appendix A.**

### 3.3.4 Error simulations

Using the phantom we were able to directly measure strain on the surface and compare these results with strain calculated using digitized two-dimensional images. To determine the accuracy of the strain measurements we first measured the error introduced by the assumption that the artery is axisymmetric and has a quadratic surface of revolution.

Table I shows the average  $r^2$  values measuring goodness-of-fit of the phantom and arterial segments to their least-square-error quadratic surface. The  $r^2$  values are all nearly unity, and therefore the arterial/phantom surfaces are very nearly quadratic.

**Table I:  $r^2$  values measuring the validity of the assumption that the artery is axisymmetric and has a quadratic surface**

Phantom		Artery	
Step number	$r^2$	Pressure (atm)	$r^2$
0	0.9997	0	0.9995
1	0.9722	2	0.9995
2	0.9842	4	0.9966
3	0.9931	6	0.9942
4	0.9945	8	0.9949

System errors, defined as the difference between the strain tensor computed by the system investigated in this thesis and the strain tensor computed by direct hand-measurement, were found to be in agreement with the errors predicted by the Monte-Carlo analysis, and so validated the Monte-Carlo simulation. Figure 17 shows 25 samples of the strain-mensuration system error, as represented by filled circles. The results of 10,000 runs of the Monte-Carlo error simulator yielded three zero-mean

Gaussian curves for each of the three components of strain. The boxed areas for each strain component in Figure 17 span a symmetric distance that encompasses one-half of the area of the corresponding Gaussian curve; i.e. a randomly-chosen value of the Monte-Carlo analysis is 50% likely to be within the boxed region. A two-tailed t-test testing the likelihood that the measured error values were samples taken from a parent distribution with parameters given by the Monte-Carlo simulation yielded p values of 0.97, 0.96, and 0.94 for the circumferential, axial, and torsional components respectively. This close agreement gives us confidence in the simulation's ability to predict the magnitude of the strain-mensuration system's error.

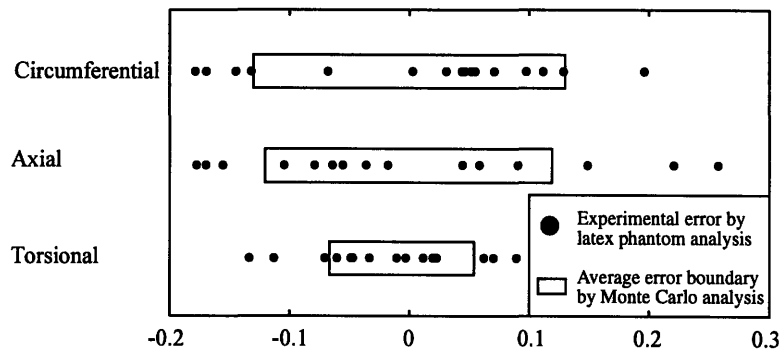


**Figure 17: Comparison of 25 samples of strain-imaging system error magnitudes from latex phantom experiments (shown by the circles) and the average error from 10,000 runs of a Monte-Carlo error simulation. Raw data is presented in Appendix A.**

New Monte Carlo simulations were then run using parameters based upon typical arterial sizes to predict the *in vivo* system errors (Table II). Because the sources of error are additive (i.e. for a given specimen and camera they are fixed and not proportional to strain), the resulting errors they cause are additive, and are therefore listed as the average of the absolute errors rather than percent error.

**Table II: Average *in vivo* errors predicted through the Monte-Carlo simulator.**

	average   error	Typical <i>in vivo</i> final strains
Circumferential	0.09	0.60
Axial	0.06	-0.20
Torsional	0.06	0.00

## 3.4 Discussion

### 3.4.1 Strain

#### 3.4.1.1 Definitions

Although there is an accepted standard measure of the scalar finite uniaxial strain  $E$ ,

$$E = (\text{initial length} - \text{final length})/\text{initial length}$$

there are several alternate definitions for multi-dimensional strain. We chose to use the

Green tensor formulation as have several other investigators of biologic strains<sup>25,26,27,28,29</sup>.

Specifically, as shown in Figure 18, the vectors  $da_i$  and  $dx_i$  connect two points before and after deformation respectively.

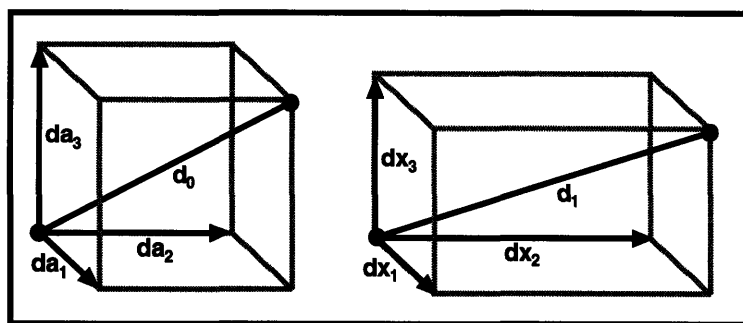


**Figure 18: Biaxial Green strain tensor**

The points are initially separated by length  $d_0$ , where  $d_0$  is the magnitude of  $da_i$ , and similarly after deformation by  $d_1$  where  $d_1$  is the magnitude of  $dx_i$ . The Green strain tensor  $E_{ij}$  is given by

$$d_1^2 - d_0^2 = 2 E_{ij} da_i da_j \quad (1)$$

The general form of the Green surface strain tensor over a tube has three unique components. As defined in cylindrical coordinates (Figure 19) these are: circumferential  $\epsilon_{\theta\theta}$  which will tend to make the cylinder increase in diameter, torsional  $\epsilon_{\theta z}$  which will tend to make the artery twist around its axis, and longitudinal  $\epsilon_{zz}$  which will tend to make the artery lengthen.

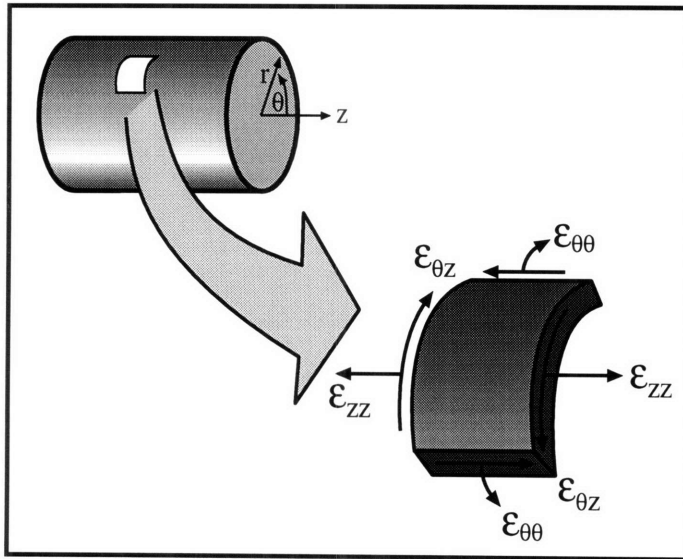


**Figure 19: The two-dimensional strain field of a tubular surface shown in cylindrical coordinates. The components  $\epsilon_{\theta\theta}$ ,  $\epsilon_{zz}$ , and  $\epsilon_{\theta z}$  are referred to in this thesis as circumferential, longitudinal, and torsional strains, respectively.**

### 3.4.1.2 Finding strain tensor from marker triads

The surface strain tensor may be calculated from the relative displacements of a marker triad. Using the cylindrical coordinates defined in Figure 19, let a surface exist in three dimensions that can be described before deformation as  $r=f(z)$  and after deformation as  $r=F(z)$  (i.e. axisymmetric). Let any differential vector  $dX_i$  exist on the surface which is deformed into vector  $dx_i$ . A deformation gradient tensor  $F_{ij}$  then exists that maps  $dX_i$  to  $dx_j$  by

$$dx_i = F_{ij} dX_j \quad (2)$$

To estimate  $F_{ij}$ , let three closely-spaced markers  $X^\alpha$ ,  $\alpha=1,2,3$  exist on a surface with components  $X_{\theta,r,z}^\alpha$  in the undeformed state which deform into points  $x^\alpha$  with components  $x_{\theta,r,z}^\alpha$ . Let the vector  $X^{\beta,\alpha}$  be directed from point  $X^\alpha$  to  $X^\beta$ , and similarly define a vector  $x^{\beta,\alpha}$  from point  $x^\alpha$  to  $x^\beta$ .

If the surface  $r=f(z)$  has the property  $dr/dz \ll 1$  (i.e. any tapering of the cylindrical surface is gradual) then the  $\theta$  and  $z$  components of  $X^{\beta,\alpha}$  will be much greater than the  $r$  component and  $X_r^\alpha$  and  $X_r^\beta$  may be replaced by  $X_r$ .  $dX_i$  and  $dx_i$  may then be approximated in local Cartesian coordinates on a plane normal to the surface, using matrix notation, as

$$dX^{\beta,\alpha} \approx \begin{bmatrix} X_r (X_\theta^{\beta,\alpha}) \\ X_z^2 - X_z^1 \end{bmatrix} \quad \text{and similarly} \quad dx^{\beta,\alpha} \approx \begin{bmatrix} x_r (x_\theta^{\beta,\alpha}) \\ x_z^2 - x_z^1 \end{bmatrix} \quad (3a,b)$$

This reduces the problem to determining the two-dimensional strain components in the Cartesian coordinate system. This transformed problem has been examined by several research teams. The remainder of this derivation follows from McCullough (28):

Substituting (3) into (2) yields

$$\begin{bmatrix} x_r(x_\theta^{\beta,\alpha}) \\ x_z^2 - x_z^1 \end{bmatrix} = \begin{bmatrix} F_{\theta\theta} & F_{\theta z} \\ F_{z\theta} & F_{zz} \end{bmatrix} \begin{bmatrix} X_r(x_\theta^{\beta,\alpha}) \\ x_z^2 - x_z^1 \end{bmatrix} \quad (4)$$

Replacing the  $(\beta, \alpha)$  pairs in equation (4) with marker pairs (2, 3a) and (2, 3b) yields four linear equations which may be solved as follows for the components of  $F_{ij}$ :

$$\begin{bmatrix} F_{\theta\theta} & F_{\theta z} \\ F_{z\theta} & F_{zz} \end{bmatrix} = \begin{bmatrix} aD - bC & bA - aB \\ cD - dC & dA - cB \end{bmatrix} \frac{1}{AD - BC}, \text{ where}$$

$$\begin{aligned} A &= X_r(X_\theta^2 - X_\theta^1) & a &= x_r(x_\theta^2 - x_\theta^1) \\ B &= X_r(X_\theta^3 - X_\theta^1) & b &= x_r(x_\theta^3 - x_\theta^1) \\ C &= X_z^2 - X_z^1 & c &= x_z^2 - x_z^1 \\ D &= X_z^3 - X_z^1 & d &= x_z^3 - x_z^1 \end{aligned}$$

The strain tensor E is then found by the relation

$$E = (F \cdot F^T - I) / 2 \quad (5)$$

### 3.4.2 How others have measured tissue strain

The determination of surface strains in low-modulus biological materials is not a new problem, and recent advances in imaging and computation systems have made several new

measurement methods possible. Large deformations experienced by compliant tissues favor the use of non-contact systems that image tissue-bound markers using a variety of media, including: visible<sup>26,27,28</sup>, infrared<sup>30</sup>, and ultraviolet light<sup>31</sup>, ultrasound<sup>32</sup>, x-rays<sup>29,33</sup>, and phase-contrast magnetic-resonance<sup>34</sup>.

It is difficult to non-invasively measure arterial wall distention *in vivo* because the material properties are similar to that of the surrounding tissue, and arteries lack suitably-distributed reference markers. Magnetic-resonance imaging has been used to determine the elastic deformation in tendons with promising results *ex vivo*<sup>34</sup>, although its applicability to vessel-wall measurements is limited by its requirement for two easily-imaged end points. Ultrasonic imaging techniques can take advantage of naturally-occurring speckles as reference points, and have been used *ex vivo* to find biaxial (circumferential and longitudinal) surface strains over complex surfaces<sup>32</sup>. Because of the large number of potential markers this method has also been used to determine the locally-varying strain as a function of position. This technique is best used to analyze small strains because the speckles change appearance significantly as they move. Experiments involving latex phantoms show that the lowest measurement error of uniaxial strain occurs only for displacements near  $100\mu\text{m}$ <sup>35</sup>. The error grows rapidly on either side of this boundary, rendering the method incapable of measuring displacements greater than  $150\mu\text{m}$ .



The most common method used to measure strain in compliant tissues involves marking the specimen before optically imaging the displacement. Water-insoluble ink has been directly applied to larger specimens<sup>36</sup>. Smaller surfaces, such as arteries, have been sprayed with ink using the bristles of a toothbrush<sup>27</sup> to achieve the small sizes needed (~20 $\mu$ m). Others have used small, inert particles such as vanilla-bean pieces pressed into the specimen surface<sup>37</sup>, fluorescently-labeled microspheres<sup>31</sup>, or strips glued to the tissue<sup>33</sup> to achieve the high-contrast needed to accurately identify the markers amidst the visual noise of ambient glare and irregular surface of moist tissue. A novel system that measures strain in real time uses small steel bearings glued to the specimen<sup>38</sup>, although visual noise limits its *in vivo* utility. More invasive methods may yield greater accuracy but by their nature alter the very tissue being studied. Bogen<sup>30</sup> was able to obtain extremely precise *ex vivo* measurements, on the order of 200 $\mu$ m, by piercing thin strips of tissue with illuminated fiber-optic strands, and Waldman<sup>29</sup> embedded radio-opaque markers into the left ventricle wall to gain 3D displacement information.

These techniques are summarized in Table 1. The *axes* column refers to whether uniaxial (e.g. longitudinal) or biaxial (e.g. longitudinal, circumferential, and torsional) information is acquired. The *flat surface* column indicates whether the method is restricted to measuring strain developed in a planar field-of-view, or can be used over a curved surface. The number of cameras required is listed in the *cam* column. Note that all optical imaging systems require two cameras to extract strain information over non-flat surfaces.

**Table III: A comparison of strain-imaging methods used in highly-compliant materials**

Investigator	Site	Illumination	Marker	Axes	Flat?	Cam	Note
Barbee	<i>ex vivo</i>	ultraviolet	fluorescent microspheres	2D	yes	1	
Bogen	<i>ex vivo</i>	infrared	fiber optic cable pushed through specimen	2D	yes	1	
Downs	latex model	visible light	glued steel bearings	2D	yes	1	1,2
Drace	<i>ex vivo</i>	MRI	tendon-bone interface	1D	yes	NA	
Fung	<i>ex vivo</i>	visible light	ink sprayed from toothbrush bristles	2D	yes	1	
Hoffman	<i>in vivo</i>	ultraviolet	resin chips affixed with grease	2D	yes	1	
Hsu	latex model	visible light	"markers affixed to specimen"	2D	no	2	3
Humphrey	<i>ex vivo</i>	visible light	vanilla-bean fragments glued	2D	yes	1	
McCulloch	<i>in vivo</i>	visible light	sutured crosses	2D	no	2	
Ryan	latex model	ultrasound	silica particles suspended in gel	2D	yes	1	
Skovoroda	latex model	visible light	marked ink dots	2D	no	2	4
Vito	<i>ex vivo</i>	visible light		1D	yes	1	5
Waldman	<i>in vivo</i>	x-ray	radio-opaque implants	3D	no	NA	
Weizsacker	<i>ex vivo</i>	visible light	marked ink dots	2D	yes	1	
Yin	<i>in vivo</i>	x-ray, vis. light	infused radio-opaque dye	1D	yes	1	

Notes:

1. System successful on rubber phantom; did not work correctly when used on *ex vivo* specimen
2. Automatically measured in real-time; up to 30Hz refresh rate
3. Used FEM to fit parameters for single and bilayer arterial cross-section to data
4. Measured local strain as a function of position for heterogeneous specimens.
5. Measured strain on face and width of slab cut from artery wall to determine bilayer constitutive parameters

Characterizing the locally-varying strain field imparted by an expanding stent to an artery *in vivo* has two unique constraints not addressed by the above techniques. First, although it is necessary to track the two-dimensional locations of arterial markers over the curved arterial surface *in vivo*, the surgical incision required to expose the artery for imaging

without altering its *in vivo* orientation and environment is deep and narrow which makes a multiple-camera approach impractical. Second, the strain field tensor varies along the length of the stent, and so must be determined locally as a function of position along the artery. The single-camera with arterial modeling approach used in this thesis is the first reported method capable of measuring the complete three-dimensional vascular strain tensor *in vivo* without damaging the vessel wall.

### 3.4.3 Error Analysis

The primary sources of error in the computed strain tensor (henceforth called calculated strain) are measurement inaccuracies caused by the limited resolution of the digitized image. Figure 11 shows that a surprisingly small component of error is derived from the assumptions that the artery is axisymmetric and fits the quadratic envelope of a cylinder, elliptical section, or hyperboloid. These assumptions contribute less than 10% of the measurement error caused by the limited resolution of the digitizing camera. Quantization error occurring during digitization is difficult to reduce. Although increasing the magnification to make the stented region completely fill the field of view of the camera would decrease this error, motion between the camera and stent from natural cardiac and respiratory cycles, and movements of the catheter during inflation make this difficult *in vivo*.

To validate the Monte-Carlo analysis of error we compared its simulated error distribution with sample system errors taken from a large-scale latex mockup. We chose

to use a large-scale mockup so we could accurately hand-measure the distance between markers, avoiding the need to back-project the points onto a mathematical three-dimensional model to prevent the effects of axial asymmetry and a non-quadratic envelope from influencing the strain-tensor measurement. Further, by hand-measuring the distances between markers on the large-scale mockup we eliminated errors from the limited resolution of the digitizing camera. Because the only source of error remaining stems from measurement inaccuracies, and this is less than 10% of the measurement error due to the limited resolution of the camera, we considered the strain tensor computed from the hand-measured inter-marker distances to be the true strain tensor.

The errors predicted by the Monte-Carlo simulation were in consonance with the differences between the hand-measured and computer-analyzed strain tensor, validating the Monte-Carlo simulation (Figure 17). The results of Monte Carlo simulations run using parameters based upon typical arterial sizes to predict the *in vivo* system errors show that axial and torsional strains greater than 0.12 and circumferential strains greater than 0.18 must be present to be reliably detected. Because the sources of error are additive (i.e. for a given specimen and camera they are fixed and not proportional to strain), the resulting errors they cause are additive, and therefore are defined as confidence bounds rather than percent error.

#### **3.4.4 Spatial resolution**

The strain tensor computed as a function of three specific markers represents the average strain experienced within that marker triad. The system's spatial resolution, or ability to localize changes in strain, is therefore limited to the average distance between these markers. We chose to examine marker triads separated by 0.75-1.0 mm which struck a reasonable balance between spatial resolution and the effect of digitization error on strain measurement accuracy. This spatial resolution allows us to examine macroscopically how vascular implants expand and move, although it does make the system insensitive to large changes in strain over a short distance such as might occur in the immediate vicinity of a 0.25 mm strut. The spatial resolution of 0.75-1.0 mm is largely limited by the choice made to envision changing patterns of strain over the surface of the entire stented region. Smaller reference marks would permit a proportionally finer spatial resolution, but would also require an expensive high-resolution camera to digitize this information over the length of the stent and custom deep-field optics to maintain focus over the curved arterial section.

#### **3.4.5 Luminal strain in the thick-walled artery model**

Although many biological interactions take place after stenting on the interior luminal surface, the strain mensuration system described in this thesis measures the strain on the exterior arterial surface. These strain tensors need not be equal. Arteries, such as the ones examined in this thesis, that are axisymmetric and do not experience torsional strain

have different circumferential components of strain on their exterior and luminal surfaces after deformation as derived below.

If  $R_0$  and  $r_0$  are designated the respective outer and inner radii of a cylindrical artery before stent expansion, and the exterior arterial surface has two reference marks separated by angle  $\theta$  and length  $l_0$ , and after an  $\epsilon_{\theta\theta}$  axisymmetric expansion,  $R_1$  and  $r_1$  are the new exterior and interior radii with the reference marks separated by length  $l_1$  at the same angle  $\theta$ , then by the definition of strain,

$$\epsilon_{\theta\theta \text{ exterior}} \equiv \frac{l_1^2 - l_0^2}{l_0^2} = \frac{(R_1\theta)^2 - (R_0\theta)^2}{(R_0\theta)^2} = \frac{R_1^2 - R_0^2}{R_0^2} \quad (6)$$

and similarly,

$$\epsilon_{\text{interior}} = \frac{r_1^2 - r_0^2}{r_0^2} \quad (7)$$

Based on the findings of Choung<sup>39</sup> the vessel wall is assumed incompressible, and therefore the area remains the same after expansion:

$$\begin{aligned} A &= \pi R_0^2 - \pi r_0^2 = \pi R_1^2 - \pi r_1^2 \\ r_1^2 &= R_1^2 - R_0^2 + r_0^2 \end{aligned} \quad (8)$$

Substituting (8) into (7) and simplifying into terms of (6) yields

$$\epsilon_{\text{interior}} = \epsilon_{\text{exterior}} \left( \frac{R_0}{r_0} \right)^2 \quad (9)$$

Thick-walled human coronaries may therefore be subjected to far greater luminal strain for a given measure of external wall strain than thin-walled arteries.

### 3.5 Summary

This computerized system is the first described that can potentially be used to determine *in vivo* how a surface strain tensor varies both as a function of distance and time. Strains must be axisymmetric, to allow three-dimensional information to be extracted from a single camera, and large, to overcome measurement error amplification that is inherent in the process of back-projection. A knowledge of how local surface strain varies with time can be used to explore and characterize the dynamics of endovascular implant expansion. This may provide a mechanical basis of understanding for the observation that different designs of implants impart varying degrees of injury to the vascular wall<sup>40</sup>, and assist in the rational development of a less-injuring device.

Although applied here to measurement of stent-induced vascular strain, the method can be used to quantify changes in external geometry for any axially-symmetric structure, such as measuring *in vivo* peristaltic intestinal movements.

Using endovascular implants as devices that impart extreme levels of chronic strain, the ability to measure *in vivo* strain may also help answer fundamental questions about the causes of and responses to vascular injury.

## 4. *In vivo* vascular strain induced by the expanding endovascular stent

### 4.1 Introduction

The strain mensuration system developed in the previous chapter was applied *in vivo* to determine the surface strain tensor induced by the expanding endovascular stent in a rabbit model. The following questions were explored:

- How do balloon-expandable stents inflate *in vivo*? Are any gross behaviors visible such as rotation or uneven expansion? Are *in vivo* tests necessary or do benchtop experiments yield the same results?
- Do the stents abrade the vascular wall during inflation through mechanical contact? Is this an important contributor of superficial/deep injury and ultimately neointimal hyperplasia?
- Can any abrasion present be reduced through catheter choice or redesign, stent choice or redesign, or operator technique?



## 4.2 Methods

New Zealand rabbits were anesthetized with ketamine and xylazine, and their femoral arteries were exposed and cleaned of fascia in preparation for marking. A black plastic cradle with registration marks was placed underneath the artery to improve contrast of the arterial envelope and provide a length scale. An arteriotomy of the femoral artery was performed, and a multilink stent (ACS, Figure 2) was inserted on a compliant polyurethane angioplasty catheter (ACS) to a position in the femoral artery approximately 2 cm cranial to the incision (Figure 20).

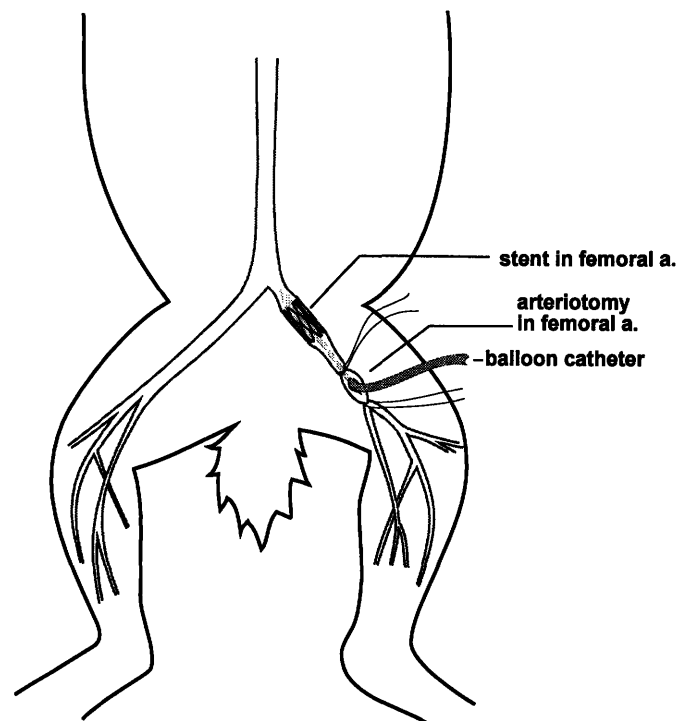


**Figure 20: Stent placement in the rabbit femoral artery**

A grid of 150  $\mu\text{m}$  marks were next inscribed upon the surface of the artery over the stented region using the ink-jet printer cartridge discussed in the previous chapter. Figure 21 shows the results of this marking technique *in vivo* on the rabbit femoral artery.

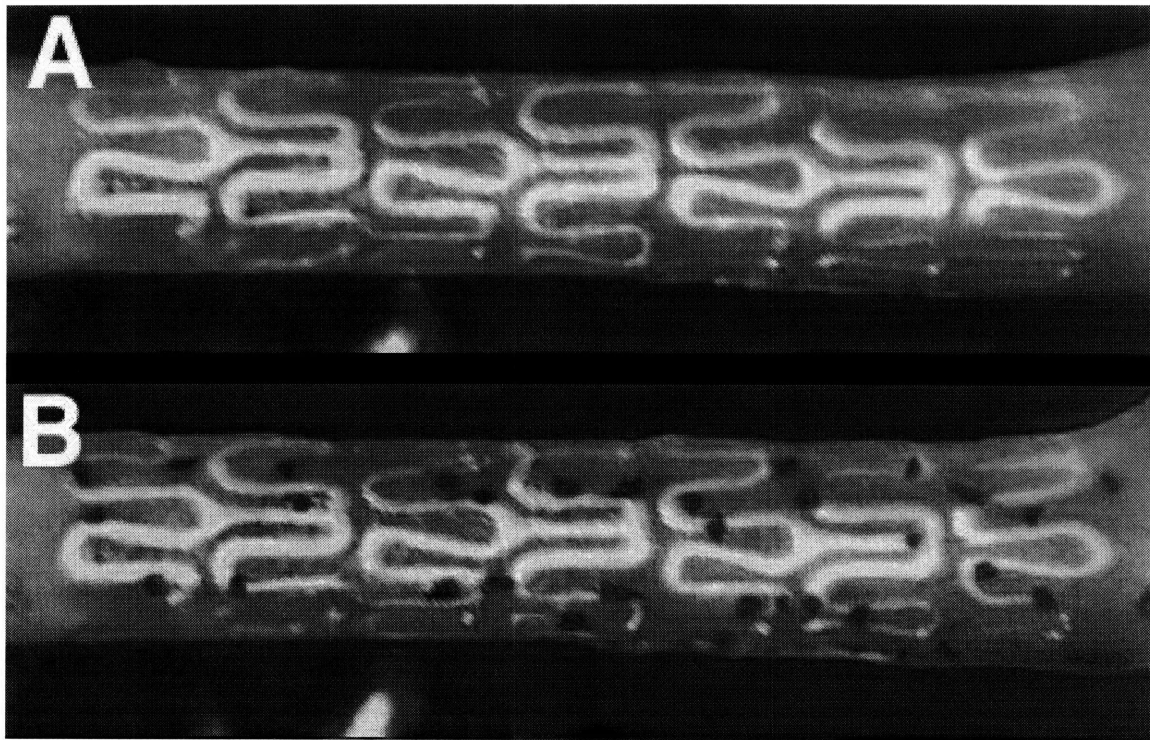


**Figure 21: Rabbit femoral artery shown in the same aspect before (A) and after (B) *in vivo* marking**

After the artery was marked the stent was expanded in 2 atm increments to 8 atm of pressure, held at maximum pressure for one minute, and released. The procedure was recorded and digitized using the same data acquisition system described in Figure 7 of the previous chapter with a polarizing lens added to the camera lens to reduce glare. As with the *ex vivo* experiments, a frame-by-frame three-dimensional mathematical model of the artery was then reconstructed using the assumption of axial symmetry, and the positions of the reference marks were back-projected onto this model. These marks were then automatically grouped and analyzed to determine the circumferential, axial, and torsional components of the strain tensor developed within each arterial subsection for each frame in time.

## 4.3 Results

### 4.3.1 *In vivo* strain components 2 to 8 atm

The strain tensor of the vessel surface as the stent was inflated to 2 atm of pressure is shown in Figure 22. As derived in the previous chapter, the accuracy of the strain measurements is  $\pm 0.10$ , and so no readings at this pressure are significant. As in the *ex vivo* case shown in Figure 11, the stent has not yet begun to expand at 2 atm.

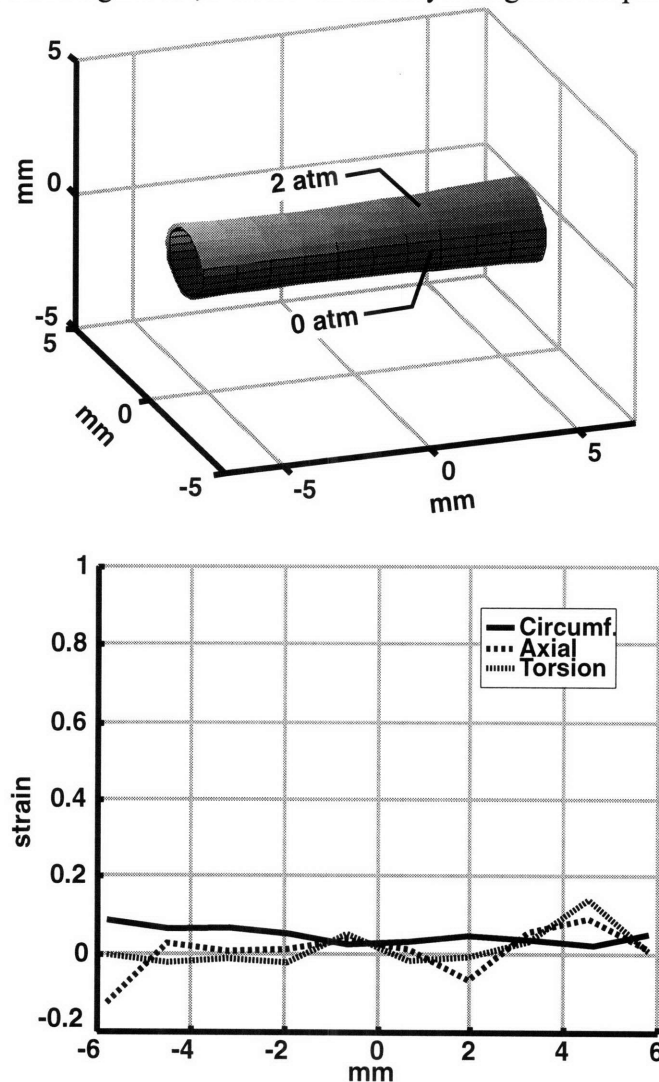
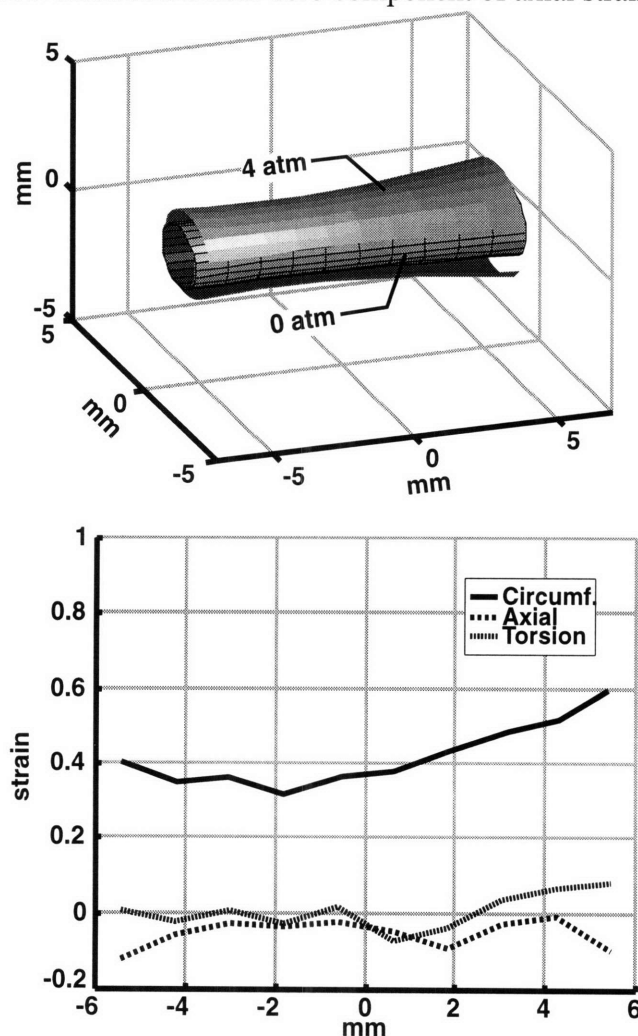


Figure 22: Reconstructed view of rabbit femoral artery segment before and after *in vivo* expansion to 2 atm (top panel). The axes represent dimensional distances in mm. The arterial surface strain tensor components are shown in the lower panel as a function of the longitudinal distance along the artery. Raw data is presented in Appendix A.

At 4 atm (Figure 23) the stent has begun to enlarge circumferentially, with the proximal (right) side to the catheter inflating first. As with the *ex vivo* data, the right panel shows the original unexpanded arterial surface in cutaway. Note that the proximal edge has inflated approximately 50% more than the center, and that both proximal and distal ends experience greater luminal gain than the center. The stent appears here shorter than at 0 atm because the surface is flared outwards at each end, making a shorter projection onto the axis of symmetry. The curved proximal-to-distal distance measured along the stent surface would reveal no change in length, as revealed in the near-zero component of axial strain.



**Figure 23: Reconstructed view of rabbit femoral artery segment before and after *in vivo* expansion to 4 atm (top panel). The axes represent dimensional distances in mm. The arterial surface strain tensor components are shown in the lower panel as a function of the longitudinal distance along the artery. Raw data is presented in Appendix A.**

As the pressure continues to rise the middle of the stent continues to enlarge (Figure 24).

Note that the stent has begun to contract in the axial direction, again similar to the *ex vivo* results.

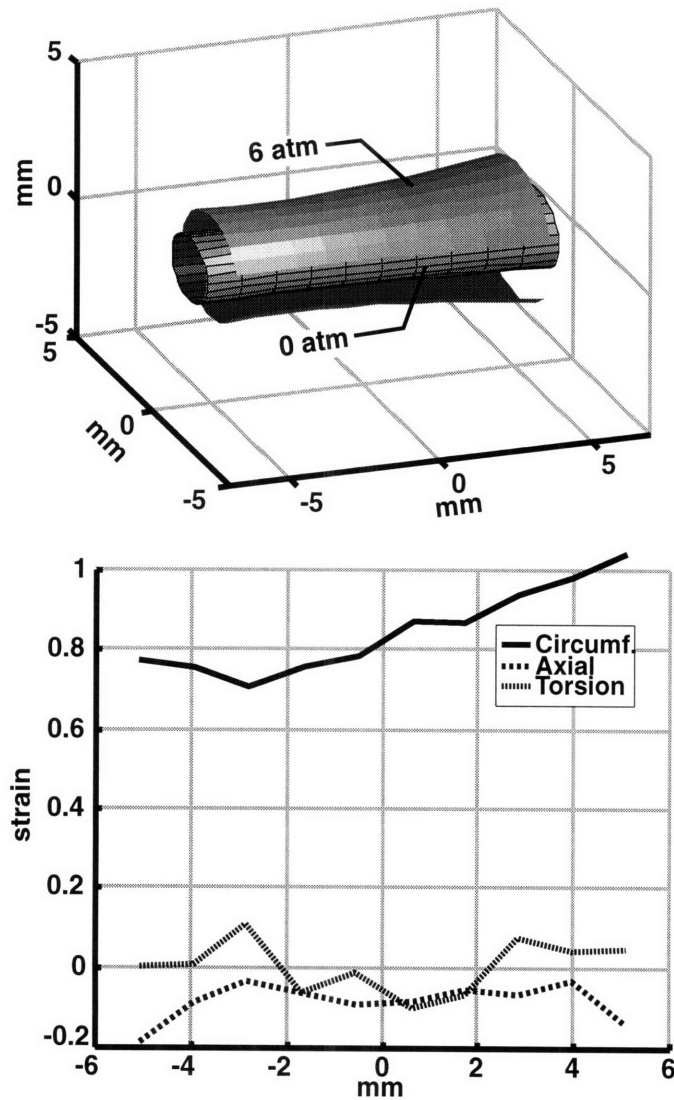


**Figure 24:** Reconstructed view of rabbit femoral artery segment before and after *in vivo* expansion to 6 atm (top panel). The axes represent dimensional distances in mm. The arterial surface strain tensor components are shown in the lower panel as a function of the longitudinal distance along the artery. Raw data is presented in Appendix A.

At the final inflation pressure of 8 atm (Figure 25) the center of the stent has risen to within 5% of the radius of the edges (corresponding to 10% of the circumferential strain, since the stent approximately doubled in diameter). In clinical practice, the stent would be further straightened with a high-pressure, low compliance balloon catheter. As the center of the stent completed its circumferential expansion it contracted 20% axially.

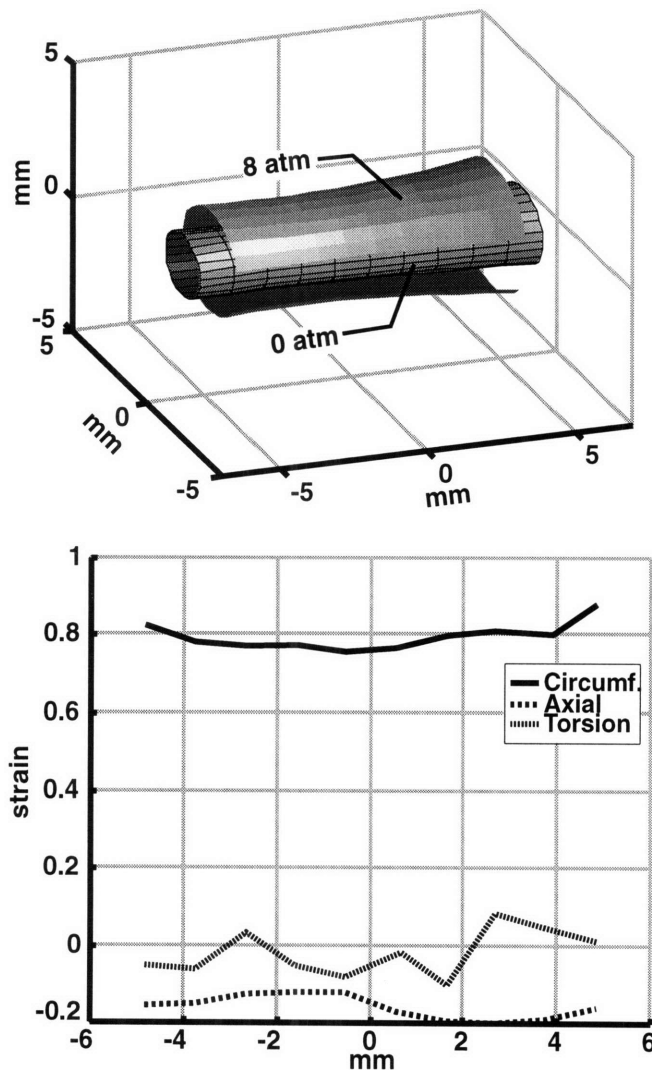


**Figure 25: Reconstructed view of rabbit femoral artery segment before and after *in vivo* expansion to 8 atm (top panel). The axes represent dimensional distances in mm. The arterial surface strain tensor components are shown in the lower panel as a function of the longitudinal distance along the artery. Raw data is presented in Appendix A.**

### 4.3.2 Pressure-differential strain

Another method of viewing the expansion data is to show the change in strain for a given change of pressure. Because strain measurements have limited accuracy, this method requires pressure steps larger than 2 atm to yields significant results; Figure 23 shows the change in the strain tensor as pressure is increased from 0 to 4 atm (which is the same as the absolute 4 atm strain tensor), and Figure 26 shows the change in the strain tensor as pressure is increased from 4 to 8 atm. Notice the locations of the greatest circumferential expansion mirror the locations of greatest axial contraction, both appearing largest at the ends of the stent. In contrast, from 4 to 8 atm the stent experienced the largest circumferential gains in the center, accompanied by a similar axial contraction.

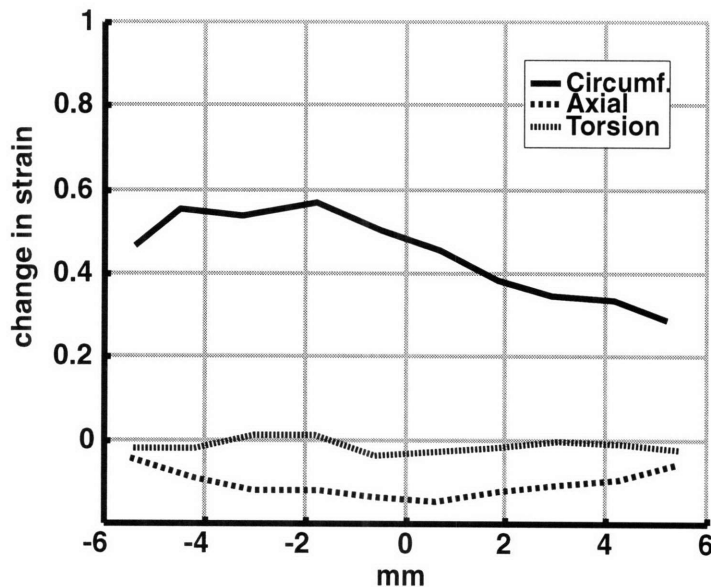


**Figure 26: Change in the strain tensor within stented rabbit femoral artery as balloon catheter pressure is increased from 4 to 8 atm, shown as a function of the longitudinal distance along the artery. Raw data is presented in Appendix A.**

## 4.4 Discussion

### 4.4.1 The dogbone effect

The hyperboloid dogbone shape that the stent transiently exhibits as it expands may contribute to both acute superficial and deep injury that later leads to narrowing of the lumen through neointimal hyperplasia.

#### *4.4.1.1 Proposed mechanism - existence depends only on stent/balloon length, not on material properties*

The stent is mounted on a slightly longer balloon catheter in order to ensure complete circumferential expansion along the length of the stent. Benchtop experiments indicate the following chain of events leading to a fully-deployed stent:

1. The proximal and distal ends of the balloon, unconstrained by the overlying stent, begin to inflate first as the applied pressure reaches approximately 4 atm.
2. Likewise, the stent begins expansion at its proximal and distal regions first. The ends begin to expand suddenly, with either end equally likely to rise first (Figure 27).

The proximal and distal ends of the stent contact the covering artery as two rings might, while the middle region remains comparatively uninflated.



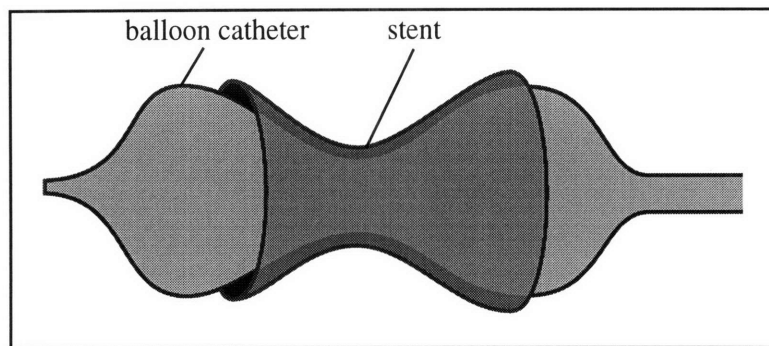


**Figure 27: Both stent (dark gray) and balloon (light gray) open end-first at approximately 4 atm of pressure (shown without artery).**

3. As the pressure increases the center of the stent circumferentially expands with concomitant axial contraction. This contraction along the axis pulls the flared stent edges inward, mechanically scraping the arterial wall under high pressure and causing superficial and deep vascular injury (Figure 28).

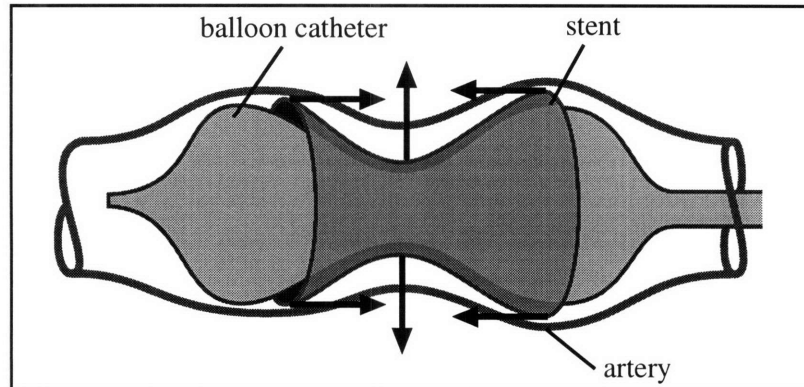


**Figure 28: As the center of the stent opens under the force of the balloon catheter, the stent and surrounding artery contracts axially.**

4. The center of the stent expands to the same diameter as the distal and proximal ends. The stent struts are fully opposed along the length of the device, and the only evidence that the transient dogbone occurred is in the injury that the arterial wall has sustained.

It is important to note that while the balloon pressure at which the stent begins to dogbone is dependent on the material properties of the stent, balloon, and artery, the *existence* of dogbone injury is not. Dogbone injury will occur whenever the ratio of balloon length to stent length is greater than one.

#### ***4.4.1.2 Validating evidence: superficial injury***

Examination of the superficial arterial wall immediately after stenting supports the hypothesis that a scraping injury occurs at the ends of the stent. Others in our group have studied superficial injury in stented rabbit iliac arteries<sup>41</sup>. Arteries were stained *in situ* using AgNO<sub>3</sub> 15 minutes after stenting to outline the luminal lining cells and the extent of superficial injury. The stented artery was harvested and an incision made along its length. The stent was removed and the artery mounted *en face* for histologic examination. Figure 29 shows a stented artery's proximal edge. The stent shielded the geometrically-patterned region to the right from the AgNO<sub>3</sub> and leaves clear tracks of the corrugated ring design. Intact endothelial cells appear as a light silver layer carpeting the region to the right (region C). The endothelial cells are completely denuded where the balloon contacts the artery to the left, revealing the darker basement membrane above the underlying smooth muscle cells (A).

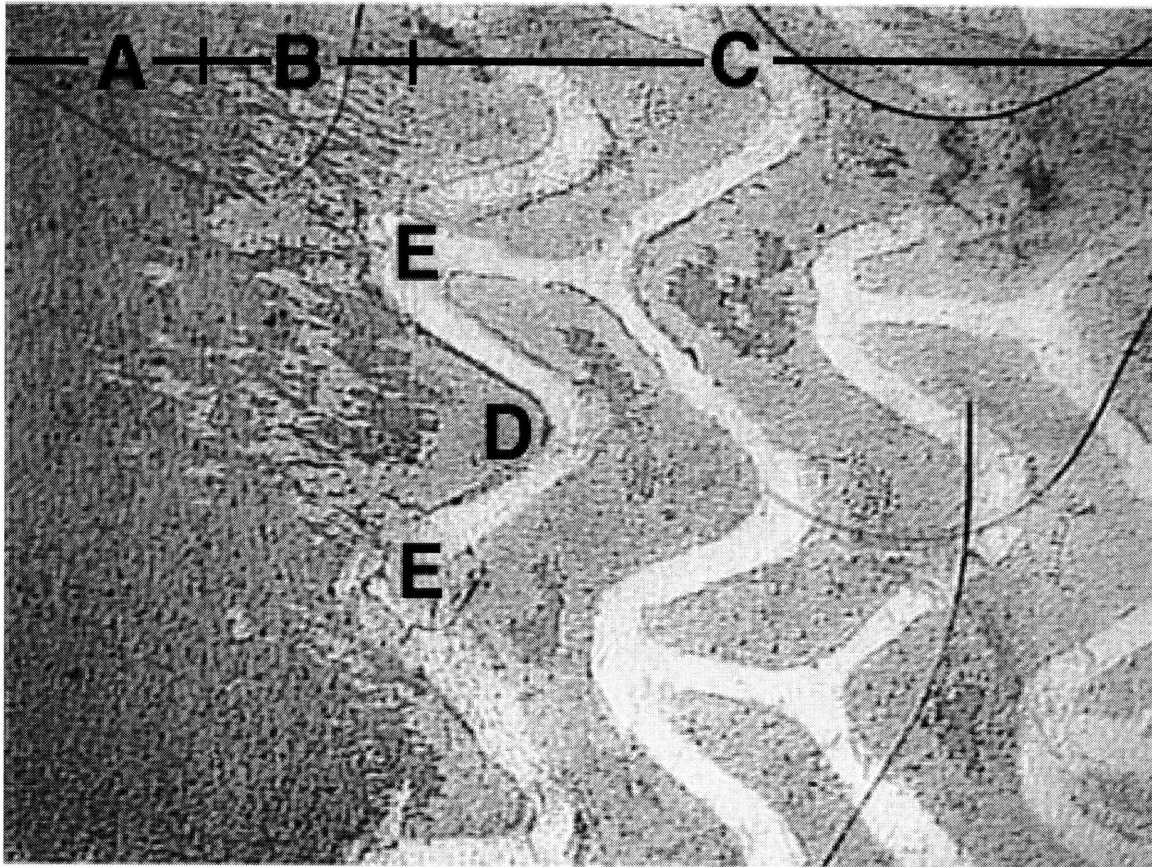


**Figure 29:  $\text{AgNO}_3$  stained *en face* rabbit femoral artery after stenting**

The center region (B) clearly shows longitudinal scraping damage in the region proximal to the stent. Note that this damage lessens in the V-shaped valley (D). This damage is consistent with injury induced from the dogbone effect. The flared stent ends impart the severe scraping damage as they begin axial contraction. The outermost struts (E) support the overlying artery, tenting it up and shielding the less-circumferentially expanded areas (D).

#### 4.4.1.3 Validating evidence: deep injury & hyperplasia

Unpublished data\* examining the magnitude of deep arterial injury and resulting hyperplasia in stented rabbit femoral arteries as a function of position along the stent also support the dogbone hypothesis (Figure 30). Deep arterial injury is measured on the scale proposed by Schwartz<sup>4</sup>, which maps increasing injury to an increasing score from zero to four. Intimal area is measured 14 days after stenting with stainless steel corrugated ring stents (ACS/Multi Link<sup>®</sup>). This data is compared to a metric of the nonuniformity, measured by the circumferential component of the arterial strain tensor at the point of greatest nonlinearity, occurring at approximately 4 atm.

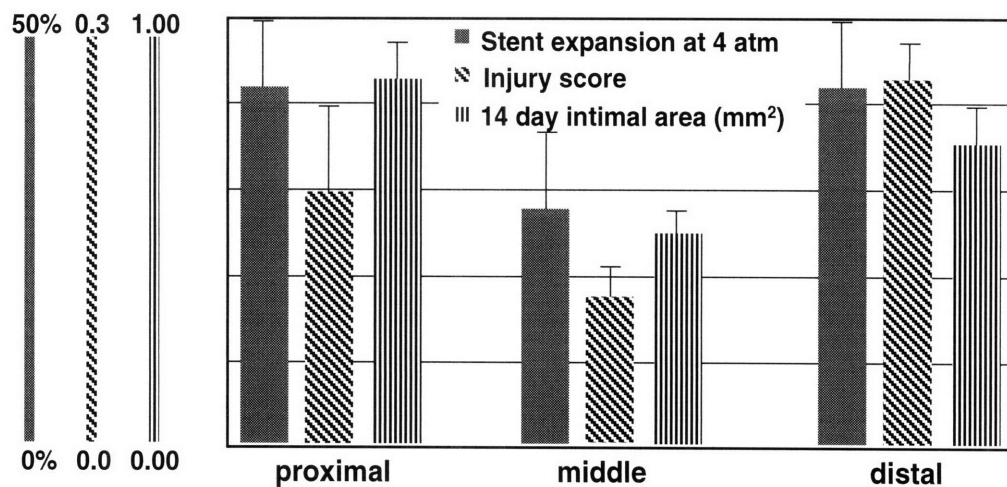


**Figure 30: Arterial injury and hyperplasia levels vs. position along the stent. Stent expansion at 4 atm is a metric of the severity of dogbone-shaped flare at the stent ends, and it closely tracks both injury score and eventual hyperplasia. Raw data is presented in Appendix A.**

\* Hyperplasia and injury score vs. position data courtesy of Sahil Parikh, Edelman laboratory, M.I.T., Cambridge, MA

These data show a significant difference of all three metrics as measured at the ends versus the middle: % nonuniformity ( $p=0.042$ ), injury score ( $p=0.046$ ), and intimal area gain ( $p=0.020$ ). Although measured at only three locations, nonuniformity shows a clear correlation with both injury score ( $r=0.87$ ) and increase in intimal area ( $r=0.91$ ).

#### 4.4.2 Other findings

Although a negligible torsional component of strain exists in the artery during and after stent deployment, video images of the translucent artery during surgery revealed that the stent rotates approximately 90 degrees during expansion. Similar observations were made in *ex vivo* tests and indicated that the torsional force originated in the catheter and was enhanced through the catheter's long moment arm; there was no differential rotation measured between the ends of the stent itself. *In vivo*, this rotation occurred before the ends first flared open; the unconstrained stent therefore first rotated freely as a unit to relieve any torsional force exerted by the catheter. The torsional moment was small compared to the tethering of the artery by surrounding *vasa vasorum*, and so the stent's angle of rotation became fixed once the stent first made contact with the artery. Early rotation of the catheter therefore could not cause vascular injury, and is unlikely to be a contributor of neointimal hyperplasia. This hypothesis is strengthened by the absence of a diagonal pattern of endothelial denudation in Figure 29.

*Ex vivo* and *in vivo* experiments yielded very similar results. The *ex vivo* testing was done on an air-filled unpressurized muscular bovine coronary artery free at one end and

tethered at the other by a vise, as opposed to the *in vivo* blood-pressurized rabbit iliac artery tethered at both ends by the surrounding vasculature. The dogbone effect was noted in both at the same pressure; resultant strain components were similar, and early catheter rotation was noted in both, despite several gross differences in the experiment. This suggests further work may be first done *ex vivo*, and validated *in vivo* with fewer animal experiments.

#### **4.4.3 Proposed methods to reduce dogbone**

The findings above are summarized in the left panel of Figure 31. Current stenting systems use an oversize balloon catheter to ensure, with a margin of safety, that the stent is fully expanded along its length after deployment. Yet, because of the dogbone effect, oversizing the balloon guarantees that at some intermediate point in expansion just the opposite will occur. We explored several ways this effect may be countered through either changes in stent or catheter design. It is important to note that the dogbone effect is only a function of the relative compliances and lengths of the balloon and catheter, and therefore cannot be reduced through any technique of balloon inflation. Furthermore, not all stents are susceptible to dogbone; self-expanding stents use the shape memory effect of nitinol to circumferentially expand and are therefore immune to dogbone injury caused by balloon/stent interaction.

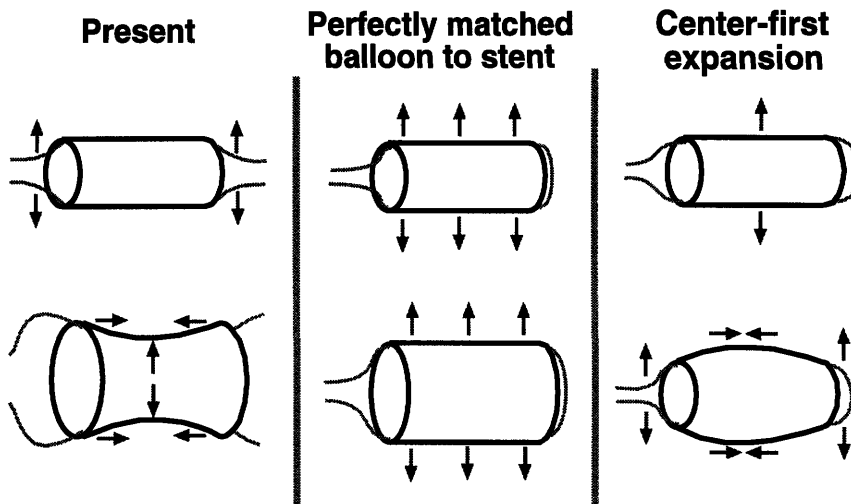


**Figure 31: Balloon/catheter designs, present and proposed. The present design expands at the far distal and proximal regions first, causing scraping damage as it axially contracts. This could be reduced by either matching the lengths of the balloon and stent or altering their material properties to cause them to expand from the center region outwards.**

#### ***4.4.2.1 Stent-based methods***

The stent may be selected to have exactly the same uninflated length as the balloon, shown in the center panel. Without having unconstrained ends, the balloon will feel equal resistance to expansion along its length and therefore expand evenly. A margin of safety to ensure complete stent expansion is still provided as many stents contract axially as they expand. This method also prevents balloon-arterial contact and subsequent deendothelialization seen previously in the histological photomicrograph of Figure 31 in arteries that have not been predilated through angioplasty.

An alternative method, shown in the right panel, is to design a stent with thinner struts towards the center than at the edges, causing it to circumferentially expand in the center first, and then smoothly outwards. Any axial contraction takes place as the stent rises to

meet the arterial surface; there is no pinching between flared ends as in the current configuration.

#### ***4.4.2.2 Catheter-based methods***

The same design goals considered above through stent modification can also be met through catheter redesign. Equivalent to a matched length stent-catheter system is a catheter that expands only in a marked center region of equal length to the stent. The far distal and proximal constrained balloon ends could then provide a crimping surface to secure the stent yet not inflate. Taken to less extremes, a catheter graded in compliance from least in the center and increasing outwards would exhibit the same center-first opening characteristic and benefits that could be obtained with the previously-examined center-first stent.

#### ***4.4.2.3 Self-expanding stents***

Self-expanding stents use the shape memory effect of nitinol to circumferentially expand and are therefore immune to dogbone injury caused by balloon/stent interaction.

## **4.5 Summary**

Stents dynamically open in a highly nonuniform fashion which leads to a pronounced edge effect during initial expansion of the proximal and distal ends. The dogbone shape that the stent temporarily assumes is caused by an interaction between the balloon



catheter and stent, and is a function of their lengths and compliances. Because it is a temporary condition, a cinematic sequence of images must be analyzed to examine this effect; before/after images alone do not reveal its presence.

This dogbone characteristic asserted during inflation causes direct, acute, local mechanical damage to the vascular wall. Such mechanical damage, measured *in vivo*, includes both superficial and deep injury, and correlates well with eventual intimal thickening.

## 5. Conclusions

### 5.1 Accomplishments

The concept of buttressing collapsible structures is certainly not new; vestiges of large wooden hoops used to scaffold walls have been found in Indian excavations that date from the early Bronze Age<sup>42</sup>. The investigation of the mechanics of endovascular stents is a fundamentally different type of problem, however, since vascular injury is not simply proportional to the final strain developed but depends upon more subtle factors such as the dynamic interaction between the stent and balloon during expansion, and demands both an understanding of the engineering behind stent expansion and appreciation of the underlying vascular biology.

In the United States, the FDA has currently approved two endovascular stent designs and has four more pending; in Europe no fewer than 20 different stent designs are currently in use. Despite this diversity and the knowledge that the degree of post-stenting intimal hyperplasia is dependent on stent design<sup>40</sup>, there existed neither an understanding of the mechanical initiators of hyperplasia nor tools to predict the efficacy of new geometries prior to clinical trials.

This thesis has described and analyzed one geometry-dependent mechanism causing arterial injury and resultant neointimal hyperplasia, and develops a tool to predict its magnitude both *in vitro* and *in vivo* for any stent design. The immediate clinical ramification is that injury from nonuniform stent expansion can be lessened through choice of catheter and stent, but not through inflation technique. Several proposed stent and balloon designs have also been explored that mitigate this mode of injury. Further, this thesis has developed both a tool and model to explore the biological effects of large strains on vascular tissue.

## 5.2 Future work

Several proposed designs were suggested that minimize the dogbone effect, and a logical continuation of this work would be to work with catheter/stent manufacturers to examine whether these changes do produce a less-injurious stent. More generally, identification of the dogbone effect permits stent/balloon design concepts to be tested for this mode of injury through finite element simulations before going to manufacturing and animal experiments. There are clearly other potential modes of mechanical injury that can be identified and correlated with eventual hyperplasia. Knowledge of a more complete set of rules measuring both the mode and significance of mechanical precursors of hyperplasia could:

1. create novel designs based upon this general set of design rules

2. shed insight on the basic biological processes causing hyperplasia
3. decrease the cost and time of the development cycle of new stent/balloon systems through the ability to simulate new concepts quickly.

A logical extension to this end of the work presented in this thesis would be to characterize more completely the various manners of mechanical injury that cause different stents to evoke different responses. Three modes appear especially suspect:

1. injury from direct balloon-arterial contact between the struts
2. blood turbulence and/or nonlaminar flow around the struts and at the far distal/proximal regions
3. mechanical integrity of vascular cells apposed to strut surfaces.

The process of identifying and measuring these characteristics to limit restenosis involves a multidisciplinary approach, binding the disciplines of solid and fluid mechanics, physics, vascular biology, physiology, and polymer chemistry with experiment, mathematical modeling, and clinical judgment. I hope this thesis contributes an understanding of the role of stent-induced vascular strain to this ongoing effort.

## Appendix A: Figure data

Figure 10										
distance (mm)	-5.80	-4.51	-3.22	-1.93	-0.64	0.64	1.93	3.22	4.51	5.80
circumferential	0.00	0.00	0.00	0.00	0.00	0.00	0.00	0.00	0.00	0.00
axial	0.00	0.00	0.00	0.00	0.00	0.00	0.00	0.00	0.00	0.00
torsional	0.00	0.00	0.00	0.00	0.00	0.00	0.00	0.00	0.00	0.00

Figure 11										
distance (mm)	-5.84	-4.54	-3.24	-1.95	-0.65	0.65	1.95	3.24	4.54	5.84
circumferential	-0.019	-0.005	0.051	0.055	0.029	0.048	0.038	0.074	-0.047	-0.048
axial	-0.054	-0.051	-0.008	-0.011	-0.007	-0.050	-0.083	0.046	-0.012	0.037
torsional	-0.005	0.002	0.003	0.004	0.011	0.009	0.007	0.004	-0.001	-0.009

Figure 12										
distance (mm)	-5.20	-4.04	-2.89	-1.73	-0.58	0.58	1.73	2.89	4.04	5.20
circumferential	0.360	0.344	0.311	0.292	0.265	0.262	0.231	0.229	0.204	0.195
axial	-0.200	-0.262	-0.155	-0.143	-0.077	-0.151	-0.175	-0.068	-0.048	0.002
torsional	0.113	0.002	0.129	0.109	-0.011	0.101	0.070	0.096	-0.015	0.039

Figure 13										
distance (mm)	-4.42	-3.44	-2.46	-1.47	-0.49	0.49	1.47	2.46	3.44	4.42
circumferential	0.690	0.619	0.574	0.541	0.516	0.500	0.457	0.437	0.433	0.433
axial	-0.188	-0.148	-0.177	-0.230	-0.210	-0.193	-0.155	-0.123	-0.151	-0.095
torsional	0.046	-0.173	-0.107	-0.037	-0.132	-0.109	-0.090	0.033	-0.029	-0.037

Figure 14										
distance (mm)	-4.40	-3.42	-2.24	-1.47	-0.49	0.49	1.47	2.24	3.42	4.40
circumferential	0.394	0.417	0.466	0.486	0.482	0.511	0.527	0.511	0.499	0.474
axial	-0.260	-0.321	-0.132	-0.276	-0.144	-0.231	-0.400	-0.157	-0.169	-0.107
torsional	0.054	0.055	0.111	0.018	-0.091	-0.045	0.070	0.021	0.049	0.074

Figure 15										
distance (mm)	-77.3	-60.1	-42.9	-25.8	-8.59	8.59	25.8	42.9	60.1	77.3
circumferential	3.072	3.304	3.362	3.420	3.339	3.072	2.783	2.203	1.391	0.638
axial	5.159	5.043	4.522	3.942	2.609	1.217	0.725	0.696	0.522	0.035
torsional	0.464	0.470	-0.203	-0.336	-0.284	0.014	0.093	0.004	0.023	0.064

Figure 16										
distance (mm)	-171.5	-133.4	-95.3	-57.2	-19.1	19.1	57.2	95.3	133.4	171.5
circumferential	8.116	9.333	10.20	10.84	11.18	11.24	11.07	10.60	9.623	8.174
axial	8.754	8.870	10.08	10.17	10.09	9.275	7.130	7.652	7.072	4.232
torsional	0.362	0.336	-0.145	-0.122	-0.272	-0.609	0.701	-0.197	-0.128	0.099

Figure 17 - computed values			
computed values	$\mu_{\text{monte-carlo}}$	$\sigma_{\text{monte-carlo}}$	$\mu_{\text{measured}}$
circumferential	0	0.1857	0.0049
axial	0	0.1714	-0.0062
torsional	0	0.1143	-0.0064

Figure 17 - measured values								
circumferential	-0.1800	-0.1704	-0.1406	-0.1343	-0.0706	0.0000	0.0248	0.0397
	0.0676	0.0506	0.0700	0.0959	0.1107	0.1193	0.1904	
axial	-0.1795	-0.1607	-0.0794	-0.0696	-0.0293	0.0596	0.1398	0.2701
	-0.1706	-0.1097	-0.0748	-0.0397	0.0406	0.0897	0.2200	
torsional	0.0796	-0.1094	-0.0495	-0.0402	-0.0095	0.0149	0.0602	0.0905
	-0.0740	-0.0754	-0.0500	-0.0298	0.0104	0.0207	0.0649	

Figure 22										
distance (mm)	-5.94	-4.62	-3.30	-1.98	-0.66	0.66	1.98	3.30	4.62	5.94
circumferential	0.089	0.067	0.069	0.055	0.022	0.035	0.050	0.040	0.024	0.055
axial	-0.123	0.030	0.010	0.012	0.040	0.015	-0.064	0.060	0.087	0.015
torsional	-0.055	-0.026	-0.009	-0.022	0.055	-0.014	-0.004	0.029	0.138	0.015

Figure 23										
distance (mm)	-5.36	-4.17	-2.98	-1.79	-0.60	0.60	1.79	2.98	4.17	5.36
circumferential	0.396	0.350	0.360	0.315	0.355	0.374	0.429	0.473	0.507	0.591
axial	-0.123	-0.054	-0.030	-0.039	-0.026	-0.052	-0.087	-0.028	-0.012	-0.091
torsional	0.009	-0.020	0.005	-0.022	0.021	-0.007	-0.032	0.039	0.060	0.079

Figure 24										
distance (mm)	-5.12	-3.98	-2.84	-1.71	-0.57	0.57	1.71	2.84	3.98	5.12
circumferential	0.768	0.754	0.700	0.749	0.778	0.862	0.857	0.931	0.975	1.034
axial	-0.185	-0.084	-0.034	-0.062	-0.091	-0.083	-0.054	-0.067	-0.032	-0.131
torsional	0.002	0.007	0.107	-0.062	-0.017	-0.100	-0.064	0.069	0.042	0.044

Figure 25										
distance (mm)	-4.88	-3.80	-2.71	-1.63	-0.54	0.54	1.63	2.71	3.80	4.88
circumferential	0.818	0.768	0.764	0.765	0.754	0.765	0.783	0.803	0.788	0.867
axial	-0.153	-0.148	-0.123	-0.118	-0.121	-0.172	-0.197	-0.200	-0.187	-0.161
torsional	-0.052	-0.062	0.032	-0.052	-0.079	-0.018	-0.099	-0.083	0.054	0.011

Figure 26										
distance (mm)	-5.18	-4.03	-2.88	-1.73	-0.58	0.58	1.73	2.88	4.03	5.18
circumferential	0.463	0.537	0.532	0.562	0.498	0.448	0.379	0.345	0.333	0.286
axial	-0.047	-0.089	-0.118	-0.121	-0.133	-0.143	-0.128	-0.108	-0.094	-0.069
torsional	-0.021	-0.021	-0.011	0.011	-0.044	-0.028	-0.018	-0.005	-0.013	-0.019

Figure 30			
region	proximal	mid-stent	distal
percent expansion at 4 atm	42 ± 8	29 ± 8	42 ± 8
injury score	0.18 ± 0.06	0.11 ± 0.02	0.25 ± 0.04
14 day intimal area (mm <sup>2</sup> )	0.83 ± 0.11	0.52 ± 0.05	0.70 ± 0.11

## Appendix B: Strain analysis/display code

The code used to determine the Green surface strain tensor from a sequence of TIFF image files of an expanding marked artery is presented below. The code is written in Matlab 4.2c programming language, and is compatible with the beta 10 version of Matlab 5.0. The code can be divided into two categories: analysis and display.

### Analysis Procedures

The procedures are listed below in the order in which they are called by the user.

**get\_dat** takes an image map from the frame grabber with a scale factor and returns the encoded matrix  $m$  that describes both the digitized arterial envelope and the two dimensional locations of all the reference points

**fit\_hypm** takes the output matrix from **get\_dat**, completes a non-linear least squares fit of a general quadratic equation to the data, and rotates it to make the axis of symmetry horizontal.

**out\_dat** takes rotates the quadratic envelope determined by **fit\_hypm** to create a data structure describing the three-dimensional arterial surface. It next back-projects the



marker locations from `get_dat` onto this surface, divides the surface into equal patches, and stores all the data in single matrix. The matrix is called `dn`, where `n` is replaced by the frame number of the original image.

**find\_key** associates a set of marker triads with every patch location determined by `out_dat`.

**findstr** takes the set of marker triads from `find_key` and their original and displaced locations from `out_dat`, computes the Green strain tensor, and adds this information to the `dn` data structure.

### **Display Procedures**

**show** is a wrapper function that draws a graphical user interface and calls `show1-show6` as required. It takes a Matlab data file composed of the set of `dn` matrices produced by `outdat` and `findstr`, and can produce still and animated two and three dimensional graphs describing the evolution of strain in time.

### function dn = dat\_fin(n1,d1,na,da,nn,dn)

```
% DAT_FIN finds e(x,y,t) and de/dt(x,y,t)
%   dn = dat_fin(n1,d1,na,da,nn,dn)
%
%   See out_dat for description of form of d1
%   See fit_hypm for description of form of n1,na,nn
%
%   James C. Squire  December 1995
```

```
% initialize variables
```

```
hdl = waitbar(0,'Determining strain...');
nblocks = size(d1,1)-1;
for i = 1:nblocks
    triplet = findkeyt(i,n1,d1);
    straint = findstnt(triplet,n1,nn);
    dstraint = findstnt(triplet,na,nn);
    dn(i,12) = straint(3);
    dn(i,15) = dstraint(3);

    ihoriz = findkeyh(i,n1,d1);
    strainh = findstnh(ihoriz,n1,nn);
    dstrainh = findstnh(ihoriz,na,nn);
    dn(i,11) = strainh;
    dn(i,14) = dstrainh;

    strainv = findstnv(i,d1,dn);
    dstrainv = findstnv(i,da,dn);
    dn(i,10) = strainv;
    dn(i,13) = dstrainv;

    waitbar(i/nblocks)
end
close(hdl)
```

### function khoriz = findkeyh(index,nn,dn)

```
% FINDKEYH finds key point indicies to determine horizontal strain about a point
%   khoriz = findkey(index,nn,dn)
%
%   khoriz is in the form [index1, index2]
%   index is an index into dn
%   See fit_hypm for description of form of nn.
%   See out_dat for description of form of dn.
%
%   James C. Squire  August 1995
```

```
% initialize variables
```

```
HORIZTOL = 1;    % Must be at least one patchwidth away from center
DEBUG = 0;      % Set to ~0 for diagnostic printout

nvert = dn(size(dn,1),2);
nhoriz = dn(size(dn,1),3);
nblocks = nvert*nhoriz;

n3 = nn(1,3);
p2 = nn(3,1);    q = sqrt(nn(3,2));
xlist = nn(n3:size(nn,1),2);    ylist = nn(n3:size(nn,1),3);    zlist = zcalc(xlist,ylist,p2,q,DEBUG);
```

```

x1 = dn(index,2);      y1 = dn(index,3);      z1 = zcalc(x1,y1,q,p2,DEBUG);
x2 = dn(index,4);      y2 = dn(index,5);      z2 = zcalc(x2,y2,q,p2,DEBUG);
x3 = dn(index,6);      y3 = dn(index,7);      z3 = zcalc(x3,y3,q,p2,DEBUG);
x4 = dn(index,8);      y4 = dn(index,9);      z4 = zcalc(x4,y4,q,p2,DEBUG);

dyleft = sqrt((y1-y3)^2+(z1-z3)^2);  dyright = sqrt((y2-y4)^2+(z2-z4)^2);
patchheight = mean([dyleft dyright]);
patchwidth = x2 - x1;
% the center is the projected value; the intersection of the diagonals
patchxcenter = -(((x2 - x4)*(x3*y1 - x1*y3) - (x1 - x3)*(x4*y2 - x2*y4))/ ...
((x2 - x4)*(-y1 + y3) - (x1 - x3)*(-y2 + y4)));
patchycenter = -((x4*y2 - x2*y4)/(x2 - x4) + ...
((-y2 + y4)*((x2 - x4)*(x3*y1 - x1*y3) - (x1 - x3)*(x4*y2 - x2*y4))/ ...
((x2 - x4)*((x2 - x4)*(-y1 + y3) - (x1 - x3)*(-y2 + y4))));
patchzcenter = zcalc(patchxcenter,patchycenter,p2,q,DEBUG);
distances=sqrt((xlist-patchxcenter).^2+(ylist-patchycenter).^2+(zlist-patchzcenter).^2);

% find horizontal key points
xtol = patchwidth * HORIZTOL;      % must be at lest xtol away from each other
[p1d,p1_index]=min(distances);
p1x = xlist(p1_index); p1y=ylist(p1_index); p1z=zlist(p1_index);
p2d = 999999999;
p2_index = -1;
for i=1:size(xlist,1)
    xt = xlist(i); yt = ylist(i); zt = zlist(i);
    xpatchdist = sqrt((xt-patchxcenter).^2+(yt-patchycenter).^2+(zt-patchzcenter).^2);
    xpointdist = abs(xt - p1x);
    if xpointdist >= xtol & xpatchdist < p2d
        p2d = xpatchdist;
        p2_index = i;
    end
end
khoriz = [p1_index p2_index];

```

### **function ntriplet = findkeyt(index,nn,dn)**

```

% FINDKEYT finds key point indicies to determine strain about a point
%   ntriplet = findkeyt(index,nn,dn)
%
%   ntriplet are in form of [index1, index2, index3]
%   where index is an index into dn
%   See fit_hypm for description of form of nn.
%   See out_dat for description of form of dn.
%
%   James C. Squire  August 1995
%   modified August 1995

% constants
NBEST = 5;      % Examine the closest NBEST points for triplets
NEARCENTERG = .3; % Narrowness (=relative importance) of near_center grade [.1,5]
NEARCENTERC = .6; % Ideal closeness to center is NEARCENTERC*patchwidth
DISTANCEAPARTG = 1; % Narrowness (=relative importance) of distance_apart grade [.1,5]
DISTANCEAPARTC = 1.25; % Ideal distance apart is DISTANCEAPARTC*patchwidth
EDGE = 4;      % Relative importance of Edge grade [.1 10]
ANGLE = 3;     % Relative importance of Angle grade [.1 10]
DEBUG = 0;     % Set to ~0 for diagnostic printout

% initialize variables

```

```

nvert = dn(size(dn,1),2);
nhoriz = dn(size(dn,1),3);
nblocks = nvert*nhoriz;

n3 = nn(1,3);
p2 = nn(3,1);      q = sqrt(nn(3,2));
xlist = nn(n3:size(nn,1),2);  ylist = nn(n3:size(nn,1),3);
zlist = zcalc(xlist,ylist,p2,q,DEBUG);
x1 = dn(index,2);  y1 = dn(index,3);
x2 = dn(index,4);  y2 = dn(index,5);
x3 = dn(index,6);  y3 = dn(index,7);
x4 = dn(index,8);  y4 = dn(index,9);

z1 = zcalc(x1,y1,q,p2,DEBUG);
z2 = zcalc(x2,y2,q,p2,DEBUG);
z3 = zcalc(x3,y3,q,p2,DEBUG);
z4 = zcalc(x4,y4,q,p2,DEBUG);
dyleft = sqrt((y1-y3)^2+(z1-z3)^2);  dyright = sqrt((y2-y4)^2+(z2-z4)^2);
patchheight = mean([dyleft dyright]);
patchwidth = x2 - x1;
% the center is the projected value; the intersection of the diagonals
patchxcenter = -(((x2 - x4)*(x3*y1 - x1*y3) - (x1 - x3)*(x4*y2 - x2*y4))/ ...
  ((x2 - x4)*(-y1 + y3) - (x1 - x3)*(-y2 + y4)));
patchycenter = -((x4*y2 - x2*y4)/(x2 - x4) + ...
  ((-y2 + y4)*((x2 - x4)*(x3*y1 - x1*y3) - (x1 - x3)*(x4*y2 - x2*y4))/ ...
  ((x2 - x4)*(x2 - x4)*(-y1 + y3) - (x1 - x3)*(-y2 + y4)));
patchzcenter = zcalc(patchxcenter,patchycenter,p2,q,DEBUG);

% Choose the NBEST closest points and arrange in matrix mbest
% mbest = [index1 index2 index3 ...
%         patchdist_score apartdist_score edge_score angle_score total_score]

distances=sqrt((xlist-patchxcenter).^2+(ylist-patchycenter).^2+(zlist-patchzcenter).^2);
[dummy,tindex]=sort(distances);
closeindex=tindex(1:NBEST); % holds indecies to NBEST closest points
ntriplets = (NBEST)*(NBEST-1)*(NBEST-2)/6; % NBEST choose 3
mbest = zeros(ntriplets,8);
count=1;
for i=1:NBEST-2
  for j=i+1:NBEST-1
    for k=j+1:NBEST
      mbest(count,1:3)=[closeindex(i) closeindex(j) closeindex(k)];
      count=count+1;
    end
  end
end
if DEBUG~=0 & DEBUG<=1
  disp(' '); disp('closest distances are');
  disp('index distance'); disp([closeindex distances(closeindex)]); pause
  disp(' '); disp('mbest = '); disp(mbest);
  disp('Note figure 1')
  n1 = nn(1,1);      n2 = nn(1,2);
  toplinex = nn(n1:n2-1,2);  topliney = nn(n1:n2-1,3);
  bottomlinex = nn(n2:n3-1,2);  bottomliney = nn(n2:n3-1,3);
  keypointxs = xlist(closeindex);  keypointys = ylist(closeindex);
  boxx = [x1 x2 x3 x4 x1];  boxy = [y1 y2 y3 y4 y1];
  figure(1)
  hold on
  for j=1:nblocks
    plot([dn(j,2),dn(j,4),dn(j,6),dn(j,8),dn(j,2)], ...
      [dn(j,3),dn(j,5),dn(j,7),dn(j,9),dn(j,3)],'b-')
  end
  plot(toplinex,topliney,'y-',bottomlinex,bottomliney,'y-', ...

```

```

        xlist,ylist,'wo',keypointx,keypointy,'rx',boxx,boxy,'g-', ...
        patchxcenter,patchycenter,'g*');
    hold off
    pause
end

% For each of the triplets determine
% near_center score from my distribution
% dist_apart score from distribution
% edge score from min(cos(theta)) (stay away from edges)
% angle score from min(sin(theta)) (don't want small angles)

% My distribution: x^a*exp(-b x). The narrowness is prop to a. Center at a/b
anc = NEARCENTERG;    bnc=anc/(NEARCENTERC*patchwidth);
ada = DISTANCEAPARTG;    bda=ada/(DISTANCEAPARTC*patchwidth);
for i=1:ntriplets
    point1x=xlist(mbest(i,1));    point1y=ylist(mbest(i,1));    point1z=zlist(mbest(i,1));
    point2x=xlist(mbest(i,2));    point2y=ylist(mbest(i,2));    point2z=zlist(mbest(i,2));
    point3x=xlist(mbest(i,3));    point3y=ylist(mbest(i,3));    point3z=zlist(mbest(i,3));

    distc1=norm([point1x-patchxcenter point1y-patchycenter point1z-patchzcenter]);
    distc2=norm([point2x-patchxcenter point2y-patchycenter point2z-patchzcenter]);
    distc3=norm([point3x-patchxcenter point3y-patchycenter point3z-patchzcenter]);
    tin = [distc1 distc2 distc3];
    tv=[distc1^anc * exp(-bnc*distc1) distc2^anc * exp(-bnc*distc2) distc3^anc * exp(-bnc*distc3)];
    [tf,ti] = min(tv);
    mbest(i,4) = tf;    % near_center grade
    distnc = tin(ti);

    dist12=sqrt((point2x-point1x)^2 + (point2y-point1y)^2 + (point2z-point1z)^2);
    dist23=sqrt((point3x-point2x)^2 + (point3y-point2y)^2 + (point3z-point2z)^2);
    dist13=sqrt((point3x-point1x)^2 + (point3y-point1y)^2 + (point3z-point1z)^2);

    tin = [dist12 dist23 dist13];
    tv = [dist12^ada*exp(-bda*dist12) dist23^ada*exp(-bda*dist23) dist13^ada*exp(-bda*dist13)];
    [tf,ti] = min(tv);
    mbest(i,5) = tf;    % dist_apart grade
    distda = tin(ti);
    point1r=sqrt(q^2*(1+point1x^2/p2));
    point1a=sqrt(point1r^2-point1y^2)/point1r;
    if imag(point1a), point1a=0; end    % point falls outside modelled surface
    point2r=sqrt(q^2*(1+point2x^2/p2));
    point2a=sqrt(point2r^2-point2y^2)/point2r;
    if imag(point2a), point2a=0; end
    point3r=sqrt(q^2*(1+point3x^2/p2));
    point3a=sqrt(point3r^2-point3y^2)/point3r;
    if imag(point3a), point3a=0; end
    ftedge=min([point1a point2a point3a]); % always from 0 to 1, 1 best
    mbest(i,6)=ftedge^EDGELEG;

    r12=[point2x-point1x point2y-point1y point2z-point1z];
    r23=[point3x-point2x point3y-point2y point3z-point2z];
    r31=[point1x-point3x point1y-point3y point1z-point3z];
    angle123=acos((-r12*r23)/(norm(r12)*norm(r23)))*180/pi;
    angle231=acos((-r23*r31)/(norm(r23)*norm(r31)))*180/pi;
    angle312=acos((-r31*r12)/(norm(r31)*norm(r12)))*180/pi;
    ftangle = min([angle123 angle231 angle312])/60;
    % 60 would be equilateral triangle, tf from 0 to 1, 1 best
    mbest(i,7) = ftangle^ANGLELEG;

    mbest(i,8) = prod(mbest(i,4:7))*10000;

```

```

if DEBUG~=0 & DEBUG<=2

    % draw the overall stent picture with current points
    n1 = nn(1,1);          n2 = nn(1,2);
    toplinex  = nn(n1:n2-1,2);    topliney  = nn(n1:n2-1,3);
    bottomlinex = nn(n2:n3-1,2);    bottomliney = nn(n2:n3-1,3);
    keypointsx = xlist(mbest(i,1:3));    keypointsy = ylist(mbest(i,1:3));
    boxx = [x1 x2 x3 x4 x1];    boxy = [y1 y2 y3 y4 y1];
    disp(sprintf('Showing point %g of %g',i,ntriplets))
    figure(1)
    clf, hold on
    for j=1:nblocks
        plot([dn(j,2),dn(j,4),dn(j,6),dn(j,8),dn(j,2)], ...
            [dn(j,3),dn(j,5),dn(j,7),dn(j,9),dn(j,3)],'b-')
    end
    plot(toplinex,topliney,'y-',bottomlinex,bottomliney,'y-', ...
        xlist,ylist,'wo',keypointsx,keypointsy,'wx',boxx,boxy,'g-');
    hold off
    axis([-3 .1 -.2 .2])
    axis('square')
    title(sprintf('Score = %g',mbest(i,8)))

    % draw distribution for near_center_point
    figure(2)
    subplot(221)
    tx=linspace(0,5*patchwidth,100);
    ty=tx.^anc.*exp(-bnc.*tx);
    % draws it with x scale in patchwidths
    plot(tx/patchwidth,ty,'y-',distnc/patchwidth,mbest(i,4),'ro');
    set(gca,'xtick',[0 1 2 3 4 5])
    title('Nearness to patch')

    % draw distribution for distance_apart
    subplot(222)
    tx=linspace(0,5*patchwidth,100);
    ty=tx.^ada.*exp(-bda.*tx);
    % draws it with x scale in patchwidths
    plot(tx/patchwidth,ty,'y-',distda/patchwidth,mbest(i,5),'ro');
    set(gca,'xtick',[0 1 2 3 4 5])
    title('Distance from each other')

    % draw graph with edge point
    subplot(223)
    tx=linspace(0,1,100);
    ty=tx.^EDGEG;
    plot(tx,ty,'y-',ftedge,mbest(i,6),'ro');
    title('Closest point to edge')

    % draw graph with angle point
    subplot(224)
    tx=linspace(0,1,100);
    ty=tx.^ANGLEG;
    plot(tx,ty,'y-',ftangle,mbest(i,7),'ro');
    title('evenly spaced angles')
    pause
end
end

% return the best points
[dummy,tindex] = max(mbest(:,8));
ntriplet = mbest(tindex,1:3);

if DEBUG~=0 & DEBUG<=3

```

```

% draw the overall stent picture with best triplets highlighted
n1 = nn(1,1);          n2 = nn(1,2);
toplinex  = nn(n1:n2-1,2);    topliney  = nn(n1:n2-1,3);
bottomlinex = nn(n2:n3-1,2);    bottomliney = nn(n2:n3-1,3);
keypointsx = xlist(ntriplet);    keypointsy = ylist(ntriplet);
boxx = [x1 x2 x3 x4 x1];    boxy = [y1 y2 y3 y4 y1];
figure(1)
hold off
cla
title("")
hold on
for j=1:nblocks
    plot([dn(j,2),dn(j,4),dn(j,6),dn(j,8),dn(j,2)], ...
        [dn(j,3),dn(j,5),dn(j,7),dn(j,9),dn(j,3)],'b-')
end
plot(toplinex,topliney,'y-',bottomlinex,bottomliney,'y-', ...
    xlist,ylist,'wo',keypointsx,keypointsy,'wx',boxx,boxy,'g-');
axis([-3 .1 -2 .2])
axis('square')
hold off
end

```

### **function shoriz = findstrh(khoriz,na,nb)**

```

% FINDSTRH finds the strain between two key normalized points
%   shoriz = findstrh(khoriz,na,nb)
%
%   khoriz is in the form of [index1, index2]
%   index is an index into dn.
%   See fit_hypm for description of form of na,nb.
%
%   James C. Squire August 1995
%   modified October 1995 to work under assumption of zero torsion
%   modified September 1996 to change uniaxial strain definition
%   to tensor definition

% initialize variables
n3a = na(1,3);          n3b = nb(1,3);
p2a = na(3,1);          p2b = nb(3,1);
qa = sqrt(na(3,2));    qb = sqrt(nb(3,2));

% Cartesian coordinates for points pairs 1,2 of before a and after b  horiz: x  vert: y  out of page: z
% start point triad is A,B,C; end triad is a,b,c

hxa1 = na(n3a+khoriz(1)-1,2);  hya1 = na(n3a+khoriz(1)-1,3);  hza1 = zcalc(hxa1,hya1,p2a,qa);
hxa2 = na(n3a+khoriz(2)-1,2);  hya2 = na(n3a+khoriz(2)-1,3);  hza2 = zcalc(hxa2,hya2,p2a,qa);
hxb1 = nb(n3b+khoriz(1)-1,2);  hyb1 = nb(n3b+khoriz(1)-1,3);  hzb1 = zcalc(hxb1,hyb1,p2b,qb);
hxb2 = nb(n3b+khoriz(2)-1,2);  hyb2 = nb(n3b+khoriz(2)-1,3);  hzb2 = zcalc(hxb2,hyb2,p2b,qb);

% distances between points 1,2
horiza = abs(hxa1-hxa2);
horizb = abs(hxb1-hxb2);

% compute strain
shoriz = (horizb-horiza)/horiza * (horiza+horizb)/(2*horiza);

```

## function strain\_tensor = findstrt(ntriplet,nb,na)

```

% FINDSTRT finds the strain tensor around three points
%   strain_tensor = findstrt(ntriplet,n1,n2)
%
%   ntriplet is in the form of [index1 index2 index3] into n1,n2
%   strain_tensor is in the form of [e_thetatheta e_zz e_ztheta]
%   See fit_hypm for description of form of na,nb.
%
%   James C. Squire   August 1995

DEBUG = 3; % set to 9999 for no debugging

% initialize variables
n3a = na(1,3);      n3b = nb(1,3);
p2a = na(3,1);      p2b = nb(3,1);
qa = sqrt(na(3,2)); qb = sqrt(nb(3,2));

% Cartesian coordinates for points A,B,C,a,b,c  horiz: x vert: y out of page: z
% start point triad is A,B,C; end triad is a,b,c
xA = na(n3a+ntriplet(1)-1,2); yA = na(n3a+ntriplet(1)-1,3); zA = zcalc(xA,yA,p2a,qa);
xB = na(n3a+ntriplet(2)-1,2); yB = na(n3a+ntriplet(2)-1,3); zB = zcalc(xB,yB,p2a,qa);
xC = na(n3a+ntriplet(3)-1,2); yC = na(n3a+ntriplet(3)-1,3); zC = zcalc(xC,yC,p2a,qa);
xa = nb(n3b+ntriplet(1)-1,2); ya = nb(n3b+ntriplet(1)-1,3); za = zcalc(xa,ya,p2b,qb);
xb = nb(n3b+ntriplet(2)-1,2); yb = nb(n3b+ntriplet(2)-1,3); zb = zcalc(xb,yb,p2b,qb);
xc = nb(n3b+ntriplet(3)-1,2); yc = nb(n3b+ntriplet(3)-1,3); zc = zcalc(xc,yc,p2b,qb);
if DEBUG<=1
    disp('   x   y   z')
    disp(sprintf('A  %7.3g %7.3g %7.3g',xA,yA,zA))
    disp(sprintf('B  %7.3g %7.3g %7.3g',xB,yB,zB))
    disp(sprintf('C  %7.3g %7.3g %7.3g',xC,yC,zC))
    disp(sprintf('a  %7.3g %7.3g %7.3g',xa,ya,za))
    disp(sprintf('b  %7.3g %7.3g %7.3g',xb,yb,zb))
    disp(sprintf('c  %7.3g %7.3g %7.3g',xc,yc,zc))
end

% Convert to cylindrical coords and store in matrices A,B,C,a,b,c
% each point of form [r theta z]
% z is measured along the stent axis (x value in screen coords), ie
% horiz: z  around axis: theta  distance from axis: r

A(1) = norm([yA zA]); A(2) = atan2(yA,zA); A(3) = xA;
B(1) = norm([yB zB]); B(2) = atan2(yB,zB); B(3) = xB;
C(1) = norm([yC zC]); C(2) = atan2(yC,zC); C(3) = xC;
a(1) = norm([ya za]); a(2) = atan2(ya,za); a(3) = xa;
b(1) = norm([yb zb]); b(2) = atan2(yb,zb); b(3) = xb;
c(1) = norm([yc zc]); c(2) = atan2(yc,zc); c(3) = xc;
if DEBUG<=1
    disp(' ')
    disp('   r   t   z')
    disp(sprintf('A  %7.3g %7.3g %7.3g',A(1),A(2),A(3)))
    disp(sprintf('B  %7.3g %7.3g %7.3g',B(1),B(2),B(3)))
    disp(sprintf('C  %7.3g %7.3g %7.3g',C(1),C(2),C(3)))
    disp(sprintf('a  %7.3g %7.3g %7.3g',a(1),a(2),a(3)))
    disp(sprintf('b  %7.3g %7.3g %7.3g',b(1),b(2),b(3)))
    disp(sprintf('c  %7.3g %7.3g %7.3g',c(1),c(2),c(3)))
end

% Compute strain

```



```

r=mean([a(1) b(1) c(1)]);
R=mean([A(1) B(1) C(1)]);
an=R*(B(2)-A(2)); bn=R*(C(2)-A(2)); cn=B(3)-A(3); dn=C(3)-A(3);
am=r*(b(2)-a(2)); bm=r*(c(2)-a(2)); cm=b(3)-a(3); dm=c(3)-a(3);

de = am*dm-bm*cm;
F=[an*dm-bn*cm bn*am-an*bm; cn*dm-dn*cm dn*am-cn*bm]/de;
E = .5*(F'*F-eye(2));

if DEBUG<=2
    disp(' ')
    disp('F:')
    disp(F)
    disp(' ')
    disp('Euler:')
    disp(E)
end

strain_tensor = [E(1,1) E(2,2) mean([E(1,2) E(2,1)])];

```

### function strainv = findstnv(index,d1,d2)

```

% FINDSTNV finds vertical strain about index point index
% strainv = findstnv(index,d1,d2)
%
%     index is an index into dn
%     See out_dat for description of form of dn.
%
%     James C. Squire  August 1995
%     modified September 1996 to change uniaxial strain definition
%     to tensor definition

% initialize variables

nvert = d1(size(d1,1),2);
nhoriz = d1(size(d1,1),3);
ibot = ceil(index/nvert)*nvert;
itop = ibot-nvert+1;

length1 = mean(d1(itop,[3,5])) - mean(d1(ibot,[7,9]));
length2 = mean(d2(itop,[3,5])) - mean(d2(ibot,[7,9]));

strainv = (length2-length1)/length1 * (length1+length2)/(2*length1);

```

### function err = fit\_hyp(lambda)

```

%FIT_HYP Used by fit_hypm
%     FIT_HYP(lambda) returns the error between the data and the
%     values computed by the current function of lambda.
%     FITFUN assumes a function of the form
%
%     
$$y = \frac{-e-bx (+/-) \sqrt{(e+bx)^2-4c(ax^2+dx-1)^2}}{2c}$$

%
%     with 0 linear parameters and 5 nonlinear parameters
%     accounting for translational(2), rotational(1), and shape(2) DOF

```

```

%
%      James C. Squire  July 1995

global Data Plothandle

n1 = Data(1,1); n2 = Data(1,2); n3 = Data(1,3);
xt = Data(n1:n2-1,2);
yt = Data(n1:n2-1,3);
xb = Data(n2:n3-1,2);
yb = Data(n2:n3-1,3);

zt = zeros(size(xt));
for j = 1:length(xt)
    ftemp = sqrt((lambda(5)+lambda(2)*xt(j))^2-4*lambda(3)*(lambda(1)*xt(j)^2+lambda(4)*xt(j)-1));
    zt(j) = (-lambda(5) - lambda(2)*xt(j) + ftemp) / (2*lambda(3));
end

zb = zeros(size(xb));
for j = 1:length(xb)
    ftemp = sqrt((lambda(5)+lambda(2)*xb(j))^2-4*lambda(3)*(lambda(1)*xb(j)^2+lambda(4)*xb(j)-1));
    zb(j) = (-lambda(5) - lambda(2)*xb(j) - ftemp) / (2*lambda(3));
end

set(Plothandle(1),'ydata',zt)
set(Plothandle(2),'ydata',zb)
drawnow
err = norm([zt;zb]-[yt;yb]);

```

### function nn=fit\_hypm(data2, auto, lambda)

```

%FIT_HYPM fits a hyperbolic model to stent data.
%      nn=fit_hypm(rn, auto, lambda)
%
%      See get_data for form of rn.
%
%      It returns nn =
%      [n1 n2 n3] n1=start row of top envelope, n2 for bottom, n3 for key points
%      [sin(theta) cos(theta) theta]
%      [p^2    q^2    0]
%      [h      k      0]
%      [hn     kn     0]
%      [-2    x1    y1] -2 means start of top envelope
%      [-1    x1    y1] -1 means start of bottom envelope
%      [1     x1    y1] key point number 1
%
%      If lambda = [a,b,c,d,e] is supplied, it works in debug mode.
%      If auto is supplied, it does not pause while showing its work
%
%      fit_hypm fits the data to the following equation
%
%      
$$y = \frac{-e-bx (+/-) \sqrt{(e+bx)^2-4c(ax^2+dx-1)^2}}{2c}$$

%
%      It uses fit_hyp as a helper function
%
%      Fits to  $(y-k)^2/q^2 - (x-h)^2/p^2 = 1$ 
%      Returns the actual derotated hyperboloid
%      James C. Squire  July 1995
%      Modified August 1995

```

```

global Data
global Plohandle

% Setup data structures
Data = data2;
figure(1)
clf
hold on
n1 = Data(1,1);
n2 = Data(1,2);
n3 = Data(1,3);
xt = Data(n1:n2-1,2);
yt = Data(n1:n2-1,3);
xb = Data(n2:n3-1,2);
yb = Data(n2:n3-1,3);
xp = Data(n3:length(Data),2);
yp = Data(n3:length(Data),3);

% Initialize first guess by taking exact soln to 5 well-thought-out sampled points
if nargin < 3

    tl=0; tr=0; br=0; bl=0; %these refer to if a corner is taken
    [minxt,indminxt]=min(xt);
    [minxb,indminxb]=min(xb);
    [maxxt,indmaxxt]=max(xt);
    [maxxb,indmaxxb]=max(xb);
    [minyb,indminyb]=min(yb);

    % x1 must be the zero x point; store position in x1p
    if minxt==0 % it's in the top
        y1=yt(indminxt);
        tl=1;
    elseif minxb==0
        y1=yb(indminxb);
        bl=1;
    else
        error('Error: r data not normalized properly')
    end
    x1=0; % by definition

    % put the zero y point (or closest if already point1) into point2.
    if xb(indminyb)==0 % uh,oh: point(0,0) exists
        disp('Sorry: point 0,0 exists. You must manually enter start point, or redigitize')
        error('Probability of this happening = machine precision ~ 10^-16')
    end
    x2=xb(indminyb);
    if indminyb==1
        bl=1;
    elseif indminyb==length(yb)
        br=1;
    end
    y2=0; % by definition

    % fill in point3 trying clockwise from tl (either tl or tr)
    if tl==0
        x3=minxt;
        y3=yt(indminxt);
        tl=1;
    elseif tr==0
        x3=maxxt;
        y3=yt(indmaxxt);
        tr=1;

```

```

else error('Error in assigning point 3')
end

% fill in point4 trying tr,br,bl
if tr==0
    x4=maxxt;
    y4=yt(indmaxxt);
    tr=1;
elseif br==0
    x4=maxxb;
    y4=yb(indmaxxb);
    br=1;
elseif bl==0
    x4=minxb;
    y4=yb(indminxb);
    bl=1;
else error('Error in assigning point 4')
end

% fill in point5 trying br,bl,middle
if br==0
    x5=maxxb;
    y5=yb(indmaxxb);
    br=1;
elseif bl==0
    x5=minxb;
    y5=yb(indminxb);
    bl=1;
else % top middle
    lastind = round(length(xt)/2);
    x5=xt(lastind);
    y5=yt(lastind);
end

% Solution to exact fit over these 5 points (thanks, Mathematica!)
c=-((-(x2*x3*x5*y1^2*(x2^2*y3*y4*(-(x4*y3) + x3*y4) + ...
    y1^2*(-(x2^2*x3*y3) + x3*x4^2*y3 + x2^2*x4*y4 - x3^2*x4*y4))* ...
    (x2*y3 - x5*y3 - x2*y5 + x3*y5)) + ...
    x2*x3*x4*y1^2*(x2*y3 - x4*y3 - x2*y4 + x3*y4)* ...
    (x2^2*y3*y5*(-(x5*y3) + x3*y5) + ...
    y1^2*(-(x2^2*x3*y3) + x3*x5^2*y3 + x2^2*x5*y5 - x3^2*x5*y5))/ ...
    (x2^3*x3*x4*y1^3*y3*(x2*y3 - x4*y3 - x2*y4 + x3*y4)*y5* ...
    (x3*y1 - x5*y1 + x5*y3 - x3*y5) + ...
    x2^3*x3*x5*y1^3*y3*y4*(x3*y1 - x4*y1 + x4*y3 - x3*y4)* ...
    (-(x2*y3) + x5*y3 + x2*y5 - x3*y5)));
c=-((-1 + e*y1)/y1^2);
d=-((x2^2*(1 - e*y1)*y3*y4*(-(x4*y3) + x3*y4) + ...
    y1^2*(x3*x4^2*y3 - x3^2*x4*y4 + ...
    x2^2*(-(x3*y3) + x4*y4 + e*x3*y3*y4 - e*x4*y3*y4))/ ...
    (x2*x3*x4*y1^2*(x2*y3 - x4*y3 - x2*y4 + x3*y4)));
a=(1 - d*x2)/x2^2;
b=-((-1 + d*x3 + a*x3^2 + e*y3 + c*y3^2)/(x3*y3));
lambda = [a b c d e];
end

end
if nargin==1
    auto = 1;
end

plot(xt,yt,'ro',xb,yb,'ro','EraseMode','none')
title('Model Stent Envelope')
if ~auto, pause, end % Strike any key to continue.

```

```

Plothandle = plot(xt,yt,'y-',xb,yb,'y-', 'EraseMode','xor');

trace = 0;
tol = .0005; % usu. .00005
options=foptions;
options(1)=trace;
options(2)=tol;
options(14)=3000;
lambda = fmins('fit_hyp',lambda,options);
if ~auto, pause, end

hold off
echo off
disp('Ax^2+Bxy+Cy^2+Dx+Ey')
disp(sprintf('%g %g %g %g %g',lambda(1),lambda(2),lambda(3),lambda(4),lambda(5)))

if lambda(2) == 0, lambda(2) = eps; end
ft = sqrt(lambda(1)^2+lambda(2)^2-2*lambda(1)*lambda(3)+lambda(3)^2);
mt1 = (-lambda(1)+lambda(3)+ft)/lambda(2);
mt2 = (-lambda(1)+lambda(3)-ft)/lambda(2);
if abs(mt1) < pi & abs(mt2) < pi
    if mt1 > 0 & mt2 > 0
        mt = min(mt1, mt2);
    else
        mt = max(mt1, mt2);
    end
else
    if abs(mt1) < abs(mt2)
        mt = mt1;
    else
        mt = mt2;
    end
end
theta = atan(mt);
l = sin(theta);
m = cos(theta);
a = lambda(1)*m^2+lambda(2)*l*m+lambda(3)*l^2;
c = lambda(1)*l^2-lambda(2)*l*m+lambda(3)*m^2;
d = lambda(4)*m+lambda(5)*l;
e = -lambda(4)*l+lambda(5)*m;

h = -d/(2*a);
k = -e/(2*c);
p2 = (-4-d^2/a-e^2/c)/(4*a);
q2 = (4*a*c+c*d^2+a*e^2)/(4*a*c^2);
disp(sprintf('theta = %g degrees', theta/pi*180))

figure(1)
clf
plot(xt, yt, 'ro', xb, yb, 'ro', xp, yp, 'yo')

% Rotation
xr1 = xt * m + yt * l;
yr1 = -xt * l + yt * m;
xr2 = xb * m + yb * l;
yr2 = -xb * l + yb * m;
xr3 = xp * m + yp * l;
yr3 = -xp * l + yp * m;
figure(2)
plot(xr1, yr1, 'ro', xr2, yr2, 'ro', xr3, yr3, 'yo')

% Translation
xt1 = xr1 - h;

```

```

yt1 = yr1 - k;
xt2 = xr2 - h;
yt2 = yr2 - k;
xt3 = xr3 - h;
yt3 = yr3 - k;
figure(3)
xtt=linspace(min([xt1;xt2]),max([xt1;xt2]),100); ytt = sqrt(q2)*sqrt(1+(xtt/sqrt(p2)).^2); ytb=-ytt;
plot(xt1, yt1, 'ro', xt2, yt2, 'ro', xt3, yt3, 'yo',xtt,ytt,'g.',xtt,ytb,'g.')

% Final normalization
% note: this does not change the data; it is only to make irregular horn-shaped
% stents appear centered (when they should actually be out to one side)
hn = mean([min(xt3),max(xt3)]);
kn = mean([min(yt3),max(yt3)]);
xn1 = xt1 - hn;
yn1 = yt1 - kn;
xn2 = xt2 - hn;
yn2 = yt2 - kn;
xn3 = xt3 - hn;
yn3 = yt3 - kn;

% This determines the r^2 value of the fit
ytcalc = zeros(size(xt));
for j = 1:length(xt)
    ftemp = sqrt((lambda(5)+lambda(2)*xt(j))^2-4*lambda(3)*(lambda(1)*xt(j)^2+lambda(4)*xt(j)-1));
    ytcac(j) = (-lambda(5) - lambda(2)*xt(j) + ftemp) / (2*lambda(3));
end

ybcalc = zeros(size(xb));
for j = 1:length(xb)
    ftemp = sqrt((lambda(5)+lambda(2)*xb(j))^2-4*lambda(3)*(lambda(1)*xb(j)^2+lambda(4)*xb(j)-1));
    ybcal(j) = (-lambda(5) - lambda(2)*xb(j) - ftemp) / (2*lambda(3));
end

ytrue = [yt;yb];
ycalc = [ytcalc;ybcalc];
r = corrcoef(ytrue,ycalc); r = r(1,2);
disp(sprintf('The r^2 value is: %g',r^2))

% output results
nn = [6          n2+4 n3+4; ...
      1          m theta; ...
      p2         q2 0; ...
      h          k 0; ...
      hn         kn 0; ...
      -2*ones(length(xn1),1) xt1 yt1; ...
      -ones(length(xn2),1) xt2 yt2; ...
      [1:length(xn3)]' xt3 yt3];

```

### function [x,y] = getlin(fig,s)

```

%GETLINE Track mouse movement with rubberbanded line.
% [X,Y] = GETLINE(FIG) tracks the movement of a mouse in
% the figure FIG. The mouse movement is tracked with a
% rubberbanded polyline. Returns the selected line endpoints,
% X and Y in axes coordinates. Left mouse button adds a new
% point to the polygon, right mouse button (shift-click
% on the Macintosh) or <cr> finishes the polygon.
% XY = GETLINE(FIG) returns the data coordinates in a 2-column
% matrix.
%
```

```

%      See also GETRECT.

%      Clay M. Thompson 1-28-93
%      Modified July 1995 James C. Squire

% How this works: This function waits for buttonpresses. After
% a button press the current point is saved, and a call-back is
% installed as a button motion function to draw a rubber-banded
% dashed line from this saved point to the current point. When
% the button is pressed again, the current point is saved and the
% process is started all over. This continues until a <cr> or
% right mouse button is pressed.

global Pt1 Pt2 hline fig ax

if nargin<1, fig = gcf; end

if nargin==2, % Process call-backs
    if strcmp(s,'motion'),
        if length(hline)>0,
            Pt2 = get(ax,'CurrentPoint'); Pt2 = Pt2(1,1:2);
            set(hline,'Xdata',[Pt1(1) Pt2(1)],'Ydata',[Pt1(2) Pt2(2)])
        end
    else
        error('Invalid call-back');
    end
    return
end

figure(fig), ax = gca;
c = [1 0 1];

% Create an invisible line to preallocate the xor line color.
handles = line(min(get(ax,'xlim'))*ones(1,2),min(get(ax,'ylim'))*ones(1,2),...
    'eraseMode','xor','linestyle','-','Color',c,'visible','off');

if any(get(ax,'view')~= [0 90]), error('GETLINE works only on 2-D plots'); end
curse = get(gcf,'pointer');
set(gcf,'pointer','crosshair');

btndown = get(gcf,'windowbuttondownfcn');
btnup = get(gcf,'windowbuttonupfcn');
btnmotion = get(gcf,'windowbuttonmotionfcn');
set(gcf,'windowbuttondownfcn','','windowbuttonupfcn','')

Pts = []; handles = []; done = 0; first = 1;
while ~done
    done = waitforbuttonpress;
    if gcf==fig,
        axes(ax) % Protect against user clicking in another axis
        Pt1 = get(ax,'CurrentPoint');
        Pt1 = Pt1(1,1:2);
        Pts = [Pts;Pt1];
        if ~strcmp(get(fig,'selectiontype'),'normal'),
            done = 1;
            hline = [];
        else
            hline = line(Pt1(1)*ones(1,2),Pt1(2)*ones(1,2),'eraseMode','xor', ...
                'linestyle','-','Color',c);
        end
        if first,
            set(fig,'WindowButtonMotionFcn','getline(gcf,"motion")')
            first = 0;
        end
    end
end

```

```

    handles = [handles hline];
end
drawnow
end
end
delete(handles)
set(fig,'pointer',curse);
clear global Pt1 Pt2 hline fig ax
set(gcf,'windowbuttondownfcn',btndown,'windowbuttonupfcn',btnup, ...
'windowbuttonmotionfcn',btmotion)
if nargin < 2, x = Pts; return, end
if ~isempty(Pts), x = Pts(:,1); y = Pts(:,2); else x = []; y = []; end

```

### function [rn,scale]=get\_dat(x,map,scale)

```

%GET_DAT Gets edge modelling data from an image.
% [rn,scale] = get_dat(x,map,scale)
% Returns a matrix of input points centered
% Input first top half, then bottom half, then the key data points
% If scale is provided as input, does not ask for user to provide reference
% If scale is returned, may use this in next get_dat to eliminate ref errors.
% Returns
% [2 4 6] 2 is index of up upper stent envelope, 6 is index of data points
% [-2 x1 y1] -2 also signifies upper envelope
% [-2 x2 y2]
% [-1 x1 y1] -1 is lower stent envelope
% [-1 x2 y2]
% [1 x1 y1] these are point numbers
% [2 x2 y2]
%
% James C. Squire July 1995
% Modified September 1995 to include reference distance

```

```

imshow(x,map)

```

```

[txx,tyy] = getlin;
nx = length(txx);
disp(setstr(7));
disp(sprintf('%g points collected',nx))

```

```

[bxx,byy] = getlin;
nt = length(bxx);
disp(setstr(7));
disp(sprintf('%g points collected',nt))

```

```

[pxx,pyy] = getpts;
np = length(pxx);
disp(setstr(7));
disp(sprintf('%g points collected',np-1))

```

```

if nargin==2
    disp('draw line over reference length')
    [refx,refy]=getlin
    ll = norm([diff(refx),diff(refy)]);
    disp(sprintf('Line length is %g pixels',ll));
    scale = input('Enter length of line in mm -> ')/ll;
end

```

```

% Scale in real units and translate so just touching Quadrant 1 boundary
in = [-2*ones(nx,1); -ones(nt,1); [1:np]'];
t yy=-tyy; byy=-byy; pyy=-pyy; % flip up/down: screen coords vs. matrix coords

```



```

xoffset = min([txx; bxx])*scale;
yoffset = min([tyy; byy])*scale;
xx = [txx; bxx; pxx]*scale - xoffset;
yy = [tyy; byy; pyy]*scale - yoffset;

% Store them
n1 = 2;
n2 = nx + n1;
n3 = nt + n2;
m = [n1 n2 n3; in xx yy];
m(length(m),:) = []; % throw out the last row given by the right button click
hold off

```

### function dn=out\_dat(nvert,nhoriz,nn)

```

%OUT_DAT calculates a list of quadrilateral patches to form a hyperboloid projection
%   dn=out_dat(nvert,nhoriz,nn)
%
%   See fit_hypm for form of nn.
%   nvert, nhoriz describe the number of vertical and horizontal patches.
%
%   It returns dn =
%   [1 x11 y11 x12 y12 x13 y13 x14 y14 ett ezz ezt d(ett)/dt d(ezz)/dt d(ezt)/dt]
%   [2 x21 y21 x22 y22 x23 y23 x24 y24 ett ezz ezt d(ett)/dt d(ezz)/dt d(ezt)/dt]
%   [n+1 nvert nhoriz 0 0 0 0 0 0 0 0 0]
%   vertices are labelled 1 2 in each patch j
%       3 4
%
%   James C. Squire August 1995
%   modified August 1995

```

```
DEBUG = 0;
```

```

p2 = nn(3,1);
q = sqrt(nn(3,2));
xpoints = nn(nn(1,3):size(nn,1),2);
ypoints = nn(nn(1,3):size(nn,1),3);
xmin = min(xpoints);
xmax = max(xpoints);
Npatch = nvert*nhoriz;
clf
% axis([-1 1 -1 1])
dn = zeros(Npatch+1,15);
dn(:,1) = [1:Npatch+1]';

for j=1:Npatch

    jrow = nvert/2 - rem(j-1,nvert);
    jcol = ceil(j/nvert);

    if rem(j-1,nvert) < nvert/2
        half = 't'; trow = jrow;
    elseif rem(j-1,nvert) >= nvert/2
        half = 'b'; trow = 1 - jrow;
    else disp('Trouble in out_dat point 1')
    end

    x1 = xmin + (xmax-xmin)/nhoriz*(jcol-1);
    x2 = xmin + (xmax-xmin)/nhoriz*jcol;

```

```

x3 = x2;
x4 = x1;
yt1 = q*sqrt(1+(x1^2/p2))*sin(pi*trow/nvert);
yt2 = q*sqrt(1+(x2^2/p2))*sin(pi*trow/nvert);
yt3 = q*sqrt(1+(x3^2/p2))*sin(pi*(trow-1)/nvert);
yt4 = q*sqrt(1+(x4^2/p2))*sin(pi*(trow-1)/nvert);

if half == 't'
    y1 = yt1; y2 = yt2; y3 = yt3; y4 = yt4;
elseif half == 'b'
    y1 = -yt1; y2 = -yt2; y3 = -yt3; y4 = -yt4;
end

dn(j,2) = x1; dn(j,3) = y1; dn(j,4) = x2; dn(j,5) = y2;
dn(j,6) = x3; dn(j,7) = y3; dn(j,8) = x4; dn(j,9) = y4;

    patch([x1,x2,x3,x4],[y1,y2,y3,y4],[1-yt1/.8]*128)
end

dn(Npatch+1, 2) = nvert;
dn(Npatch+1, 3) = nhoriz;

if DEBUG
    hold on
    plot(xpoints,ypoints,'wo')
    while 1
        [xx,yy] = getlin;
        zz=zcalc(xx,yy,p2,q,DEBUG);
        dx = diff(xx)
        dy = diff(yy)
        dz = diff(zz)
        ds = norm([dx dy dz]);
        disp(sprintf('x1 = %g  y1 = %g  z1 = %g',xx(1),yy(1),zz(1)))
        disp(sprintf('x2 = %g  y2 = %g  z2 = %g',xx(2),yy(2),zz(2)))
        disp(sprintf('dx = %g  dy = %g  dz = %g',dx,dy,dz))
        disp(sprintf('Total distance separation is %g',ds))
        if (input('Again? ','s')) == 'n',break,end
    end
    hold off
end
end

```

### **function show(filename,skip,action)**

```

%SHOW          Displays results of stent data
%             function show(filename,skip)
%             filename holds data in variables d0,d2,d4,d6, etc.
%             skip is the jump between variable names (eg 2 above)

%             James Squire
%             September 1995

% Information regarding the movie play status will be held in
% the axis user data according to the following table:
play= 1;
stop=-1;

if nargin==2,
    action='initialize';
else
    action = 'display';
end
end

```

```

if strcmp(action,'initialize'),

    figNumber=figure( ...
        'Name','Endovascular Stent Strain', ...
        'NumberTitle','off', ...
        'Visible','off', ...
        'BackingStore','off', ...
        'Position', get(0,'screensize'));
    %'Colormap','hsv

    axes( ...
        'Units','normalized', ...
        'Position',[0.05 0.05 0.82 0.90], ...
        'Visible','on', ...
        'NextPlot','replace');

    axis([-1 1 -1 1]);
    set(gca,'userdata',0)

%=====
% Information for all buttons
%labelColor=[0.8 0.8 0.8];
yInitPos=0.90;
xPos=0.912;
btnWid=0.079;
btnHt=0.06;
% Spacing between the button and the next command's label
spacing=0.05;

%=====
% The Console frame
frmBorder=0.01;
yPos=0;
frmPos=[xPos-frmBorder yPos btnWid+2*frmBorder 1];
h=icontrol( ...
    'Style','frame', ...
    'Units','normalized', ...
    'Position',frmPos);
    %'BackgroundColor',[0.5 0.5 0.5]

%=====
% The Tensor Component popup button
btnNumber=1;
yPos=0.95-(btnNumber-1)*(btnHt+spacing);
textStr='Component';
popupStr=reshape(' Axial  Circumfr. Torsion All  None  ',10,5);

% Generic button information
btnPos1=[xPos yPos-spacing+btnHt/1.5 btnWid btnHt/2];
btnPos2=[xPos yPos-spacing btnWid btnHt/2];
popupHndlc=icontrol( ...
    'Style','text', ...
    'Units','normalized', ...
    'Position',btnPos1, ...
    'String',textStr);
    btnPos=[xPos yPos-spacing btnWid btnHt/2];
    popupHndlc=icontrol( ...
        'Style','popup', ...
        'Units','normalized', ...
        'Position',btnPos2, ...
        'String',popupStr);

```

```

%=====
% The Differential popup button
btnNumber=2;
  yPos=0.95-(btnNumber-1)*(btnHt+spacing);
textStr='Differential?';
popupStr=reshape(' No Yes',4,2);

% Generic button information
btnPos1=[xPos yPos-spacing+btnHt/1.5 btnWid btnHt/2];
btnPos2=[xPos yPos-spacing btnWid btnHt/2];
popupHndld=icontrol( ...
  'Style','text', ...
  'Units','normalized', ...
  'Position',btnPos1, ...
  'String',textStr);
btnPos=[xPos yPos-spacing btnWid btnHt/2];
popupHndld=icontrol( ...
  'Style','popup', ...
  'Units','normalized', ...
  'Position',btnPos2, ...
  'String',popupStr);

%=====
% The Frame popup button
btnNumber=3;
  yPos=0.95-(btnNumber-1)*(btnHt+spacing);
textStr='Frame';
eval(['load ' filename]);
num_data_sets = 0;
while exist(sprintf('d%g',num_data_sets))
  num_data_sets = num_data_sets + skip;
end
num_data_sets = num_data_sets - skip;

popupStr=[];
for i=0:skip:num_data_sets
  popupStr=[popupStr sprintf('%3g',i)];
end

% Generic button information
btnPos1=[xPos yPos-spacing+btnHt/1.5 btnWid btnHt/2];
btnPos2=[xPos yPos-spacing btnWid btnHt/2];
popupHndlf=icontrol( ...
  'Style','text', ...
  'Units','normalized', ...
  'Position',btnPos1, ...
  'String',textStr);
btnPos=[xPos yPos-spacing btnWid btnHt/2];
popupHndlf=icontrol( ...
  'Style','popup', ...
  'Units','normalized', ...
  'Position',btnPos2, ...
  'String',popupStr);

%=====
% The Movie popup button
btnNumber=4;
  yPos=0.95-(btnNumber-1)*(btnHt+spacing);
textStr='Movie?';
popupStr=reshape(' No Yes',4,2);

% Generic button information
btnPos1=[xPos yPos-spacing+btnHt/1.5 btnWid btnHt/2];

```

```

    btnPos2=[xPos yPos-spacing btnWid btnHt/2];
    popupHndl=icontrol( ...
        'Style','text', ...
        'Units','normalized', ...
        'Position',btnPos1, ...
        'String',textStr);
    btnPos=[xPos yPos-spacing btnWid btnHt/2];
    popupHndl=icontrol( ...
        'Style','popup', ...
        'Units','normalized', ...
        'Position',btnPos2, ...
        'String',popupStr);

%=====
% The Display button
btnNumber=5;
yPos=0.95-(btnNumber-1)*(btnHt+spacing);
labelStr='Display';
cmdStr='display';
callbackStr=[show("'" filename "' , num2str(skip) ','display'");

% Generic button information
btnPos=[xPos yPos-spacing btnWid btnHt];
startHndl=icontrol( ...
    'Style','pushbutton', ...
    'Units','normalized', ...
    'Position',btnPos, ...
    'String',labelStr, ...
    'Interruptible','yes', ...
    'Callback',callbackStr);

%=====
% The Interrupt button
btnNumber=6;
yPos=0.95-(btnNumber-1)*(btnHt+spacing);
labelStr='Interrupt';
% Setting userdata to -1 (=interrupt) will stop the movie.
callbackStr='set(gca,"Userdata",-1)';

% Generic button information
btnPos=[xPos yPos-spacing btnWid btnHt];
stopHndl=icontrol( ...
    'Style','pushbutton', ...
    'Units','normalized', ...
    'Position',btnPos, ...
    'Enable','off', ...
    'String',labelStr, ...
    'Callback',callbackStr);

%=====
% The Close button
labelStr='Close';
callbackStr='close(gcf)';
closeHndl=icontrol( ...
    'Style','push', ...
    'Units','normalized', ...
    'Position',[xPos 0.05 btnWid 0.10], ...
    'String',labelStr, ...
    'Callback',callbackStr);

% Uncover the figure
hdlCB = 0; % Since no colorbar yet

```

```

    axispos = get(gca,'position');
    hndlList=[startHndl stopHndl closeHndl popupHndlc popupHndld popupHndlf popupHndlm hndlCB
axispos];
    set(figNumber,'Visible','on', ...
        'UserData',hndlList);
    figure(figNumber);

elseif strcmp(action,'display'),
    axHndl=gca;
    figNumber=gcf;
    hndlList=get(figNumber,'UserData');
    startHndl=hndlList(1);
    stopHndl=hndlList(2);
    closeHndl=hndlList(3);
    popupHndlc=hndlList(4);
    popupHndld=hndlList(5);
    popupHndlf=hndlList(6);
    popupHndlm=hndlList(7);
    hndlCB = hndlList(8);

% ===== Display data
component = get(popupHndlc,'Value');
differential = get(popupHndld,'Value');
frame = get(popupHndlf,'Value');
movie = get(popupHndlm,'Value');

if component <= 3 & movie == 1
    show1(filename,skip)
elseif component <= 3 & movie ==2
    show2(filename,skip)
elseif component == 4 & movie == 1
    show3(filename,skip)
elseif component == 4 & movie == 2
    show3(filename,skip)
elseif component == 5 & movie == 1
    show5(filename,skip)
elseif component == 5 & movie == 2
    show6(filename,skip)
else
    error('internal error-invalid component/movie in show.m')
end

end; % if strcmp(action, ...

```

### **function show1(filename,skip)**

```

% initialize graphics
hndlList=get(gcf,'UserData');

startHndl=hndlList(1);
stopHndl=hndlList(2);
closeHndl=hndlList(3);
popupHndlc=hndlList(4);
popupHndld=hndlList(5);
popupHndlf=hndlList(6);
popupHndlm=hndlList(7);
hndlCB = hndlList(8);
axispos = hndlList(9:12);

component = get(popupHndlc,'Value');

```

```

differential = get(popupHndld,'Value');
frame       = get(popupHndlf,'Value');

set([startHndl closeHndl ],'Enable','off');
set(stopHndl,'Enable','on');

% initialize data
load(filename)
dn = eval(['d' num2str((frame-1)*skip)]);

nvert = dn(size(dn,1),2);
nhoriz = dn(size(dn,1),3);
nblocks = nvert*nhoriz;
if component == 1 & differential == 1 % axial
    y = dn(1:nblocks,11);
elseif component == 1 & differential == 2 % axial difference
    y = dn(1:nblocks,14);
elseif component == 2 & differential == 1 % circum.
    y = dn(1:nblocks,10);
elseif component == 2 & differential == 2 % circum. difference
    y = dn(1:nblocks,13);
elseif component == 3 & differential == 1 % torsion
    y = dn(1:nblocks,12);
elseif component == 3 & differential == 2 % torsion difference
    y = dn(1:nblocks,15);
else
    error('Error in show1.m; incorrectly called')
end

cla
set(gca,'position',axispos)
axis('auto')
axis('equal')
view(0,90)
grid off
colormap(jet(200));
if hndlCB~=0 % colorbar present
    close(hndlCB);
    hndlCB=0;
end

xmin = dn(1,2);
xmax = dn(nblocks,8);
nsub = mean([xmin xmax]);

hold on
for j=1:nblocks
    fill([dn(j,2),dn(j,4),dn(j,6),dn(j,8)]-nsub,[dn(j,3),dn(j,5),dn(j,7),dn(j,9)],y(j))
end
hold off
cmin = min(y);
cmax = max(y);
if cmin < 0 & cmax < 0
    cmax = 0;
elseif cmin > 0 & cmax > 0
    cmin = 0;
elseif cmin==0 & cmax == 0
    cmax = cmax + eps;
end
caxis([cmin cmax])

hndlList(8)=colorbar('v');

```

```

set(gcf,'userdata',hdlList);

set([startHndl closeHndl],'Enable','on');
set(stopHndl,'Enable','off');

end

```

### **function show2(filename,skip)**

```

% initialize graphics
hdlMainWin = gca;
hdlList=get(gcf,'UserData');

startHndl=hdlList(1);
stopHndl=hdlList(2);
closeHndl=hdlList(3);
popupHndlc=hdlList(4);
popupHndld=hdlList(5);
popupHndlf=hdlList(6);
popupHndlm=hdlList(7);
hdlCB = hdlList(8);
axispos = hdlList(9:12);

component = get(popupHndlc,'Value');
differential = get(popupHndld,'Value');

set([startHndl closeHndl ],'Enable','off');
set(stopHndl,'Enable','on');

% initialize data
load(filename)
num_data_sets = 0;
while exist(sprintf('d%g',num_data_sets))
    num_data_sets = num_data_sets + skip;
end
num_data_sets = num_data_sets/skip;
if component == 1 & differential == 1 % axial
    keycol=11;
elseif component == 1 & differential == 2 % axial difference
    keycol=14;
elseif component == 2 & differential == 1 % circum.
    keycol=10;
elseif component == 2 & differential == 2 % circum. difference
    keycol=13;
elseif component == 3 & differential == 1 % torsion
    keycol=12;
elseif component == 3 & differential == 2 % torsion difference
    keycol=15;
else
    error('Error in show1.m; incorrectly called')
end

% find the axis,x,range (so colorbar and scale do not change);
% y is set to make it square with x (y always smaller for thin stent)
minc = 99999;
maxc = -99999;
widest = 0;
for i=0:skip:(num_data_sets-1)*skip;
    dn = eval(['d' num2str(i)]);
    nblocks = size(dn,1)-1;

```



```

if min(dn(1:nblocks,keycol)) < minc
    minc = min(dn(1:nblocks,keycol));
end
if max(dn(1:nblocks,keycol)) > maxc
    maxc = max(dn(1:nblocks,keycol));
end
if (dn(nblocks,8) - dn(1,2)) > widest
    widest = dn(nblocks,8) - dn(1,2);
end
end
if minc < 0 & maxc < 0
    maxc = 0;
elseif minc > 0 & maxc > 0
    minc = 0;
elseif minc==0 & maxc == 0
    maxc = maxc + eps;
end
caxis([minc maxc])
axlim = widest/2;

% do the drawing
first = 1;
for i=0:skip:(num_data_sets-1)*skip
    dn = eval(['d' num2str(i)]);
    view(0,90)
    grid off
    colormap(jet(200));
    hndlList=get(gcf,'UserData');
    hndlCB = hndlList(8);
    cla
    set(gca,'xlim',[-axlim axlim]);
    set(gca,'ylim',[-axlim axlim]);
    axispos = hndlList(9:12);
    if hndlCB~=0 % colorbar present
        close(hndlCB);
        hndlCB=0;
        set(gca,'position',axispos)
    end
    xmin = dn(1,2);
    xmax = dn(nblocks,8);
    nsub = mean([xmin xmax]);

    hold on
    caxis([minc maxc])
    for j=1:nblocks
        fill([dn(j,2),dn(j,4),dn(j,6),dn(j,8)]-nsub,[dn(j,3),dn(j,5),dn(j,7),dn(j,9)],dn(j,keycol))
    end
    hold off
    hndlList(8)=colorbar('v');
    set(gcf,'userdata',hndlList);

if first
    m = moviein(num_data_sets);
    first = 0;
end
axes(hndlMainWin)
m(:,i/skip+1) = getframe;
if get(gca,'userdata')== -1
    break
end
end
end

if get(gca,'userdata')==0

```

```

    movie(m,15,2.5);
else
    set(gca,'userdata',0)
end
caxis('auto')

show1(filename,skip);

```

### **function show3(filename,skip)**

```

% initialize graphics
hdlList=get(gcf,'UserData');

startHndl=hndlList(1);
stopHndl=hndlList(2);
closeHndl=hndlList(3);
popupHndlc=hndlList(4);
popupHndld=hndlList(5);
popupHndlf=hndlList(6);
popupHndlm=hndlList(7);
hdlCB = hndlList(8);
axispos = hndlList(9:12);

differential = get(popupHndld,'Value');
frame      = get(popupHndlf,'Value');

%set([startHndl closeHndl ],'Enable','off');
set(stopHndl,'Enable','on');

% initalize data
load(filename)
dn = eval(['d' num2str((frame-1)*skip)]);

nvert = dn(size(dn,1),2);
nhoriz = dn(size(dn,1),3);
nblocks = nvert*nhoriz;
data = zeros(nhoriz,3); % data of form [circum axial torsion]
if differential == 1 % regular
    for i=1:nhoriz
        data(i,:) = mean(dn((i-1)*nvert+1:i*nvert,10:12));
    end
elseif differential == 2
    for i=1:nhoriz
        data(i,:) = mean(dn((i-1)*nvert+1:i*nvert,13:15));
    end
end
xmin = dn(1,2);
xmax = dn(nblocks,8);
xlim = (xmax-xmin)/2;
datax = linspace(-xlim,xlim,nhoriz);

if hdlCB~=0 % colorbar present
    close(hdlCB);
    hndlList(8)=0;
end
cla
set(gca,'position',axispos)
axis('normal')
axis('auto')
view(0,90)

```

```

hold on

plot(datax,data)
grid on
hdlList(8) = legend('Circumf.','Axial','Torsion',-1);
set(gcf,'userdata',hdlList);

set(startHndl,closeHndl,'Enable','on');
set(stopHndl,'Enable','off');

end

```

### function show5(filename,skip)

```

% initialize graphics
hdlList=get(gcf,'UserData');
startHndl=hdlList(1);
stopHndl=hdlList(2);
closeHndl=hdlList(3);
popupHndlf=hdlList(6);
hdlCB = hdlList(8);
axispos = hdlList(9:12);
frame    = get(popupHndlf,'Value');

set([startHndl closeHndl ],'Enable','off');
set(stopHndl,'Enable','on');

% initialize data
load(filename)
dn = eval(['d' num2str((frame-1)*skip)]);
d0 = eval('d0');
nvert = dn(size(dn,1),2);
nhoriz = dn(size(dn,1),3);
nblocks = nvert*nhoriz;

cla
set(gca,'position',axispos)
if hdlCB~=0 % colorbar present; get rid of it
    close(hdlCB);
    hdlList(8) = 0;
    set(gcf,'userdata',hdlList);
end
set(gca,'xlimmode','auto')
set(gca,'aspectratio',[NaN NaN])
grid on
hold on

xnmin = dn(1,2);      xnmax = dn(nblocks,8);
x0min = d0(1,2);     x0max = d0(nblocks,8);
xnscale = xnmax-xnmin;
x0scale = x0max-x0min;
ynlist = zeros(nhoriz+1,1);
y0list = zeros(nhoriz+1,1);
for i=0:nhoriz-1
    ynlist(i+1)=dn(i*nvert+1,3);
    y0list(i+1)=d0(i*nvert+1,3);
end
ynlist(nhoriz+1) = dn(nblocks-nvert+1,5);
y0list(nhoriz+1) = d0(nblocks-nvert+1,5);

```

```

[z0,y0,x0] = cylinder(y0list,25);
x0 = x0*x0scale; x0 = x0-x0scale/2;
surf(x0',y0',z0')

[zn,yn,xn] = cylinder(ynlist,25);
xn(:,18:19) = NaN*zeros(nhoriz+1,2);
xn = xn*xnscale; xn = xn-xnscale/2;
hdlSurf=surf(xn',yn',zn');
set(hdlSurf,'edgecolor','none')
set(hdlSurf,'facecolor','interp')

view(340,30)
colormap(bone(200))
axlim = diff(get(gca,'xlim'))/2;
set(gca,'ylim',[-axlim axlim]);
set(gca,'zlim',[-axlim axlim]);
hold off

set([startHndl closeHndl],'Enable','on');
set(stopHndl,'Enable','off');

end

```

### function show6(filename,skip)

```

% initialize graphics
hdlList=get(gcf,'UserData');
startHndl=hdlList(1);
stopHndl=hdlList(2);
closeHndl=hdlList(3);
hdlCB = hdlList(8);
axispos = hdlList(9:12);

set([startHndl closeHndl ],'Enable','off');
set(stopHndl,'Enable','on');

% initialize data
load(filename)
num_data_sets = 0;
while exist(sprintf('d%g',num_data_sets))
    num_data_sets = num_data_sets + skip;
end
num_data_sets = num_data_sets/skip;

% find the movie's x axis limits range (so axes do not change);
widest = 0;
for i=0:skip:(num_data_sets-1)*skip;
    dn = eval(['d' num2str(i)]);
    nvert = dn(size(dn,1),2);
    nhoriz = dn(size(dn,1),3);
    nblocks = nvert*nhoriz;
    if (dn(nblocks,8) - dn(1,2)) > widest
        widest = dn(nblocks,8) - dn(1,2);
    end
end
axlim = widest/2;

% do the drawing

```

```

first = 1;
for i=0:skip:(num_data_sets-1)*skip
    dn = eval(['d' num2str(i)]);
    d0 = eval('d0');
    cla
    set(gca,'position',axispos)
    if hndlCB~=0 % colorbar present; get rid of it
        close(hndlCB);
        hndlCB = 0;
        hndlList(8) = 0;
        set(gcf,'userdata',hndlList);
    end
    axis('auto')
    hold on

    xnmin = dn(1,2);      xnmax = dn(nblocks,8);
    x0min = d0(1,2);     x0max = d0(nblocks,8);
    xnscale = xnmax-xnmin;
    x0scale = x0max-x0min;
    ynlist = zeros(nhoriz+1,1);
    y0list = zeros(nhoriz+1,1);
    for j=0:nhoriz-1
        ynlist(j+1)=dn(j*nvert+1,3);
        y0list(j+1)=d0(j*nvert+1,3);
    end
    ynlist(nhoriz+1) = dn(nblocks-nvert+1,5);
    y0list(nhoriz+1) = d0(nblocks-nvert+1,5);
    y0list=y0list-100*eps; % so when both are shown together...

    [z0,y0,x0] = cylinder(y0list,25);
    x0 = x0*x0scale; x0 = x0-x0scale/2;
    surf(x0',y0',z0')

    [zn,yn,xn] = cylinder(ynlist,25);
    xn(:,18:19) = NaN*zeros(nhoriz+1,2);
    xn = xn*xnscale; xn = xn-xnscale/2;
    hndlSurf=surf(xn',yn',zn');
    set(hndlSurf,'edgecolor','none')
    set(hndlSurf,'facecolor','interp')

    view(340,30)
    colormap(bone(200))
    set(gca,'xlim',[-axlim axlim]);
    set(gca,'ylim',[-axlim axlim]);
    set(gca,'zlim',[-axlim axlim]);
    grid('on')
    hold off

    if first
        m = moviein(num_data_sets);
        first = 0;
    end
    if get(gca,'userdata')==1
        break
    end
    m(:,i/skip+1) = getframe;

end
if get(gca,'userdata')==0
    movie(m,20,1.5);
else
    set(gca,'userdata',0)
end
end

```

```
show5(filename,skip)
```

### **function zlist=zcalc(xlist,ylist,p2,q,debug)**

```
%ZCALC finds the z value of a hyperbola (part of thesis2)
%      zlist=zcalc(xlist,p,q,debug)
%
%      set debug~0 for diagnostic information
%      See get_data for form of m.
%      This assumes a hyperbola of form  $(y/q)^2 - (x/p)^2 = 1$ 
%
%      James C. Squire August 1995

debug=1;
rlist = sqrt(q^2*(1+(xlist.^2/p2)));
zlist = sqrt(rlist.^2 - ylist.^2);
tindex = find(imag(zlist));
if debug
    for j=1:length(tindex)
        disp(' ')
        disp(sprintf('Warning: point #%g passed to zcalc outside model',tindex(j)))
    end
end
zlist(tindex) = zeros(size(tindex));
```

## References

---

- 1 Cheng, G. C., Libby, P., Grodzinsky, A. J., and Lee, R., "Induction of DNA synthesis by a single transient mechanical stimulus of human vascular smooth muscle cells: Role of fibroblast growth factor-2," *Circulation*, vol. 93, pp. 99-105, 1996.
- 2 Sumpio, B.E., Barnes, A. J., Buckley, M. and Johnson, G. Jr., "Alterations in aortic endothelial cell morphology and cytoskeletal protein synthesis during cyclic tensional deformation," *J. Vasc. Surgery*, vol. 7, pp. 130-8, 1988.
- 3 Reidy, M. A., "Factors controlling smooth muscle cell proliferation," *Arch. Pathol. Lab. Med.*, vol. 116, pp. 1276-1280, 1992.
- 4 Schwartz, R. S., Huber, K. C., and Murphy, J. G., "Restenosis and the proportional neointimal response to coronary artery injury: results in porcine model," *JACC*, vol. 19, pp. 267-274, 1992.
- 5 Ross R., "The pathogenesis of atherosclerosis – an update," *The New England Journal of Medicine*, vol. 314, pp. 488-500, 1986.
- 6 American Heart Association, "Heart and Stroke Facts: 1995 Statistical Supplement," p. 2, 1995.
- 7 Wilson R., "Simple device to prop clogged arteries open changes coronary care", *Wall Street Journal*, Oct. 23, pp. 1-2, 1995.
- 8 Parikh S., Rogers C., and Edelman E. R., "Endovascular Stents: Experimental Data," in Endoluminal Stenting, by Sigwart, U., W. B. Saunders, London, p. 6, 1996.
- 9 Sigwart, U., Puel, J., Mirkovitch, V., Joffre, F., and Kappenberger, L., "Intravascular stents to prevent occlusion and restenosis after transluminal angioplasty," *The New England Journal of Medicine*, vol. 316, pp. 701-706, 1987.

- 
- 10 Schomig, A., Kastrati, A., Mudra, H., Blasini, R., Schuhlen, H., Klaus, V., Richardt, G., and Neumann, F. J., "Four-year experience with Palmaz-Schatz stenting in coronary angioplasty complicated by dissection with threatened or present vessel closure," *Circulation*, vol. 90, pp. 2716-24, 1994.
  - 11 Ross R., "The Pathogenesis of atherosclerosis: A perspective for the 1990's," *Nature*, vol. 362, pp. 801-809, 1993.
  - 12 Buck, R. C., "Behavior of vascular smooth muscle cells during repeated stretching of the substratum in-vitro," *Atherosclerosis*, vol. 46, pp. 217-223, 1983.
  - 13 Rosenberg, R. D., "Vascular smooth muscle cell proliferation: Basic investigations and new therapeutic approaches," *Thromb. Haemost.*, vol. 70, pp. 10-16, 1993.
  - 14 Edelman, E. R., Nugent, M. A., Smith, L. T., and Karnovsky, M. J., "Basic Fibroblast Growth Factor Enhances the Coupling of Intimal Hyperplasia and Proliferation of Vasa Vasorum in Injured Rat Arteries," *J. Clin. Invest.*, vol. 89, pp. 465-473, 1992.
  - 15 Ross, R., and Glomset J. A., "The pathogenesis of atherosclerosis (first of two parts)," *The New England Journal of Medicine*, vol. 295, pp. 369-377, 1976.
  - 16 Gotlieb, A. I. and Langille, B. L., Atherosclerosis and Coronary Artery Disease, Philadelphia: Lippincott-Raven Publishers, 1996.
  - 17 Dewey, C. F., Jr., "Effects of fluid flow on living vascular cells," *ASME J. Biomech. Eng.*, vol. 106, pp. 31-35, 1984.
  - 18 Frangos, J. A., McIntire, L. V., Eskin, S. G., and Ives, C. L., "Effects of flow on prostacyclin production by cultured human endothelial cells," *Science*, vol. 227, pp. 1477-1479, 1985.
  - 19 Gorfien, S. F., Winston, S. K., Thibault, L. E., and Macarak, E. J., "Effects of biaxial deformation on pulmonary artery endothelial cells," *J. Cell Physiology*, vol. 139, pp. 492-500, 1989.
  - 20 Lin, S. J., Jan, K. M., Weinbaum, S., and Chien S., "Transendothelial transport of low density lipoprotein in association with cell mitosis in rat aorta," *Arteriosclerosis*, vol. 9, pp. s30-s36, 1989.
  - 21 Nerem, R. M. and Girard, P. G., "Hemodynamic influences on vascular endothelial biology," *Toxicol Pathol.*, vol. 18, pp. 572-582, 1990.



- 
- 22 Peacock, J., Hankins, S., Jones, T., and Lutz, R., "Flow instabilities induced by coronary artery stents: assessment with an in-vitro pulse duplicator," *J. Biomech.*, vol. 28, pp. 17-26, 1995.
  - 23 Volk, T. and Geiger, B., "A 135-kd membrane protein of intercellular adherens junctions," *EMBO J.*, vol. 3, pp. 2249-2260, 1984.
  - 24 Nelder, J. A. and Mead, R., "A simplex method for function minimization," *Computer Journal*, vol. 7, pp. 308-313, 1987.
  - 25 Hoffman, A. H. and Grigg, P., "A method for measuring strains in soft tissues," *J. Biomech.*, vol. 17, pp. 795-800, 1984.
  - 26 Humphrey, J. D., Vito, R. P., and Vawter, D. L., "Quantification of strains in biaxially tested soft tissues," *J. Biomech.*, vol. 20, pp. 59-65, 1987.
  - 27 Fung, Y. C., Biomechanics: Mechanical Properties of Living Tissues (2nd Ed.), New York: Springer-Verlag, 1993.
  - 28 McCulloch, A. D., Smaill, B. H., and Hunter, P. J., "Left ventricular epicardia deformation in isolated arrested dog heart," *American Physiological Society*, vol. 252, pp. H233-H241, 1987.
  - 29 Waldman, L. K., Fung, Y. C., and Covell, J. W., "Transmural myocardial deformation in the canine left ventricle: Normal in-vivo three-dimensional finite strains," *Circ. Res.*, vol. 57, pp. 152-163, 1985.
  - 30 George, D. T. and Bogen, D. K., "A low cost fiber-optic strain gauge system for biological applications," Proc. Thirteenth Annu. Bioeng. Conf., Philadelphia, PA, 1987.
  - 31 Barbee, K. A., Macarak, E. J., and Thibault, L. E., "Strain measurements in cultured vascular smooth muscle cells subjected to mechanical deformation," *Annals of Biomedical Engineering*, vol. 22, pp. 14-22, 1994.
  - 32 Skovoroda, A. R., Emelianov, S. Y., Lubinski, M. A., Sarvazyan, A. P., O'Donnell, M., "Theoretical Analysis and Verification of Ultrasound Displacement and Strain Imaging," *IEEE Transactions on Ultrasonics, Ferroelectrics, and Frequency Control*, vol. 41, pp. 302-313, 1994.

- 
- 33 Yin, F. C. P., Tompkins, W. R., Peterson, K. L., et al., "A video dimension analyzer," *IEEE Trans. Biomed. Eng.*, vol. 19, pp. 376-381, 1972.
- 34 Drace, J. E. and Pelc, N. J., "Elastic deformation in tendons and myotendinous tissue: Measurement by phase-contrast MR imaging," *Radiology*, vol. 191, pp. 835-839, 1994.
- 35 Ryan, L. K., Lockwood, G. R., Bloomfield, T. S., and Foster, F. S., "Speckle tracking in high frequency ultrasound images with application to intravascular imaging," IEEE 1993 Ultrasonics symposium Proceeding, , Baltimore, MD, Oct. 31-Nov. 3, 1993.
- 36 Weizsacker, H. W., "Isotropy and anisotropy of the arterial wall," *Biomechanics*, vol. 21, pp. 477-487, 1988.
- 37 Vito, R. P., Whang, M. C., Glagov, S., and Aoki, T., "The distribution of strains and stresses in the arterial cross section," 1991 Advances in Bioengineering Conference, ASME, Atlanta, Georgia, Dec. 1-6, 1991.
- 38 Downs, J., Halperin, H. R., Humphrey, J., and Yin, F., "An improved video-based computer tracking system for soft biomaterials testing," *IEEE Transactions on Biomedical Engineering*, vol. 37, pp. 903-907, 1990.
- 39 Choung, C. J. and Fung, Y. C., "Compressibility and constitutive equations of arterial wall in radial compression experiments," *J. Biomechanics*, vol. 17, pp. 35-40, 1984.
- 40 Rogers, C. and Edelman, E. R., "Endovascular stent design dictates experimental restenosis and thrombosis," *Circulation*, vol. 91, pp. 2995-3001, 1995.
- 41 Rogers, C., Parikh, S., Seifert, P. and Edelman, E. R., "Endothelial cell seeding: remnant endothelium after stenting enhances vascular repair," *Circulation.*, vol. 94, pp. 2099-2914, 1996.
- 42 Liu, X., Ancient India / Ancient China, Oxford: Oxford University Press, 1988.